1. Report No.	2. Government Accession No.	3. Recipient's Catalog No.
FHWA/TX-05/0-1707-10		

4. Title and Subtitle	5. Report Date
DEVELOPMENT OF SPECIFICATION-TYPE TESTS TO ASSESS THE IMPACT OF FINE AGGREGATE AND MINERAL FILLER ON FATIGUE DAMAGE	July 2005
	6. Performing Organization Code

7. Author(s)	8. Performing Organization Report No.
Yong-Rak Kim and Dallas N. Little	Report 0-1707-10

9. Performing Organization Name and Address	10. Work Unit No. (TRAIS)
Texas Transportation Institute The Texas A&M University System College Station, Texas 77843-3135	11. Contract or Grant No. Project No. 0-1707

12. Sponsoring Agency Name and Address	13. Type of Report and Period Covered
Texas Department of Transportation Research and Technology Implementation Office P. O. Box 5080 Austin, Texas 78763-5080	Technical Report: February 2003 – August 2004
	14. Sponsoring Agency Code

15. Supplementary Notes

Research performed in cooperation with the Texas Department of Transportation and the Federal Highway Administration.

Project Title: Long-Term Research on Bituminous Coarse Aggregate

url://http:tti/tamu.edu/documents/0-1707-10.pdf

16. Abstract

This report presents a specification-type test method to characterize the impact of fine aggregate and material filler on the complex nature of fatigue behavior of asphalt mixtures. Dynamic mechanical tests using the dynamic mechanical analyzer (DMA) were performed for cylindrical sand asphalt samples made with pure binders, modified binders, and mastics to estimate viscoelastic characteristics and fatigue behavior. Test results were analyzed using viscoelastic theories and fatigue prediction models based on continuum damage mechanics. The mechanical effects of additives were investigated. In addition, researchers identified a reasonable definition of fatigue failure. This DMA protocol can also be used to investigate the impact of moisture on the cohesive strength and damage resistance of the matrix and/or the fine aggregate matrix.

17. Key Words	18. Distribution Statement
Matrix, Mastic, Dynamic Mechanical Analyzer, Aggregate	No restrictions. This document is available to the public through NTIS: National Technical Information Service Springfield, Virginia 22161 http://www.ntis.gov

19. Security Classif.(of this report)	20. Security Classif.(of this page)	21. No. of Pages	22. Price
Unclassified	Unclassified	116	

DEVELOPMENT OF SPECIFICATION-TYPE TESTS TO ASSESS THE IMPACT OF FINE AGGREGATE AND MINERAL FILLER ON FATIGUE DAMAGE

by

Yong-Rak Kim
Graduate Research Assistant
Texas Transportation Institute

and

Dallas N. Little, Ph.D.
Senior Research Fellow
Texas Transportation Institute

Report 0-1707-10
Project 0-1707
Project Title: Long Term Research on Bituminous Coarse Aggregate

Performed in cooperation with the
Texas Department of Transportation
and the
Federal Highway Administration

July 2005

TEXAS TRANSPORTATION INSTITUTE
The Texas A&M University System
College Station, Texas 77843-3135

DISCLAIMER

The contents of this report reflect the views of the authors, who are responsible for the opinions, findings, and conclusions presented herein. The contents do not necessarily reflect the official views or policies of the Texas Department of Transportation (TxDOT) or the Federal Highway Administration (FHWA). This report does not constitute a standard, specification, or regulation. Additionally, this report is not intended for construction, bidding, or permit purposes. Dr. Dallas N. Little, P.E. (40392) is the principal investigator for the project.

ACKNOWLEDGEMENT

The authors wish to thank Ms. Caroline Herrera of the Construction Division of TxDOT for her guidance and support during this project. We also thank TxDOT and the FHWA for the cooperative sponsorship of this project.

TABLE OF CONTENTS

Page

TABLE OF CONTENTS (con't)

Page

LIST OF FIGURES

FIGURE Page

LIST OF FIGURES (Cont'd)

LIST OF FIGURES (Cont'd)

LIST OF FIGURES (Cont'd)

FIGURE Page

LIST OF FIGURES (Cont'd)

FIGURE Page

LIST OF TABLES

TABLE Page

CHAPTER 1. INTRODUCTION

A better understanding of fatigue behavior of asphalt mixtures is required to improve asphalt mixture design and hot mix performance. In project 0-1707, we are charged to investigate the impact of aggregate hot mix asphalt (HMA) performance. However, accurate prediction and evaluation of fatigue is a difficult task not only because of the complex nature of fatigue phenomena but also because fatigue testing is expensive and time-consuming. In 1992, the Strategic Highway Research Program (SHRP) considerably improved the understanding of fatigue behavior of asphalt mixtures; however, the development of a reasonable testing protocol for binders and mastic (combination of binder, filler, and entrapped air) remains a challenge. Recently, Anderson et al. examined binder fatigue performance using the dynamic shear rheometer (DSR) and concluded that the DSR is not suitable for characterizing the fatigue behavior because of unstable flow and edge fracture effects (2001). An appropriate fatigue test must allow one to monitor fatigue by observing how a material changes during the test, and failure must be based on a well-defined fatigue failure point.

In addition to the need for development of a reasonable fatigue testing method, the definition of fatigue life (the number of loading cycles to failure) has been a controversial issue. Recently, the popular and arbitrary failure criterion of 50 percent loss in stiffness or modulus from its initial value in controlled-strain tests has been questioned. Instead, other criteria based on changes in phase angle during fatigue testing as proposed by Reese (1997) or 50 percent loss in pseudo stiffness as proposed by Lee (1996), Kim et al. (1997), and Lee et al. (2000) may be more realistic criteria. Still other dissipated energy concepts, including reduced energy ratio, have been advocated in studies by Hopman et al. (1989), Rowe (1993), and Rowe and Bouldin (2000), and these are indeed promising and scientifically sound.

Based on a reasonable definition of fatigue failure, a fatigue life prediction model can be developed. In general, there are two main approaches: phenomenological and mechanistic. The phenomenological fatigue model is simple to use; however, it does not account for damage evolution throughout the fatigue process. On the other hand, mechanistic models are derived from fundamental principles of fracture mechanics or damage mechanics. The mechanistic approach is inherently more complex than the phenomenological approach but is more widely accepted because it is based on material properties and damage characteristics.

The quality of the binder and/or mastic influences fatigue damage and fracture of asphalt mixtures, since the fatigue damage initiates with cohesive and/or adhesive microcracking in the mastic. Because crack phenomena (cohesive and adhesive fracture) are governed substantially by properties of the binder and/or mastic, many researchers including Anderson and Goetz (1973) and Bahia et al. (1999) have studied binder

modification and mastic quality improvement. However, the synergistic mechanisms due to the addition of binder modifiers and fillers have not been fully understood.

PROBLEM STATEMENTS AND RESEARCH OBJECTIVES

Fatigue cracking in asphalt concrete pavements is considered one of four primary distresses, along with rutting, low-temperature cracking, and moisture damage. As discussed earlier, fatigue cracks initiate as microcracks and are followed by a crack propagation process including coalescence of the microcracks. Since microcracking is mostly governed by mastic properties, better prediction of mixture performance is possible if the fatigue behavior of the mastic is appropriately evaluated. A relatively accurate and repeatable testing methodology in assessing the fatigue behavior of mastics and/or binders is necessary. Successful development of the testing protocol can allow one:

- to understand fatigue behavior in asphalt mixtures more accurately using comprehensive investigation of fatigue performance;
- to define fatigue failure more reasonably;
- to understand the effects of the addition of fillers and/or modifiers; and
- to develop a better model for predicting fatigue performance.

Phenomenological approaches have been utilized to model damage-induced behavior, such as fatigue cracking, since phenomenological modeling is easy to do and simple to use. However, this type of modeling is not based on fundamental material characteristics and damage evolution; consequently, the phenomenological models are limited in use. Development of a mechanic-based damage model is necessary to predict damage evolution and overall structural behavior of asphalt mixtures.

The specific objective of this research was to develop a specification-type test capable of evaluating the import of the fine aggregate and mineral filler fraction of aggregate on fatigue damage in HMA.

RESEARCH METHODOLOGY

An organization chart illustrated in Figure 1 presents research methods used to meet the objectives of this study. A primary task was development of rapid, repeatable, and accurate mechanical tests to characterize constitutive relations and to assess fatigue damage of bitumen or mastic systems. The newly developed method used cylindrical sand asphalt mixtures under the strain-controlled mode to avoid unstable permanent deformation and to derive microcracks initially and coalescence of the microcracks eventually.

To meet the research objective, the material selection took into account:

- various compositional combinations of bitumen;
- bitumen modified with polymer additives;
- filled bitumen or mastics (especially with active fillers or those that demonstrate an interaction between the filler and the bitumen, i.e., hydrated lime); and
- bitumen with and without aging. The experimental design, which is based on the material selection, was established to define material-dependent mechanical characteristics and fatigue behavior.

Researchers performed two main categories of tests, including constitutive tests to determine linear viscoelastic material properties of sand asphalt mixtures and strain-controlled fatigue tests to evaluate fatigue damage resistance and healing potential. Linear viscoelastic material properties were determined by performing well-known constitutive tests, such as dynamic frequency sweep tests within the linear viscoelastic region. Long-time constitutive relations can be obtained by using the time-temperature superposition concept after performing tests at several different temperatures. In an attempt to evaluate fatigue damage, strain-controlled cyclic tests (time sweep mode) were performed at several strains at 25^{o}C and 10 Hz. Selected strain levels are high enough to develop fatigue damage. Stiffness reduction and phase angle change due to damage accumulation was monitored as the number of loading cycles increased. Based on comprehensive observation of the fatigue behavior of various sand asphalt mixtures, identification of the general fatigue phenomenon and a reasonable definition of fatigue failure were made. Material-dependent fatigue behavior was also investigated. Hysteretic stresses and strains at each loading cycle were measured to quantify the fatigue damage using nonlinear viscoelastic theory.

Researchers performed mechanical analyses of test data for both non-damaged and damaged behavior. Time-dependent linear viscoelastic material properties of sand asphalt mixtures were identified to understand fundamental material characteristics. Effects of filler addition and binder modification on the mechanical behavior of neat materials were evaluated by monitoring the viscoelastic material properties.

The research team performed stress analyses of damage-induced fatigue behavior by employing Schapery's nonlinear viscoelastic model (1984). Schapery proposed the extended elastic-viscoelastic correspondence principle, which is applicable to both linear and nonlinear viscoelastic materials. Based on pseudo variable concepts, the extended correspondence principle separates the linear viscoelastic relaxation mechanism from damage accumulation in viscoelastic materials. Specimens that experience significant damage typically deviate from the linear stress – pseudo strain domain. The deviation can be identified by synergistic nonlinearities, and it is hypothesized that structural damage is the most dominant factor causing nonlinearity. Damage accumulation was demonstrated by observing the stress – pseudo strain behavior during fatigue testing. This analytical technique was applied to fatigue testing data to assess each material's fatigue resistance.

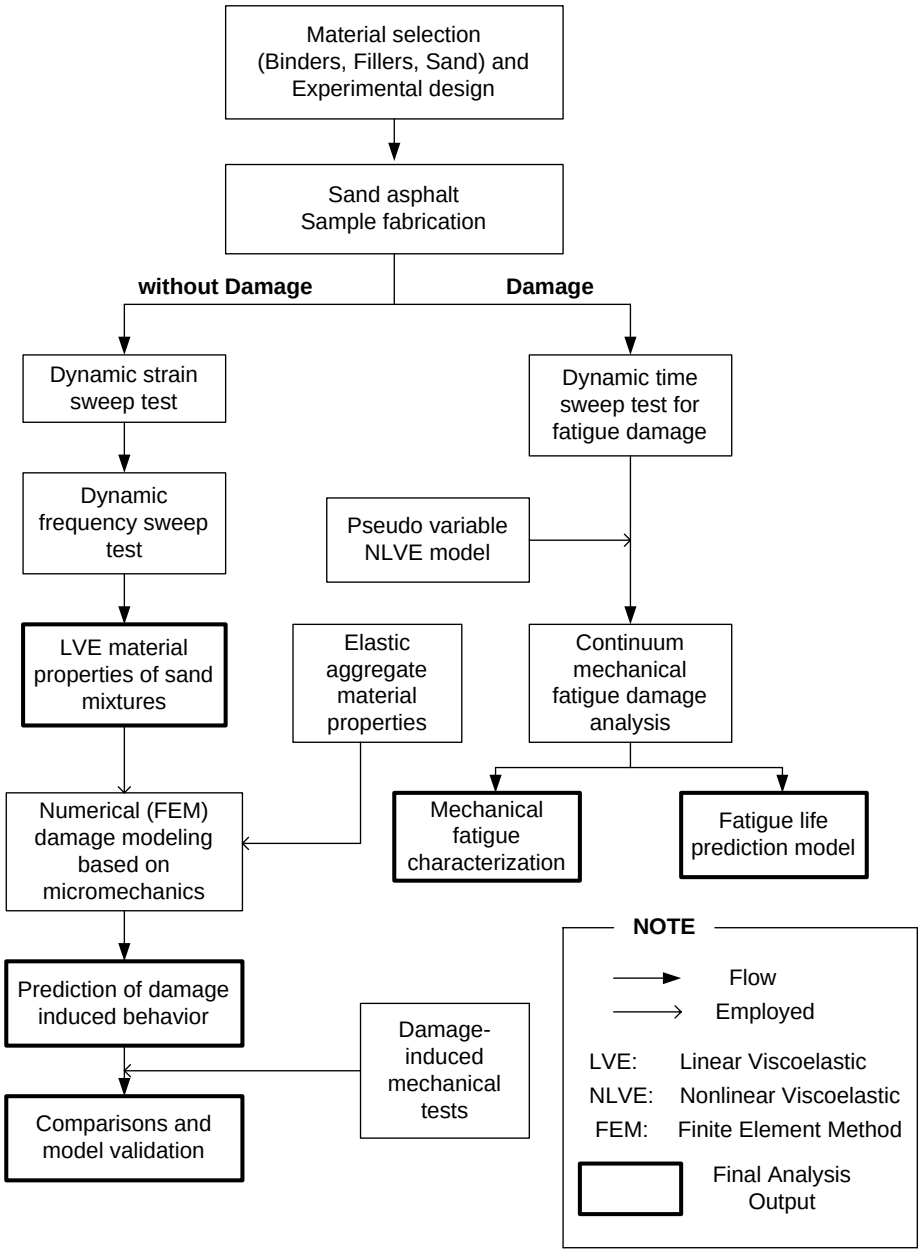

Figure 1. Organization Chart Describing Research Methodology.

In addition, the pseudo variable nonlinear viscoelastic theory was incorporated with the analytical continuum damage mechanics and work potential theory. Park (1994) and Lee (1996) have applied the technique for multiaxial viscoelastic bars and uniaxial asphalt concrete samples, respectively, to develop continuum damage mechanical models. In particular, Lee et al. developed a fatigue performance prediction model of asphalt concrete under uniaxial cyclic loading (2000). A fatigue life prediction model for this study was achieved based on modification of the original model by Lee et al. (2000). Newly defined fatigue failure criteria and a different mode of loading condition were taken into account in this study.

ORGANIZATION OF THE REPORT

This report is composed of seven chapters. Following this introduction, Chapter II describes newly developed testing methods to determine fundamental viscoelastic material properties and fatigue damage characteristics of asphalt binders and mastics. The initial testing protocol developed by Kim and Little is discussed in detail in the chapter. Selected materials used to validate the approach and background associated with the material selection are presented in Chapter III. A description of laboratory testing and representative testing results are presented in Chapter IV. Based on theories presented in Chapter II, Chapter V shows mechanical data analyses for the results with and without damage. Effects of additives (filler and/or polymer), and material aging on fundamental material characteristics and damage behavior are discussed in this chapter using the theory of viscoelasticity and continuum damage mechanics. Chapter VI describes a method developed to evaluate moisture damage in dynamic mechanical analysis (DMA) experiments. Chapter VII describes the evolution of the DMA method to not only consider the bitumen or mastic but also different fine aggregate (smaller than about the No. 16 sieve). Chapter VII describes the work done by Zollinger to validate the approach (2005). Finally, Chapter VIII provides a summary of findings and conclusions of the study. Recommendations for future research are also presented in this chapter.

CHAPTER 2. DEVELOPMENT OF TESTING METHODS

Fatigue damage and fracture initiates with cohesive and/or adhesive microcracking and propagates as the microcracks grow and coalesce. Since crack phenomena (cohesive and adhesive fracture) are governed substantially by properties of the mastic, mixture performance can be improved if the mastic is engineered to resist fracture and fatigue. Furthermore, several studies by Kim (1988), Kim et al. (1990, 1994, and 1995), and Bahia et al. (1999) have shown that microcracks heal during rest periods. In particular, Bahia et al. showed significant effects of rest periods on fatigue damage recovery in dynamic shear rheometer tests using various binders. The general findings from those studies are that fatigue damage and healing potential are strongly related to binder characteristics, additive properties in the binder, interaction between the binder and additives, and various phenomenon that affect microcrack development and growth in the mastic. Many researchers including Soenen and Eckmann (2000), Anderson et al. (2001), and Bonnetti et al. (2002) have used DSR to evaluate fatigue behavior of binders and mastics. However, DSR is not suitable for characterizing the fatigue behavior because of unstable flow and edge fracture effects at intermediate (realistic fatigue performance) temperatures such as 25°C. This fact was demonstrated in a study by Anderson et al. (2001). For this reason, the development of a reasonable testing protocol for binders and mastics is required. An appropriate fatigue test must allow one to monitor fatigue by observing how a material changes during the test, and failure must be based on a well-defined fatigue failure point.

This chapter presents a testing instrument and methods to replace the DSR fatigue tests. The current approach is expected to be suitable to monitor fatigue damage, starting with microcracks, as well as fundamental material characteristics of binders and mastics. Linear and/or nonlinear viscoelastic theories associated with testing data are also presented to perform stress analyses.

DYNAMIC MECHANICAL ANALYZER

To derive reasonable fatigue cracks and to measure fatigue damage, a dynamic mechanical analyzer, RMS-800/RDS-II of Rheometrics, Inc., was employed. The DMA was originally intended to be used as a mechanical test system for evaluating viscoelastic properties of materials, especially polymers. The materials can be in solid, melt, or liquid state. The DMA system consists of three main components: a test station, a system controller, and control computers. An environmental controller is optionally used for temperature control. The environmental controller provides low temperatures down to –150°C using liquid nitrogen and high temperatures up to 600°C using a controlled electric heater. The DMA setup is shown in Figure 2.

Figure 2. Dynamic Mechanical Analyzer.

The impetus for the DMA testing of asphalt was originally from work performed by Goodrich (1988, 1991), Christensen and Anderson (1992), and Smith and Hesp (2000). Specifically, Smith and Hesp demonstrated that controlled-strain testing of mastics in a DMA leads to a controlled rate of microcrack development and growth, whereas controlled-stress testing would lead to rapid and uncontrolled crack growth (2000). Differences between the current study and those studies include the sample geometry used, the sample composition, and the loading sequence (including rest periods). A cylindrical rather than a rectangular sample was adopted in an attempt to avoid complex stress distribution in the samples and to make calculation easier. Rectangular samples have been the typical testing geometry for DMA. Sand asphalt mixtures were employed so that samples could be tested at an intermediate temperature to minimize unstable plastic flow. A sample holder capable of properly securing the cylindrical sample was developed. Epoxy glue was used to secure the sand asphalt sample to the holder. In the gluing process, care was taken not to cause any undesirable stress concentrations. Figure 3 shows a schematic diagram of the cylindrical DMA sample with holders. Each sample was mounted in the DMA instrument, and the chamber was closed and allowed to equilibrate to the desired testing temperature. All tests were started after at least a 20-minute equilibration period at the test temperature. Figure 4 shows the cylindrical sand asphalt sample configuration installed in the DMA.

The DMA machine measures resisting torque of a sample due to sinusoidal displacement-controlled rotational input. According to a study by Reese, torsional loading is a better simulation of damage than bending loads when considering traffic movements(1997). Test data (applied displacement and corresponding torque response) were collected by a data acquisition (DAQ) system with a 16-bit multichannel board.

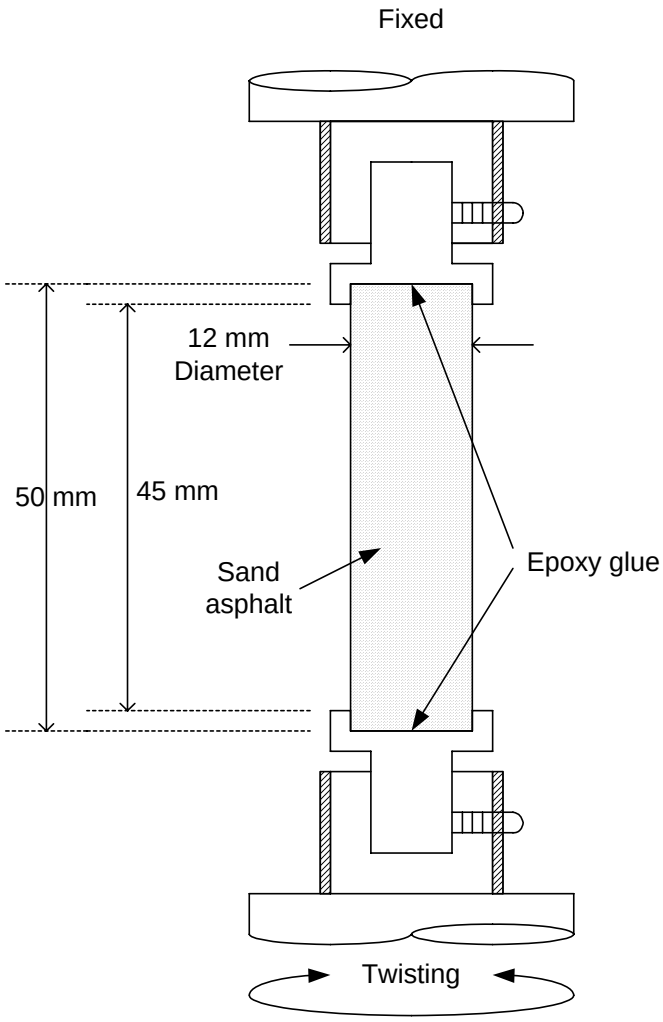

Figure 3. Schematic Diagram of the Cylindrical DMA Sample with Holders.

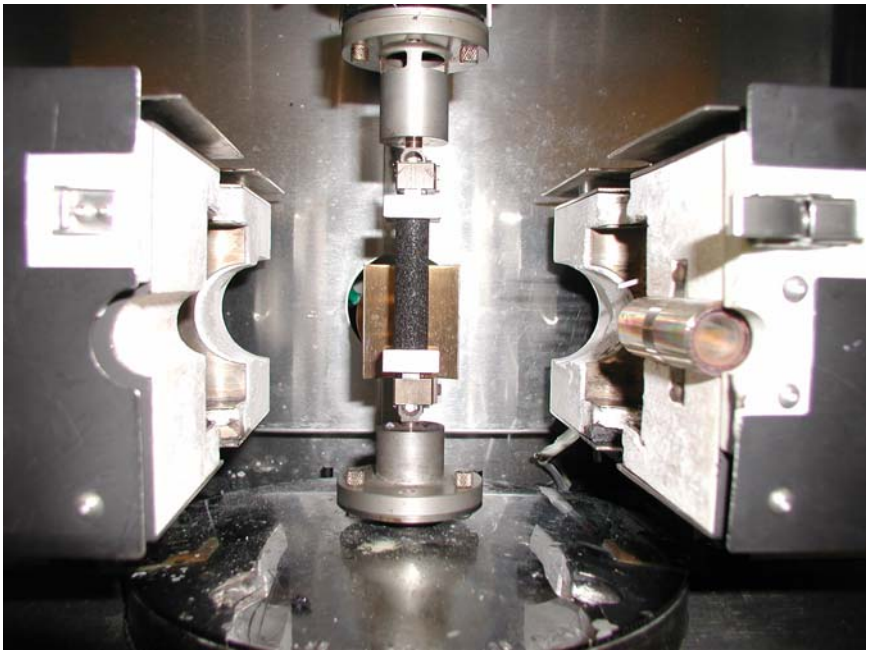

Figure 4. Cylindrical Sand Asphalt Sample Installed in the DMA.

VISCOELASTIC STRESS ANALYSIS OF TORSIONAL CIRCULAR BARS

Figure 5 simply illustrates a sand asphalt sample installed in the DMA. The solid circular sand asphalt sample of length L and constant radius R is subjected to a twisting moment (torque) T, so as to produce a prescribed angle of twist φ. For a viscoelastic material, this problem can be treated by an approximate method to solve for the torque and stress distribution as a function of time resulting from the prescribed angle of twist. Equilibrium equations governing the problem are automatically satisfied because the problem is statically determinate.

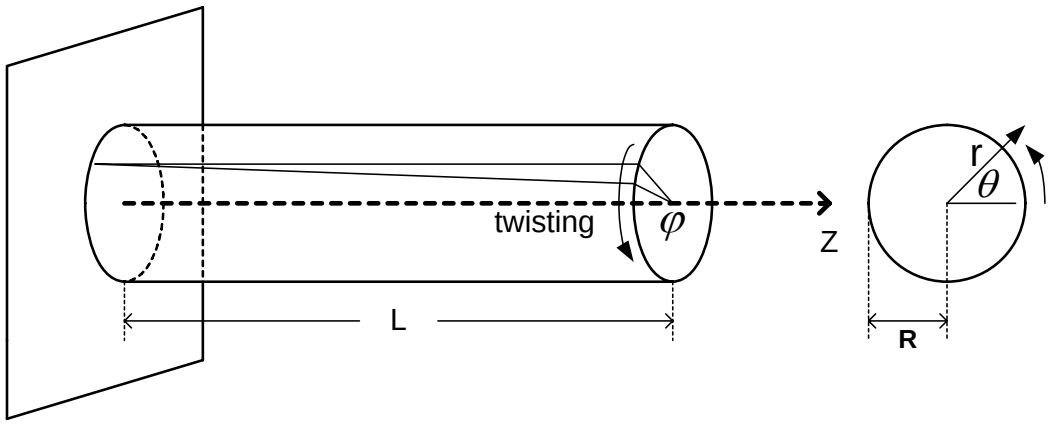

Figure 5. Simple Illustration of the Cylindrical Bar under Torsion.

Displacement of a general point can be reasonably expressed as a tangential direction displacement, u_θ, in cylindrical coordinates r, θ, z:

$$u_\theta(t) = \Theta(t) r z \tag{1}$$

Where $\Theta(t) = \dfrac{\varphi(t)}{L}$ = angle of twist per unit length. (2)

The only valid strain-displacement relationship considering the tangential displacement, u_θ, is given by:

$$\gamma(t) = \frac{\partial u_\theta(t)}{\partial z} + \frac{1}{r}\frac{\partial u_z(t)}{\partial \theta} \tag{3}$$

Where $\gamma(t)$ = shear strain as a function of time.

It should be noted that the second term in Equation 3 is negligible, because vertical displacement $u_z(t)$ is assumed to be zero. If the material is isothermal linear viscoelastic, the constitutive equation in terms of a convolution integral is given as follows:

$$\tau(t) = \int_0^t G(t-\xi)\frac{\partial \gamma}{\partial \xi} d\xi \tag{4}$$

$$\gamma(t) = \int_0^t J(t-\xi)\frac{\partial \tau}{\partial \xi} d\xi \tag{5}$$

Where $\tau(t)$ = time-dependent shear stress,
$\gamma(t)$ = time-dependent shear strain,
$G(t)$ = shear relaxation modulus,
$J(t)$ = shear creep compliance,
t = time of interest, and
ξ = time-history integration variable.

The torque $T(t)$ required to maintain a constant angle of twist $\Theta(t)$ can be calculated as follows by summing the moment of tangential force increments over the cross-sectional area:

$$T(t) = \int_0^{2\pi}\int_0^r r\,\tau(t) r dr d\theta \tag{6}$$

It should be noted that the shear stress in Equation 6 is not necessarily linear viscoelastic. Equation 6 can be expressed in the following simple form:

$$\tau(t) = \frac{T(t)}{J} r \tag{7}$$

Where $J = \int_0^{2\pi}\int_0^r r^3 dr d\theta$ = polar moment of inertia. (8)

Substituting Equation 1 into Equation 3 yields shear strain resulting from the displacement measurements:

$$\gamma(t) = \frac{\varphi(t)}{L} r \tag{9}$$

With the displacement function $\varphi(t)$, linear viscoelastic material property $G(t)$, and sample geometry, corresponding shear stress and shear strain as a function of time can be calculated by Equations 4 and 9. Alternatively, the shear stress can also be determined by Equation 7, when the resisting torque is measured. Given measurements of the displacement and torque, the linear viscoelastic material property is identified based on the constitutive relation, and viscoelastic stress analyses can be conducted

analytically and/or numerically. The DMA instrument typically requires an oscillatory twisting displacement as input and provides resisting transducer torque responses.

Under dynamic loading conditions, viscoelastic materials normally produce frequency-domain dynamic properties such as storage modulus, loss modulus, and the phase angle between stress and strain due to time-dependency. The combined form of the storage and loss properties reduces to a complex modulus and a dynamic modulus:

$$\left|G^*(\omega)\right| = \sqrt{\left[G'(\omega)\right]^2 + \left[G''(\omega)\right]^2} \tag{10}$$

$$G^*(\omega) = G'(\omega) + iG''(\omega) \tag{11}$$

$$\phi(\omega) = \tan^{-1}\left[\frac{G''(\omega)}{G'(\omega)}\right] \tag{12}$$

Where $\left|G^*(\omega)\right|$ = dynamic shear modulus,

$G^*(\omega)$ = complex shear modulus,

$G'(\omega)$ = storage shear modulus,

$G''(\omega)$ = loss shear modulus,

$\phi(\omega)$ = phase angle,

ω = angular frequency, and

$i = \sqrt{-1}$.

The shear stress-shear strain relation under the sinusoidal harmonic dynamic loading condition can be represented by:

$$\tau(t) = G^*(\omega)\gamma(t) \tag{13}$$

The relaxation modulus as a function of time can be determined by static creep, static relaxation, and/or dynamic frequency sweep tests within the linear viscoelastic region. Because DMA usually employs dynamic loading, such as oscillatory vibration, the dynamic frequency sweep tests are performed to determine the linear viscoelastic relaxation behavior of materials. This is based on the theory of linear viscoelasticity inferring correspondence between frequency-domain and time-domain.

Data plots of the linear viscoelastic modulus and frequency require a curve-fitting function to be used in determining the linear viscoelastic relaxation modulus. Among many candidate models, the generalized Maxwell model, which is shown in Figure 6, is frequently used because it fits the data more precisely and provides better efficiency in mathematical implementation than other models. Mathematical expression of the

generalized Maxwell model is typically called a Prony series. Prony series representations (Christensen, 1982) of storage and loss modulus as a function of frequency are presented in Equations14 and15 as follows:

$$G'(\omega) = G_{\infty} + \sum_{i=1}^{n} \frac{G_i \omega^2 \rho_i^{\,2}}{\omega^2 \rho_i^{\,2} + 1} \tag{14}$$

$$G''(\omega) = \sum_{i=1}^{n} \frac{G_i \omega \rho_i}{\omega^2 \rho_i^{\,2} + 1} \tag{15}$$

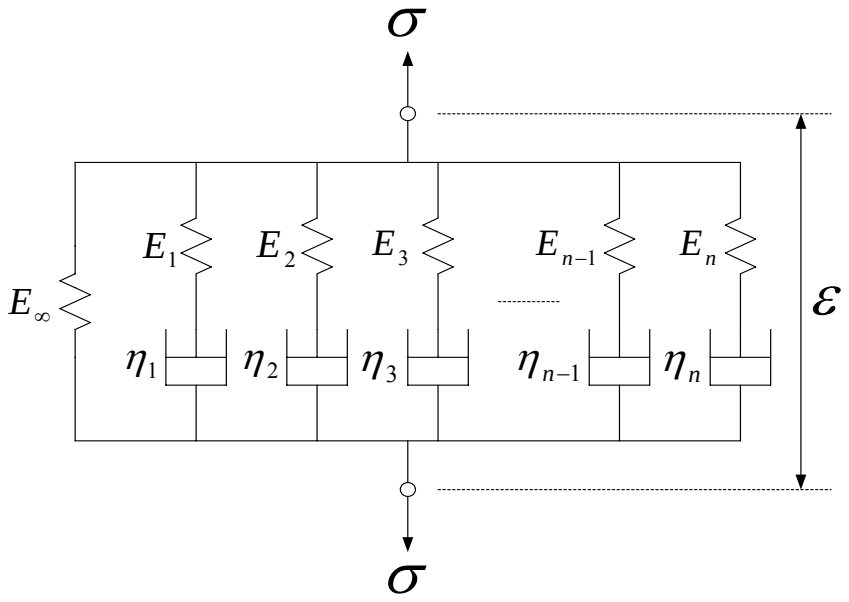

Figure 6. Generalized Maxwell Model Analog for Viscoelastic Relaxation.

The regression constants in Equations 14 or 15 can be determined by a so-called collocation method that is a matching procedure between the measured data and the analytical representation at several collocation points. More detailed information on the collocation method is given by Huang (1993).

Given parameters from a Prony series representation determined from the dynamic frequency sweep test, static relaxation modulus as a function of time can be illustrated by Equation 16. The static relaxation modulus is easily formulated by using

the same Prony series material parameters G_∞, G_i, and ρ_i, which are determined from linear viscoelastic dynamic frequency sweep testing.

$$G(t) = G_\infty + \sum_{i=1}^{n} G_i e^{-\frac{t}{\rho_i}} \tag{16}$$

As discussed, the dynamic shear modulus is defined as an absolute value of the complex shear modulus. However, in typical DMA testing, the dynamic shear modulus is determined by monitoring the ratio of the peak stress to the peak strain at each cycle, as shown in Equation 17:

$$\left|G^*\right| = \frac{\tau_0}{\gamma_0} \tag{17}$$

Where $\left|G^*\right|$ = dynamic shear modulus,

τ_0 = peak stress measured at each cycle, and

γ_0 = applied cyclic strain amplitude.

Equation 17 can be defined in both linear and nonlinear viscoelastic behavior. The linear viscoelastic dynamic modulus is determined by measuring peak stress and peak strain within the linear viscoelastic region. If the material is behaving in a nonlinear viscoelastic manner due to damage, nonlinear moduli can be introduced. As Golden et al. presented, a nonlinear complex modulus may be written as (1999):

$$G^*_{NL} = \frac{\tau_0}{\gamma_0} e^{i\delta} \tag{18}$$

Where G^*_{NL} = nonlinear complex shear modulus, and

δ = nonlinear viscoelastic phase angle.

With the nonlinear complex shear modulus (Equation 18), the nonlinear storage, loss, and dynamic moduli are, respectively, as follows:

$$G'_{NL} = \frac{\tau_0}{\gamma_0} \cos\delta \tag{19}$$

$$G''_{NL} = \frac{\tau_0}{\gamma_0} \sin\delta \tag{20}$$

$$\left|G_{NL}^{*}\right| \equiv \sqrt{\left[G_{NL}^{'}\right]^2 + \left[G_{NL}^{''}\right]^2} = \frac{\tau_0}{\gamma_0} \tag{21}$$

Where $G_{NL}^{'}$ = nonlinear storage shear modulus,

$G_{NL}^{''}$ = nonlinear loss shear modulus, and

$\left|G_{NL}^{*}\right|$ = nonlinear dynamic shear modulus.

Once the linear viscoelastic relaxation modulus is defined, Schapery's extended elastic-viscoelastic correspondence principle based on pseudo variables can be employed to evaluate damage-induced nonlinear viscoelastic behavior (1984). Schapery stated that constitutive equations for certain viscoelastic media are identical to those for the elastic cases, but stresses and strains are not necessarily physical quantities in the viscoelastic body. Instead, they are pseudo variables.

Assuming that Poisson's ratio is independent of time, torsional shear pseudo strain under the pure shear condition is written as (Schapery, 1974):

$$\gamma^R(t) \equiv \frac{1}{G_R}\int_0^t G(t-\xi)\frac{\partial \gamma}{\partial \xi}d\xi \tag{22}$$

Where $\gamma^R(t)$ = pseudo strain in the shear mode, and

G_R = reference shear modulus that is an arbitrary constant.

As shown in Equation 22, the calculation of pseudo strain can be performed by presenting the relaxation modulus and the strain as analytical functions of time and integrating the product of these functions. With the use of the definition of pseudo strain in Equation 22, Equation 4 can be rewritten as follows:

$$\tau(t) = G_R\gamma^R(t) \tag{23}$$

The extended correspondence principle separates the viscoelastic relaxation mechanism from damage accumulation in viscoelastic materials. Specimens that experience significant damage exhibit hysteretic loops when plotted in the stress – pseudo strain domain. Damage accumulation can be demonstrated by observing changes in the loop area and loop chord-slope during mechanical tests, such as fatigue testing.

In an attempt to quantify damage accumulation, Kim et al. (1994, 1995) introduced a simple damage parameter, pseudo stiffness, S^R:

$$S^R = \frac{\tau_m}{\gamma_m^R} \tag{24}$$

Where S^R = pseudo stiffness,
γ_m^R = maximum pseudo strain in each physical stress-pseudo strain cycle, and
τ_m = physical stress corresponding to γ_m^R.

The analytical harmonic representation of the twisting displacement at time t under the zero means the cyclic displacement condition can be expressed as:

$$\varphi(t) = \varphi_o \sin(\omega t + \psi) H(t) \tag{25}$$

Where φ_o = twisting amplitude of the sinusoidal vibration,
ω = angular velocity,
ψ = regression constant, and
$H(t)$ = Heaviside step function.

The regression constant is necessary to match the analytical functions of displacement history with measured displacement data at the same loading time. Substituting Equation 25 into Equation 9 yields the respective oscillatory shear strain history at time t:

$$\gamma(t) = \frac{\varphi_0 r}{L} \sin(\omega t + \psi) H(t) \tag{26}$$

$$\frac{\varphi_0 r}{L} = \gamma_0$$

Where γ_0 = shear strain amplitude.

Substituting Equation 26 in the definition of pseudo strain, Equation 22, analytically yields the respective pseudo strain at time t as:

$$\gamma^R(t) = \frac{1}{G_R}\left[\gamma_0 \left|G^*(\omega)\right| \sin(\omega t + \psi + \phi)\right] \tag{27}$$

Where $\left|G^*(\omega)\right|$ = linear viscoelastic dynamic modulus in shear mode, and
ϕ = linear viscoelastic phase angle.

This shear pseudo strain calculation requires knowledge of linear viscoelastic dynamic shear modulus and phase angle. These mechanical properties can be determined from constitutive testing, such as DMA dynamic frequency sweep testing. Therefore, pseudo strain at any time can be easily predicted with a well-defined strain history as a function of time and two linear viscoelastic material properties: dynamic modulus and phase angle.

In the study of fatigue, only the peak pseudo strain within each cycle is typically used. The pseudo strain reaches the peak pseudo strain in each cycle when the sine function in Equation 27 becomes 1. By assuming the value of the reference shear modulus, G_R to be unity, Equation 27 can be rewritten as:

$$\gamma_m^R = \gamma_0 \left| G^*(\omega) \right| \tag{28}$$

Where γ_m^R = peak pseudo strain in each cycle.

Thus, the peak pseudo strain at any loading cycle can be easily obtained whenever the linear viscoelastic dynamic modulus and the strain amplitude are known.

CHAPTER 3. MATERIALS AND SAMPLE FABRICATION

This chapter presents selected materials for this study and the background associated with the material selection. Then, procedures of sample fabrication are briefly described. Cylindrical sand asphalt samples installed in the dynamic mechanical analyzer were fabricated to estimate fatigue damage, including viscoelastic material characteristics. A newly developed fabrication technique of the sand asphalt samples is presented.

MATERIALS

Researchers selected two SHRP-classified neat binders, AAD-1 and AAM-1, because of their very different compositions showing a wide range of aromatics, amphoterics, and wax contents. Little et al. demonstrated that the binders AAD-1 and AAM-1 showed the greatest difference among various SHRP-classified binders in terms of fracture and healing characteristics (1999). They found that fracture and healing are both related to surface energy (cohesive and adhesive, depending on the proximity of the crack) through fundamental principles of viscoelastic fracture mechanics. The experimental results demonstrated an inverse relationship between the healing potential and Lifshitz-Van der Waals surface energy and a direct relationship between the healing potential and acid-base surface energy. Binder AAM-1 has a higher acid-base and much lower Lifshitz-Van der Waals surface energy than AAD-1. The selection of the binders AAD-1 and AAM-1 is based on the fact that the two distinct, compositionally different asphalt binders will show significantly sensitive behavior to fracture and healing. Table 1 shows rheological properties and compositional characteristics of binders AAD-1 and AAM-1 (Moulthrop, 1990; Little et al., 1998).

Table 1. Rheological Properties and Compositional Characteristics of Binder AAD-1 and AAM-1 (Moulthrop, 1990; Little et al., 1998).

		AAD-1	AAM-1
Rheological Properties			
Viscosity of Original Binder	60°C, poise	1055	1992
	135°C, cSt	309	569
Viscosity after RTFO[1] Aging	60°C, poise	3420	3947
	135°C, cSt	511	744
Penetration of Original Binder	25°C, dmm	135	64
	4°C, dmm	9	4
Compositional Characteristics			
Amphoteric Content		High	Low
Aromatic Content		Low	Low
Wax Content		Low	High

Note
RTFO[1]: Rolling Thin Film Oven

Many experimental results demonstrate the substantial influence of binder modification on asphalt mixtures. Polymer additives have shown the ability to change the microstructure, morphology, and fracture mechanisms that occur in asphalt binders. A series of studies by Shin et al. (1996) and Bhurke et al. (1997) demonstrated that the fracture morphology of asphalt concrete is highly dependent on the morphology of the binder. They observed a network structure of various polymer-modified binders in thin asphalt binder films and correlated the network structural characteristics to fracture toughness. Hui et al. (1994) and Lee and Hesp (1994) demonstrated that rubber-modified or polyethylene-modified binders improve low temperature fracture performance, and that greater toughening occurs with more finely dispersed polymers and with greater compatibility at the interface between the polymer and binder. Recently, Bahia et al. presented the effects of binder modification by assessing nonlinear viscoelastic and fatigue properties of various polymer-modified binders based on testing results using DSR (1999). They found

that both strain dependency and fatigue are highly sensitive to the composition of binders, type of additive, temperature, aging, and interactions of these factors.

In an attempt to evaluate physical/mechanical effects of binder modification on fracture fatigue, several different polymer-modified binders and one particular fabricated rubber particle modified binder was selected. All the polymer-modified binders are combinations of the two unmodified binders, BASE and FLUX. Polymer addition was achieved through high shear blending. The binder combinations and the percentage of modifier are shown in Table 2. The base material for the rubber particle modified binder was originally soft with a low viscosity. The viscosity increased considerably after air blowing and some light component evaporation. The air blown modified binder was then blended with 12 percent (by weight) of rubber particles at 260^{o}C while stirring at 1600 rpm for three hours. Since the blend is composed of a high rubber content cured at a relatively high temperature with a high-shear mixer, the generic term, high cure rubber (HCR) is used.

Furthermore, the HCR binder was aged at two different levels to investigate effects of material aging on damage and healing characteristics. A 1-mm thick HCR binder film in a tray was stored in a 60^{o}C environmentally controlled room for three months and six months, respectively. It is assumed that one month of aging in the laboratory is equivalent to one year in the field. Thus, three months and six months laboratory aging are equivalent to three and six years of field aging, respectively. A detailed description of HCR binder fabrication and the aging process can be found elsewhere (Glover et al., 2000).

Table 2. Binder Combinations and Percentage of Modifier.

Binder	Binder Combinations	% of Modifier
BASE	Unmodified	
AirBlown	100% FLUX	
SBS-LG	58.9% FLUX 41.1% BASE	3.75
EVA	100% FLUX	5.5
ELVALOY	50% FLUX 50% BASE	2.2

In addition to the significant effects from binder modification with polymeric materials, mineral fillers also play a major role in the behavior of the asphalt mixtures, and it is the primary focus of the project 0-1707 to investigate the role of the mineral filler. The importance of fillers in asphalt mixtures has been studied extensively by Anderson and Goetz (1973), Anderson (1987), Harris and Stuart (1995), Kavussi and Hicks (1997), Cooley et al. (1998), and many others. Fillers fill voids between coarse aggregates in the mixture and alter properties of the binder because the filler acts as an integral part of the mastic (combination of bitumen, filler, and entrapped air). The quality of the mastic influences the overall mechanical performance of asphalt mixtures as well as placement workability. An interactive physico-chemical effect between the filler and the binder related to the fineness and surface characteristics of the filler typically influences fatigue fracture characteristics. According to a study by Craus et al., the physico-chemical aspect is related to adsorption intensity at the filler-binder interface, and higher surface activity significantly contributes to stronger bonds at the filler-binder interface (1978). It can be inferred that the interactive role associated with the physico-chemical reaction is influenced by the type of binder and filler as well. Lesueur and Little demonstrated that hydrated lime reacts quite differently as a filler with asphalt AAD-1 than with asphalt AAM-1 (1999). They hypothesized that hydrated lime interacts with some of the plentiful polar components of AAD-1 but is relatively inert in the well-dispersed AAM-1. The different interactions between hydrated lime and asphalt have subsequently been documented by Hopman et al. (1999) and Buttlar et al. (1999). Based on these findings, two fillers (limestone and hydrated lime) were selected to assess the filler effect for this study. Figure 7 presents the particle size distribution of each filler. Geometric characteristics of the filler particles were inspected using the environmental scanning electron microscope (ESEM). Figures 8 and 9 demonstrate that both limestone and hydrated lime particles show geometric irregularity in surface texture and non-spherical shape.

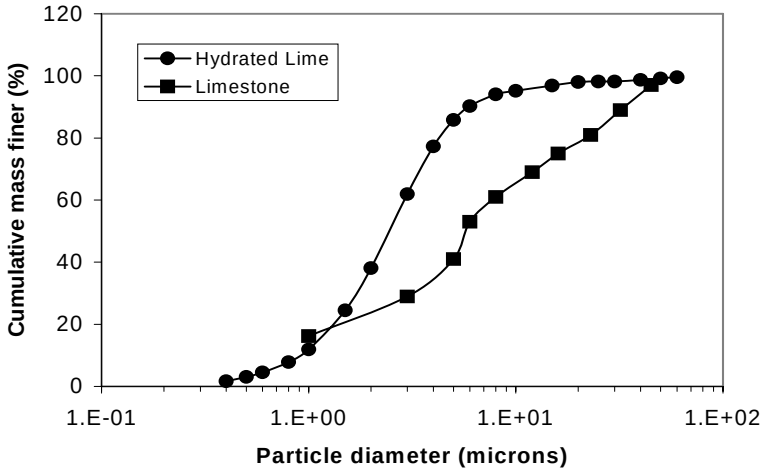

Figure 7. Particle Size Distribution of Each Filler.

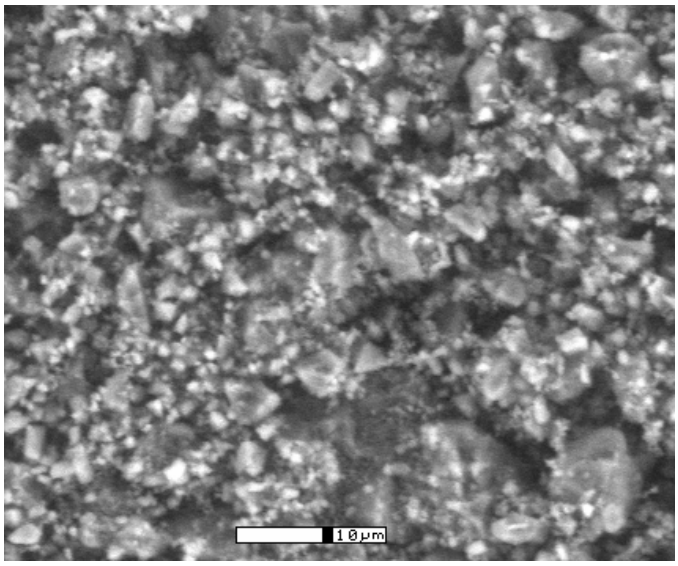

Figure 8. Environmental Scanning Electron Microscopy Image of Limestone Filler.

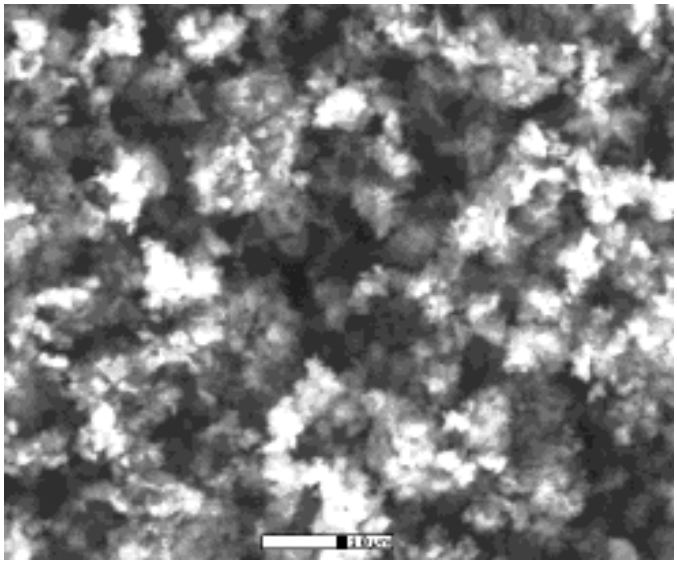

Figure 9. Environmental Scanning Electron Microscopy Image of Hydrated Lime.

As mentioned in previous chapters, this study employed cylindrical sand asphalt mixtures installed in the DMA instrument. Each binder and mastic was mixed with Ottawa sand to form the sand asphalt. Ottawa sand is a relatively clean and uniformly graded aggregate, as shown in Figure 10. Approximately 70 percent sand particles are within #30 sieve (0.6 mm mesh size) to #50 sieve (0.3 mm mesh size). The selected Ottawa sand satisfied the particle gradation required for standard sand (ASTM C 778-99). Table 3 summarizes all selected materials for this study.

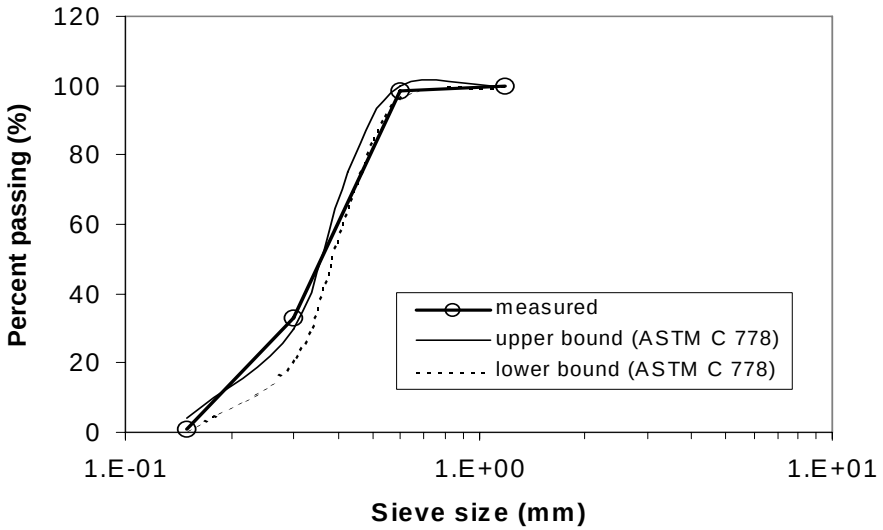

Figure 10. Gradation of Ottawa Sand and Upper and Lower Bound Required for Standard Sand.

Table.3. Summary of Selected Materials.

Material Category	Material Selected	Remarks
Neat Binder	AAD-1	SHRP binder
	AAM-1	SHRP binder
	BASE	One of two unmodified binders (BASE and FLUX)
Modified Binder	AirBlown	Modified by air blowing
	SBS-LG	Styrene-Butadiene-Styrene (Linear-Grafted)
	EVA	Ethylene-Vinyl-Acetate
	ELVALOY	Particularly fabricated binder
	HCR	High cure crumb rubber modified binder
Binder Conditioning	Unaged	Two different levels of aging were simulated for the HCR
	Aged	
Fillers	Limestone	Control filler
	Hydrated Lime	Active filler
Aggregate	Ottawa Sand	Clean standard sand

SAMPLE FABRICATION

Each binder and mastic was mixed with Ottawa sand to form a sand asphalt mixture. Eight percent binder by weight of dry sand was mixed and compacted at pre-determined mixing and compaction temperatures. The 8-percent asphalt content was selected as a reasonable arbitrary value to provide an average "film thickness" of approximately 10 microns. The term "film thickness" is used with the understanding that it is a controversial term. The mixing and compaction temperatures were determined by using the rotational viscometer according to ASTM D 4402.

Each loose sand asphalt mixture was compacted in a specially fabricated mold, as shown in Figure 11. The inside area of the mold was machined to produce a smooth surface on the compacted sample without significant flaws. This treatment helps obtain repeatable test results because the smooth surface is an important factor in minimizing random behavior in terms of fatigue crack initiation and propagation in the torsional

loading mode. The 11.5 grams of loose sand asphalt was determined by trial and error as the required mass for one sample, and the compacting mold was designed to produce a cylinder 50-mm long with a 12-mm diameter. A 30-minute cooling period was employed to facilitate specimen removal from the mold without undue distortion.

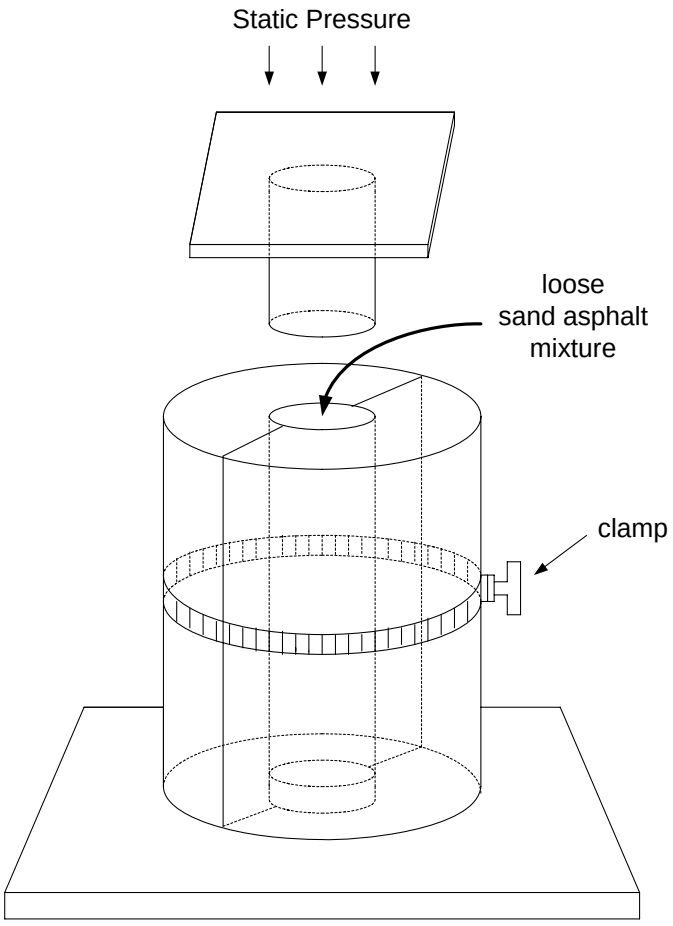

Figure 11. Compaction Mold Assembly for Sand Asphalt Sample Fabrication.

CHAPTER 4. LABORATORY TESTING AND RESULTS

In this chapter, representative results are described to show general behavior from the laboratory experiments. Various dynamic mechanical tests using the dynamic mechanical analyzer were performed for cylindrical sand asphalt samples mixed with pure binders and/or mastics to estimate viscoelastic characteristics and fatigue behavior. More comprehensive discussion and data analyses are presented in Chapter V.

DYNAMIC MECHANICAL ANALYZER TESTING

Three different tests—dynamic strain sweep, dynamic frequency sweep, and dynamic time sweep—were conducted on sand asphalt specimens in the displacement-controlled torsional shear mode. Figure 12 illustrates each DMA testing scheme. The torsional shear strain sweep test was performed to determine strain levels that satisfy the homogeneity principle of linear viscoelasticity. Dynamic strains beginning at 0.0065 percent were applied on replicate samples, and corresponding values of shear modulus were monitored, as shown in Figure 13. Since strain dependency is a function of temperature and frequency, strain sweep tests were performed at different temperatures and frequencies, as shown in Figure 13. Any strain can be selected for constitutive testing, such as dynamic frequency sweep testing, as the strain is within the linear viscoelastic region over a specified range of temperature and frequency. Table 4 presents linear viscoelastic dynamic shear moduli at three different frequencies (0.1, 1.59, and 10 Hz) and at 25°C determined from the torsional shear strain sweep test.

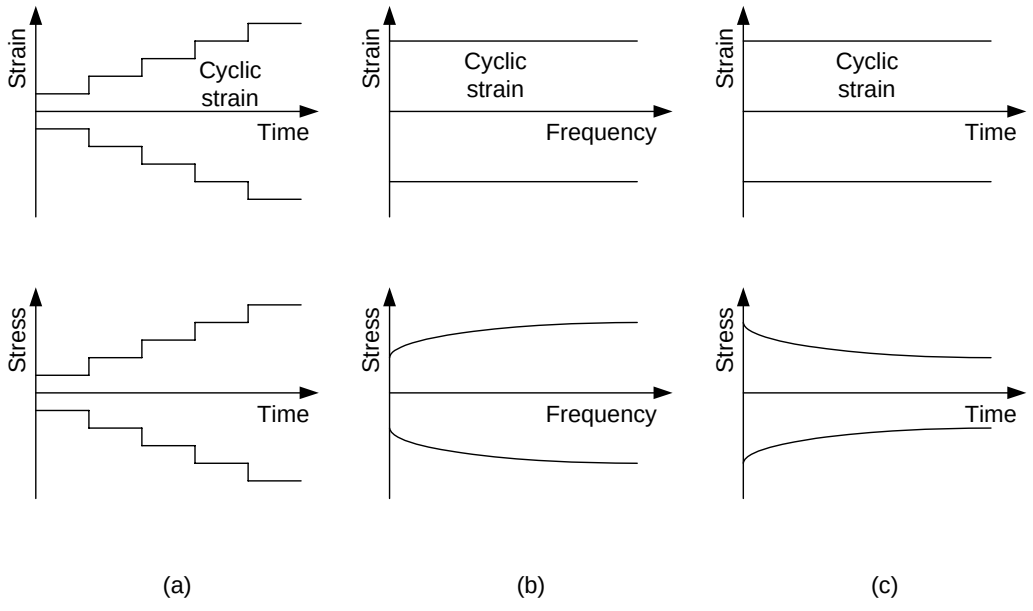

Figure 12. DMA Testing Schemes: (a) Dynamic Strain Sweep Test, (b) Dynamic Frequency Sweep Test, (c) Dynamic Time Sweep Test.

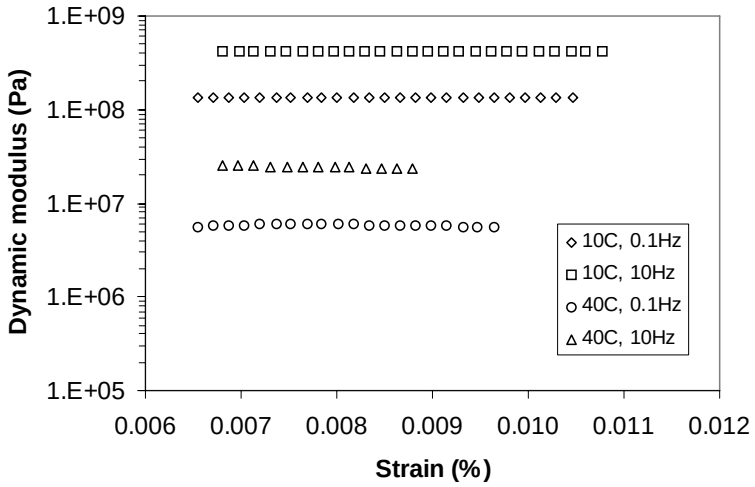

Figure 13. Representative Dynamic Strain Sweep Test Results at Different Temperatures and Frequencies.

Table 4. Linear Viscoelastic Dynamic Shear Modulus (Unit: MPa) at 25°C from DMA Strain Sweep Testing.

	Frequency (Hz)		
Sand Asphalt Mixture	0.1	1.59	10
AAD-1	7.56	16.1	52.6
AAM-1	19.0	62.8	138
AAD-1+LS[1]	9.20	27.5	69.2
AAD-1+HL[2]	9.58	28.6	71.8
AAM-1+HL[3]	28.0	90.4	184
HCR-1[4]	10.2	23.3	47.1
HCR-2[5]	28.4	67.7	119
HCR-3[6]	49.9	92.4	164
BASE	14.3	55.0	138
AirBlown	14.5	49.5	114
SBS-LG	12.1	40.4	97.0
EVA	11.4	34.2	78.8
ELVALOY	10.8	30.1	70.8

Note
[1]: AAD-1 mixed with 10 percent volume of limestone filler
[2]: AAD-1 mixed with 10 percent volume of hydrated lime
[3]: AAM-1 mixed with 10 percent volume of hydrated lime
[4]: Unaged high cure rubber
[5]: 3-month aged high cure rubber
[6]: 6-month aged high cure rubber

Based on strain sweep testing results, researchers performed frequency sweep tests at low strains without causing any nonlinear damage. In an attempt to predict relaxation behavior over a long time domain, testing was done at three different temperatures (10, 25, and 40°C), and the frequency-temperature superposition concept was applied to AAD-1, AAM-1, AAD-1+LS, AAD-1+HL, AAM-1+HL, HCR-1, HCR-2, and HCR-3, while the frequency sweep tests were performed at only 25°C for BASE, AirBlown, SBS-LG, EVA, and ELVALOY. Since the frequency sweep tests were performed under a steady-state vibrational loading condition, master curves at a certain temperature can be represented by storage, loss, and/or dynamic modulus. Figure 14 shows each master curve (storage, loss, and dynamic modulus) representation of the sand asphalt mixture AAD+LS (AAD-1 mixed with 10 percent volume of limestone filler) at 25°C after superposition in the frequency domain. Curve fitting with a Prony series was then conducted for the storage modulus master curve using Equation 14. Parameters

determined from the Prony series representation using the storage modulus data were employed to calculate the loss modulus and the dynamic modulus by Equations 15 and 10. Figures 15 through 17 present measured modulus plots (storage, loss, and dynamic) after the frequency-temperature superposition and their corresponding Prony series fit. The predicted moduli generally show good agreement with the measured moduli.

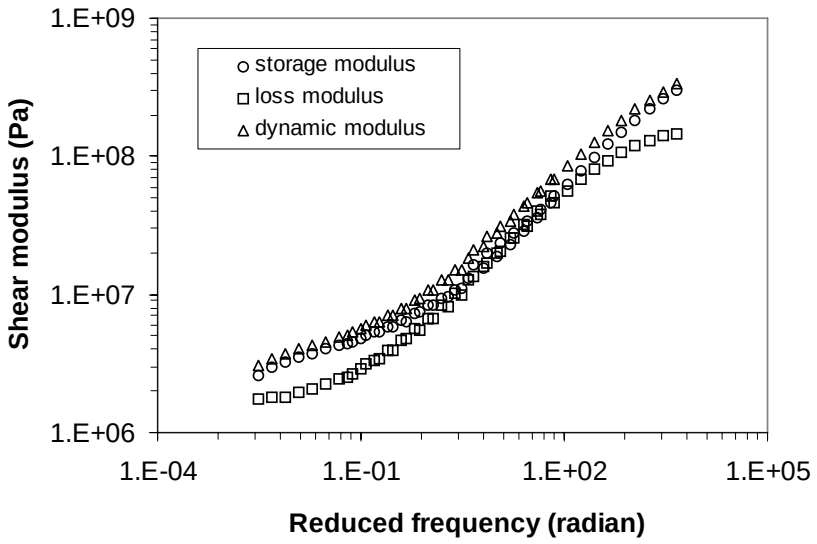

Figure 14. Each Master Curve (Storage, Loss, and Dynamic Modulus) after Superposition.

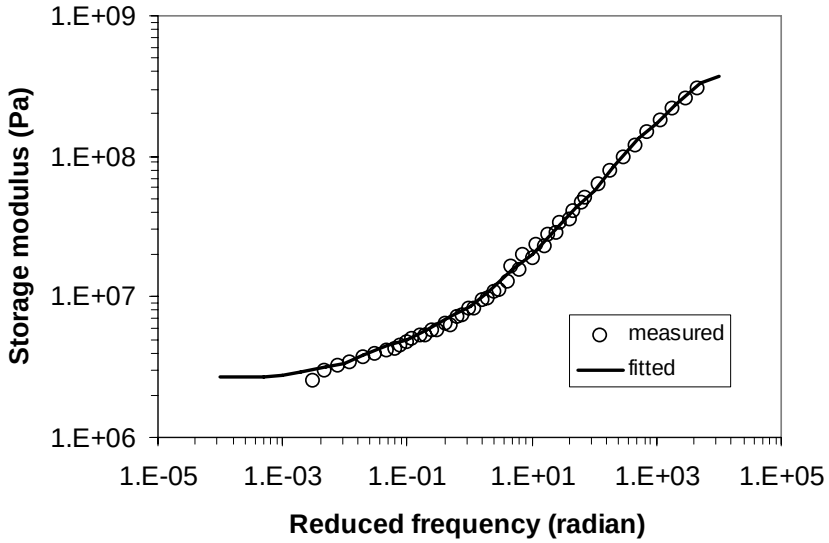

Figure 15. Storage Modulus Master Curve and Prony Series Fit.

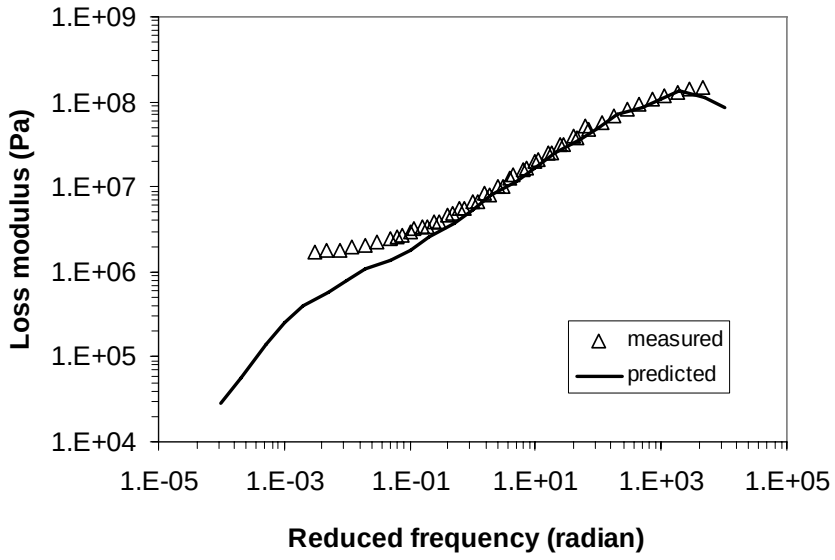

Figure 16. Loss Modulus Master Curve and Prony Series Fit.

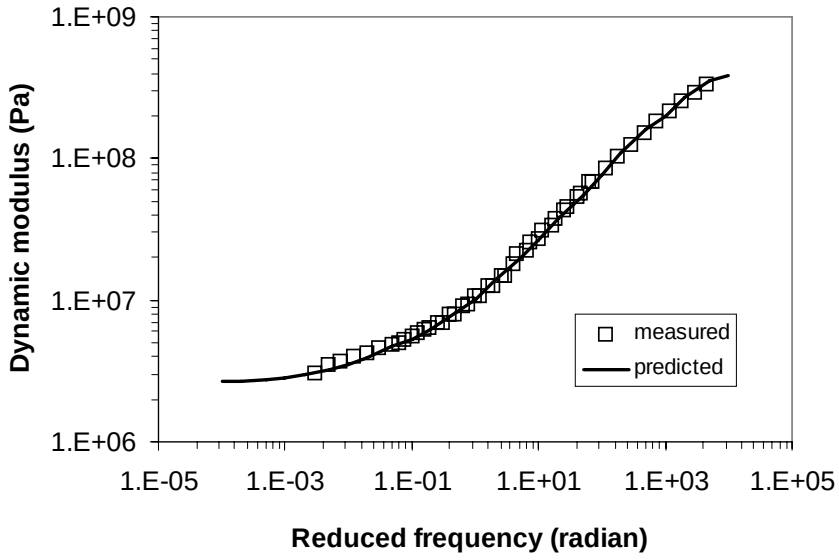

Figure 17. Dynamic Modulus Master Curve and Prony Series Fit.

Dynamic time sweep tests were performed in two different ways: (1) low strain levels for validation of linear viscoelastic behavior and (2) high strain levels for fatigue damage simulation. To validate linear viscoelastic behavior without any damage, low strain, such as 0.007 percent, was employed at 25°C and at 10 Hz. Figures 18 and 19 show hysteretic stress-strain and stress-pseudo strain behavior, respectively. As expected, the hysteretic behavior due to loading/unloading and repetitive loading does not depend on the number of loading cycles in stress-strain plots. Furthermore, hysteresis loops in the stress versus pseudo strain plots disappear, because the sample is tested in the linear viscoelastic region without damage. It can be inferred that Schapery's extended elastic-viscoelastic correspondence principle using the pseudo variables is clearly validated based on these results.

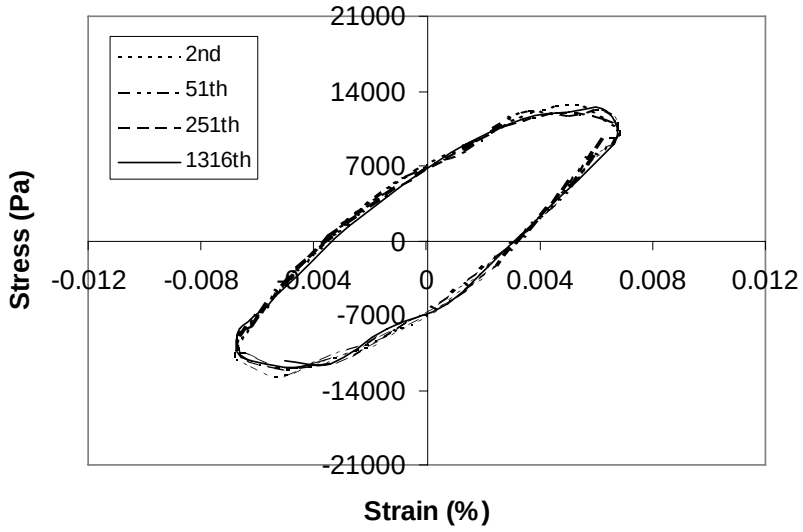

Figure 18. Linear Viscoelastic Stress-Strain Hysteresis Loops without Damage.

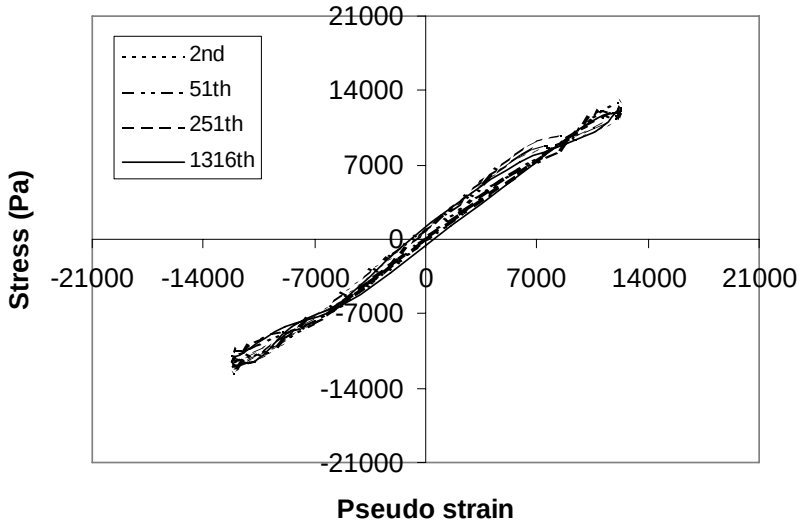

Figure 19. Linear Viscoelastic Stress-Pseudo Strain Loops without Damage.

To simulate fatigue damage, researchers conducted strain-controlled torsional shear cyclic tests at different strain levels from 0.20 to 0.844 percent (high enough to derive fatigue damage) at 25°C and 10 Hz. Every fatigue test was continued to complete failure on each sample. Many hairline cracks were observed on the surface, and a clean macrocrack was observed at the end of testing. Typically, the macrocrack was formed within the middle third of the sample. It can be inferred that the fatigue damage and crack development were governed by the fatigue process and not by geometric characteristics and/or gluing conditions at the ends of the sample. It is obvious that this testing protocol is repeatable and can result in a specification-type test method.

Typical hysteretic stress-strain behavior resulting from the high-strain cyclic loading is presented in Figure 20 at the selected 80th and 3000th cycles. Stress-strain loops shifted downward with the reduction of dissipated energy, which is determined from the area inside the stress-strain curve. The effect of the damage accumulation in a specimen was also investigated using pseudo strain, as described in Figure 21. The changes in area (dissipated pseudo strain energy) and slope (pseudo stiffness) of the hysteresis loop during the continuous cyclic loading reflect that microdamage has occurred. The dissipated pseudo strain energy is defined as dissipated energy calculated from measured physical stress versus the pseudo strain domain. By applying the pseudo strain concept, linear viscoelastic time-dependency is eliminated, and additional time-dependency can be expressed as a quantity due to non-linearity and/or damage. The dissipated pseudo strain energy at each loading cycle was calculated and plotted on a linear-log scale, as shown in Figure 22. Figure 22 demonstrates that samples experience damage at an increasing rate in the early stage, but the rate of damage then decreases and eventually decelerates, because the sample is close to complete failure. The area below the curve between the dissipated pseudo strain energy and number of loading cycles represents cumulative dissipated pseudo strain energy. Figure 23 presents the changes in cumulative dissipated pseudo strain energy as a function of loading cycles. Correspondingly, cumulative dissipated pseudo strain energy at fatigue failure can be employed as a quantitative indicator to explain fatigue resistance and/or the damage accumulation capability of a material.

Figure 25 compares a representative data set at a 0.40 percent strain level for AAD-1 using three different indicators of damage: reduction in normalized values of a) pseudo stiffness (PS); b) nonlinear dynamic modulus (NDM); and c) dissipated strain energy (DSE). Normalized values, the ratio of each indicator at certain loading cycles to the initial value, were used to eliminate variability among the indicators. Clearly, each indicator showed similar reduction due to damage accumulation.

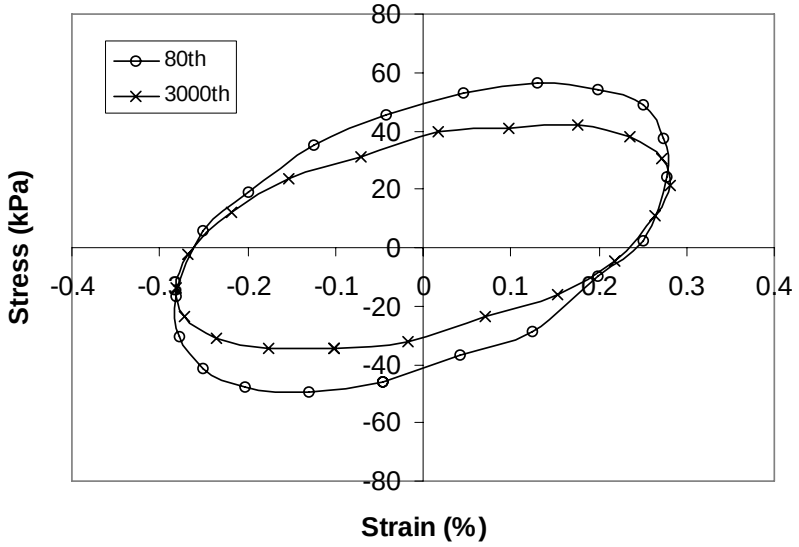

Figure 20. Stress-Strain Hysteresis Loops with Damage.

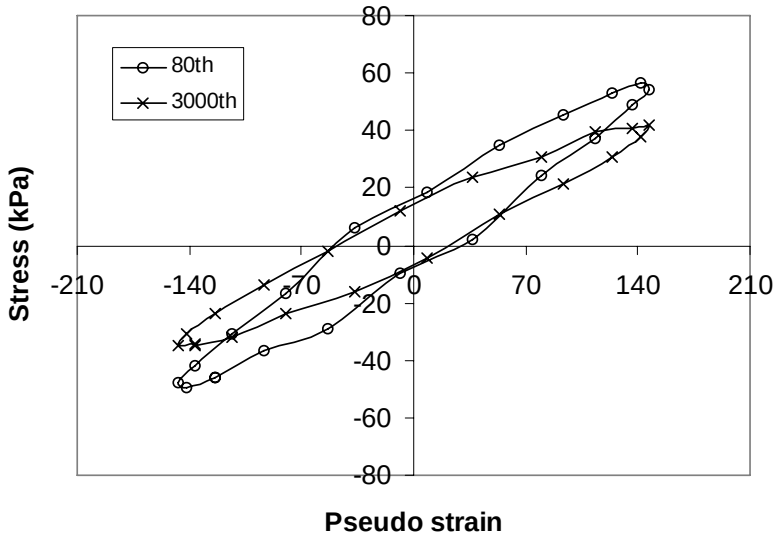

Figure 21. Stress-Pseudo Strain Hysteresis Loops with Damage.

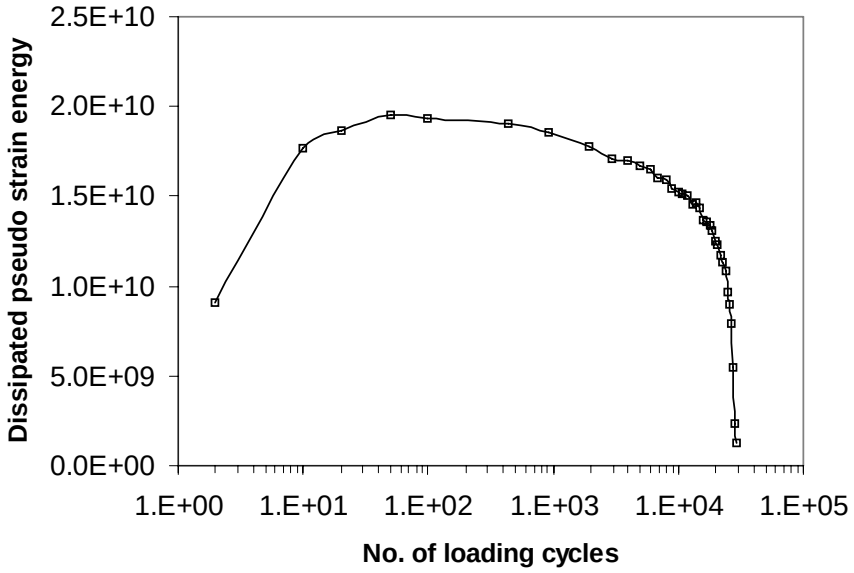

Figure 22. Linear-Log Plots of Dissipated Pseudo Strain Energy versus Number of Loading Cycles.

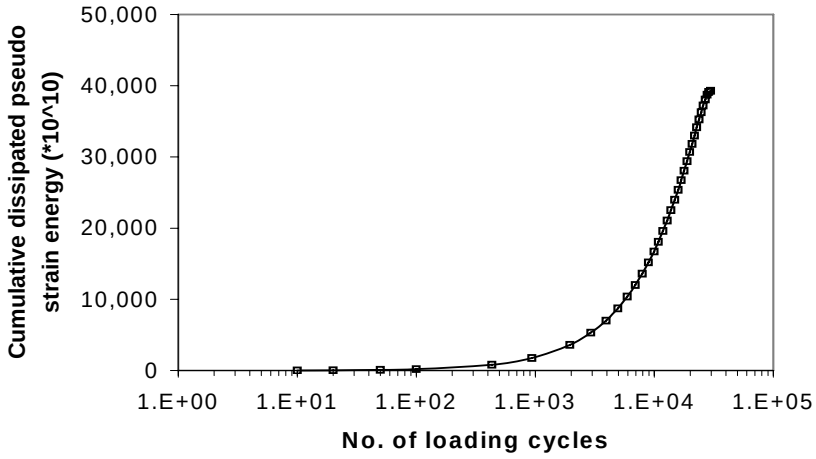

Figure 23. Linear-Log Plots of Cumulative Dissipated Pseudo Strain Energy versus Number of Loading Cycles.

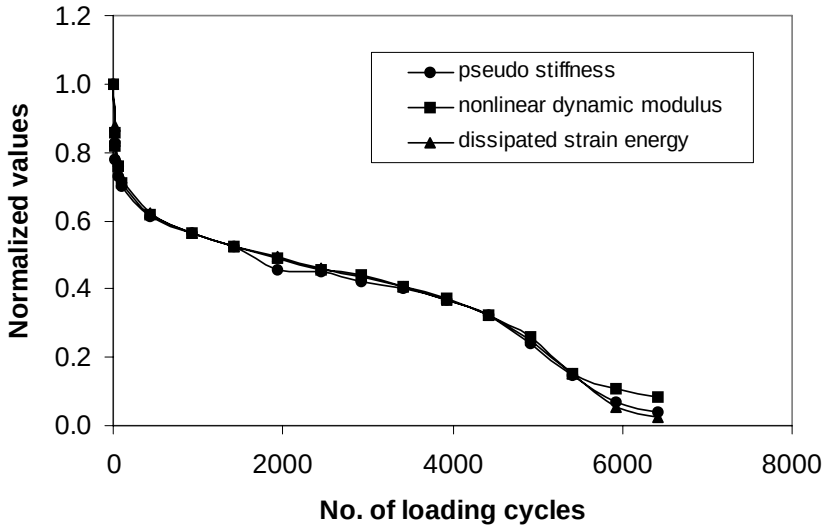

Figure 24. Fatigue Plots Based on Three Different Indicators of Damage.

CHAPTER 5. MECHANICAL ANALYSIS OF TESTING RESULTS

This chapter discusses laboratory testing results from the dynamic mechanical analyzer in detail. Linear viscoelastic material properties of sand asphalt mixtures from the DMA testing are compared to investigate effects of binder modification, aging, and filler addition on fundamental material characteristics. Then, the measured sand asphalt material properties are employed to perform stress analyses associated with nonlinear fatigue damage. Reasonable fatigue failure criteria are determined based on detailed observation of fatigue testing results from the DMA testing. Two mechanistic fatigue life prediction models for the torsional loading mode are derived based on the original model by Lee et al. (2000). The effects of binder modification and mineral fillers on fatigue fracture are discussed.

ANALYSIS OF DMA TESTING RESULTS

Figure 25 shows master storage modulus curves of each sand asphalt mixture at 25^{o}C after superposition in the frequency domain. The frequency domain master storage curves were then fit by a Prony series representation using Equation14. Once the Prony series parameters are determined, the measured dynamic shear moduli at any frequency from the dynamic strain sweep test can be compared to calculated dynamic shear moduli using the Prony series parameters. Storage moduli, loss moduli, and corresponding dynamic moduli at any frequency were calculated by Equations14, 15, and 10. Cross-plotting between the calculated and measured dynamic moduli, which were presented in Table 4, at three different frequencies (0.1, 1.59, and 10Hz) and at 25^{o}C was performed and is illustrated in Figure 26. Based on the good agreement between calculated and measured moduli, it can be concluded that every sand asphalt mixture was tested within the linear viscoelastic region, and Prony series fitting was accurately conducted.

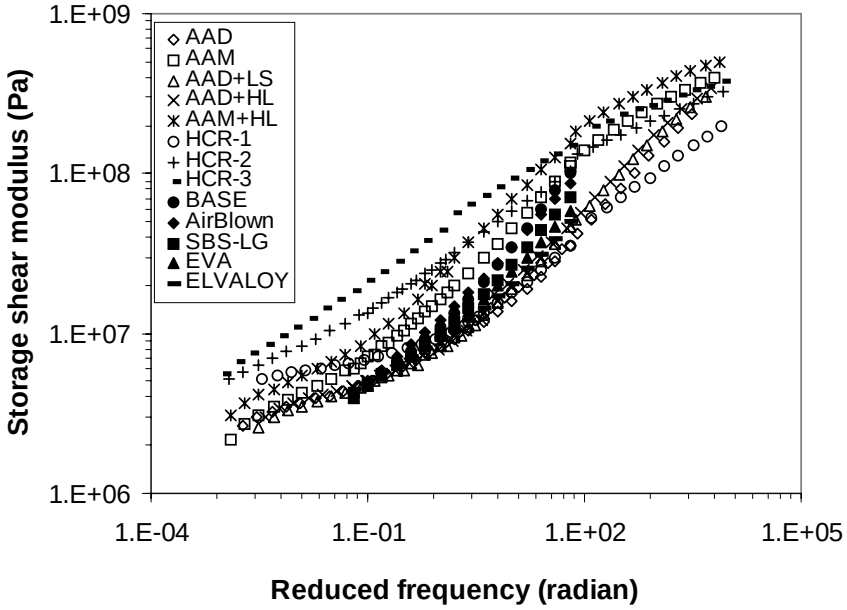

Figure 25. Master Storage Shear Modulus Curves of Each Sand Asphalt Mixture.

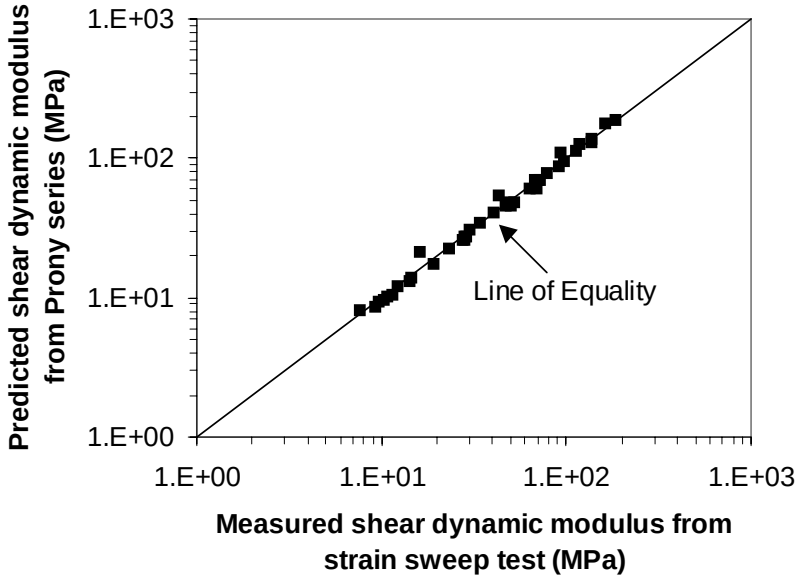

Figure 26. Cross-Plots between Measured Dynamic Modulus from Strain Sweep Tests and Predicted Dynamic Modulus from Calculation Using Prony Series Parameters.

Given parameters from a Prony series curve fitting determined from the dynamic frequency sweep test, static relaxation modulus as a function of time can be illustrated by Equation 16. Converted time domain relaxation moduli from the frequency domain master curves are shown in Figure 27 for sand asphalt mixtures of neat binders AAD-1 and AAM-1 and corresponding filler-mixed binders. Figure 28 shows these results for sand asphalt mixtures of unaged and aged high cure rubber binders HCR-1, HCR-2, and HCR-3. The converted time domain relaxation moduli for BASE, AirBlown, SBS-LG, EVA, and ELVALOY are presented in Figure 29. The position of relaxation curves in Figure 27 demonstrates that AAM-1 is stiffer than AAD-1, and fillers clearly contribute to mechanical stiffening of the binder. Another feature observed from Figure 27 is that AAD-1 mixed with hydrated lime shows higher moduli than a similar blend of AAD-1 and limestone filler. The relaxation curve slope decreases as aging increases, as demonstrated in Figure 28. This is an indication of the increasing stiffness of the asphalt mixture as it ages. The aging of asphalt binders typically reduce relaxation capability and increases brittle mechanical behavior.

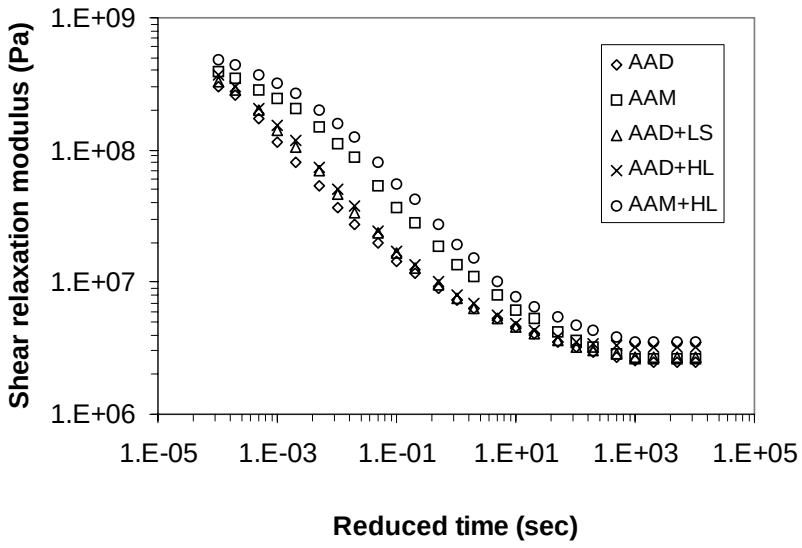

Figure 27. Transient Relaxation Moduli of Sand Asphalt Mixtures Mixed with Neat Binders and Mastics.

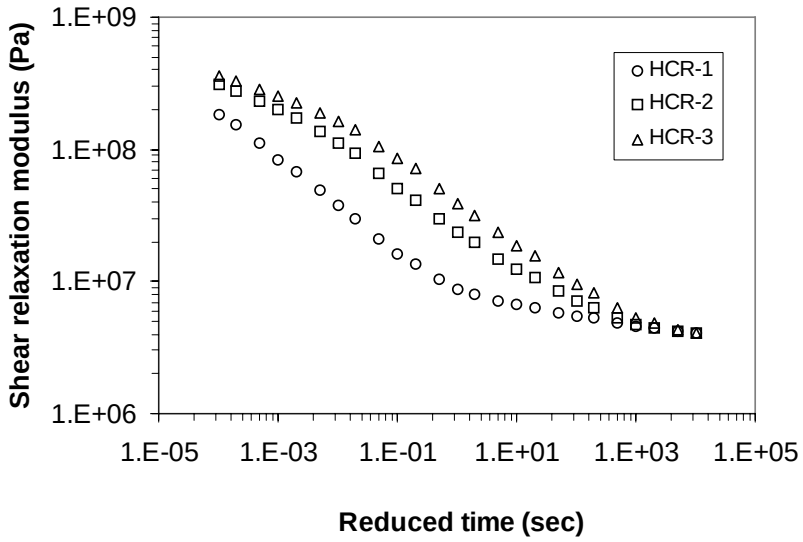

Figure 28. Transient Relaxation Moduli of Sand Asphalt Mixtures Mixed with Unaged and Aged HCR Binders.

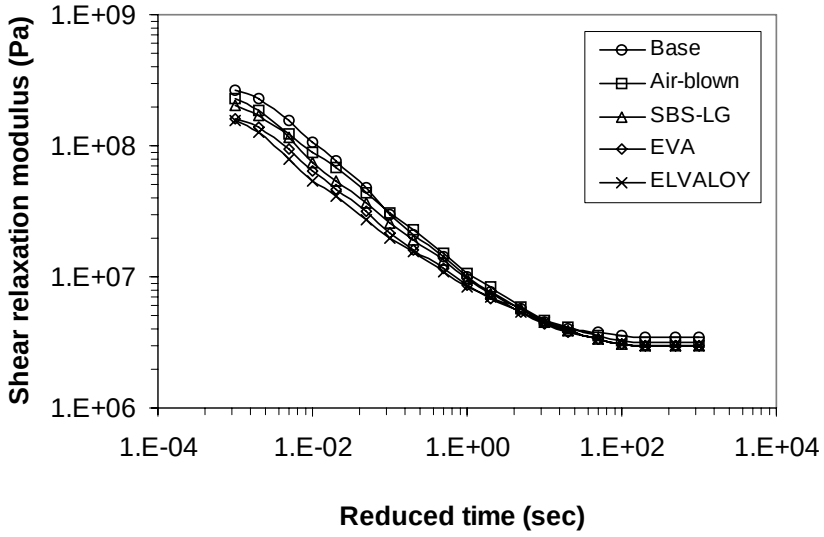

Figure 29. Transient Relaxation Moduli of Sand Asphalt Mixtures Mixed with BASE, AirBlown, SBS-LG, EVA, and ELVALOY.

Determination of Fatigue Failure

Figure 30 shows stiffness loss due to fatigue damage accumulation in a typical strain-controlled fatigue experiment. In general, two inflection points are observed. The first inflection point (FIP) defines a decreasing rate of change in stiffness associated with microcracking in the sample. The second inflection point (SIP) also infers a mechanical behavioral change possibly associated with macrocracking. A transition point (N_t) between the two inflection points represents the shift from microcracking to macrocracking. The rate of stiffness reduction abruptly increases at this transition point.

As Rowe and Bouldin skillfully proposed, the meaning of the transition point can be explained mathematically using the Taylor's series expansion (2000):

$$E^* = E_o^* + n\frac{dE^*}{dn} + \frac{n^2}{2!}\frac{d^2E^*}{dn^2} + \frac{n^3}{3!}\frac{d^3E^*}{dn^3} + ... \quad (29)$$

$$E^*n = E_o^*n + n^2\frac{dE^*}{dn} + \frac{n^3}{2!}\frac{d^2E^*}{dn^2} + \frac{n^4}{3!}\frac{d^3E^*}{dn^3} + ... \quad (30)$$

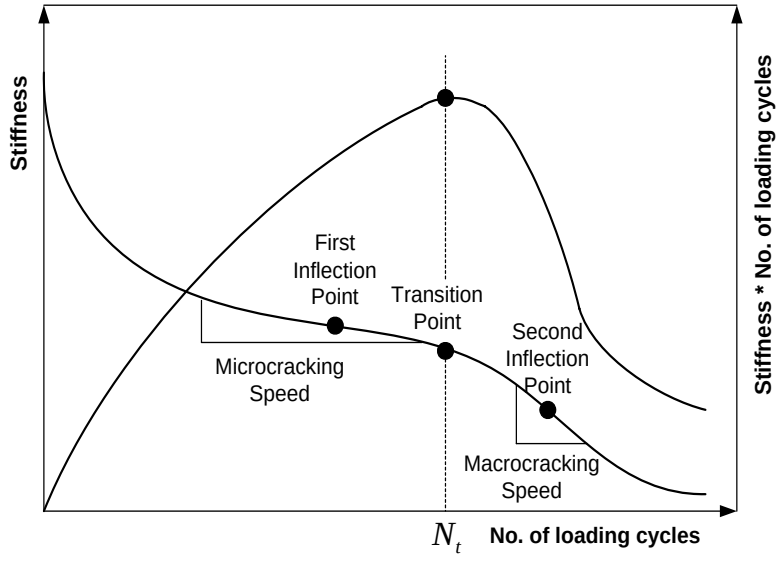

Figure 30. Typical Strain-controlled Fatigue Test Results (Rowe and Bouldin, 2000).

Where E^* = stiffness or modulus,

E_o^* = initial stiffness or modulus, and
n = number of load cycles.

In the microcracking region, the first derivative (dE^*/dn) is negative and decreasing, and the second derivative (d^2E^*/dn^2) is positive and decreasing until it reaches zero at the first inflection point. The second derivative (d^2E^*/dn^2) is then negative and increasing in magnitude until it reaches a maximum value where the third derivative (d^3E^*/dn^3) is equal to zero at the transition point where the material behavior changes from microcracking to macrocracking. The second derivative (d^2E^*/dn^2) remains negative and of decreasing magnitude until it reaches zero at the second inflection point. The second derivative becomes positive passing the second inflection point, and the rate of change of stiffness begins to reduce toward zero. In Figure 30, plotting the product E^*n against n demonstrates a peak at the transition point. This peak is a potential fatigue failure point as are the two inflection points.

Figure 31 illustrates changes in the normalized nonlinear dynamic modulus, one of the damage indicators, and the phase angle due to damage accumulation at a 0.28 percent strain level for sand asphalt mixtures with binder AAM-1. The phase angle increased and approached a peak value followed by a precipitous drop as cyclic loading continued. The importance of the phase angle in fatigue has been described by Reese (1997). According to his argument, a point showing the maximum phase angle (MPA) is a reasonable fatigue failure point since a plot of phase angle versus load cycles shows a rapid loss of phase angle when materials under fatigue loading stop accumulating distress.

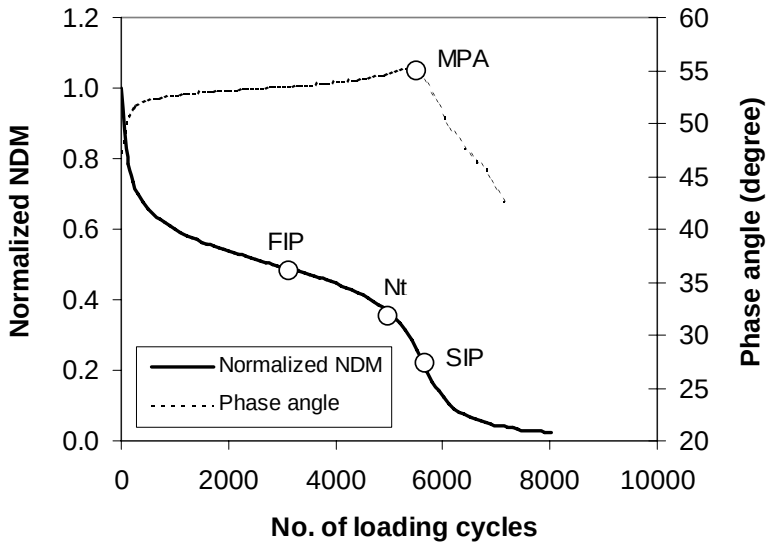

Figure 31. Plots of Normalized Nonlinear Dynamic Modulus and Phase Angle versus Number of Loading Cycles in Fatigue Testing.

An evaluation of acceptable fatigue failure criteria was performed by cross-plotting the number of loading cycles at the MPA and the number of loading cycles at the FIP, SIP, or N_t. This analysis is based on test results showing correspondence between the maximum phase angle and the three failure criteria candidates: FIP, SIP, and N_t. Figure 32 demonstrates that the number of loading cycles at the MPA is consistent with the number of load cycles at the SIP for AAD-1, AAM-1, and corresponding filler mixed sand asphalt mixtures. However, the MPA for the HCR-3 mixture corresponds better with the FIP, as shown in Figure 33. In an attempt to increase generality in determining a reasonable fatigue failure point, five different types of sand asphalt mixtures: AAD-1 (neat SHRP binder), AAM+HL (filled binder), HCR-1 (unaged rubber-modified binder), HCR-3 (aged rubber-modified binder), and EVA (polymer-modified binder) were selected, and the number of loading cycles at MPA and the number of loading cycles at FIP, SIP, or N_t are cross-plotted as presented in Figures 34 to 36. By calculating total deviation error, which is defined as the total absolute deviation from the line of equality, N_t can be inferred to be a reasonably acceptable failure point since it shows minimum deviation error.

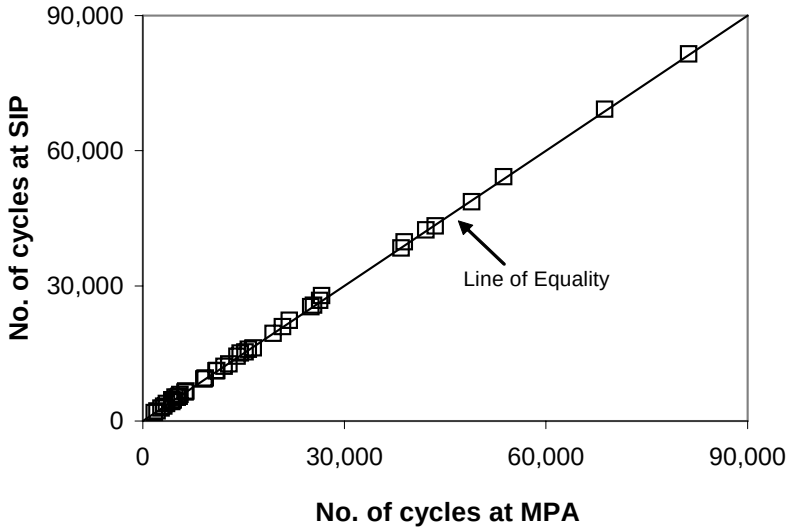

Figure 32. Cross-Plot between the Number of Loading Cycles at the Second Inflection Points and the Number of Loading Cycles at the Maximum Phase Angle (Sand Asphalt Mixtures: AAD, AAM, AAD+LS, AAD+HL, and AAM+HL).

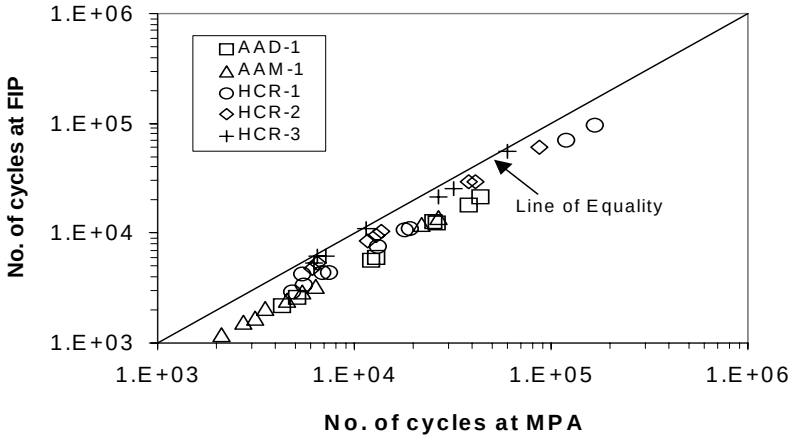

Figure 33. Cross-Plot between the Number of Loading Cycles at the First Inflection Points and the Number of Loading Cycles at the Maximum Phase Angle (Sand Asphalt Mixtures: AAD, AAM, HCR-1, HCR-2, and HCR-3).

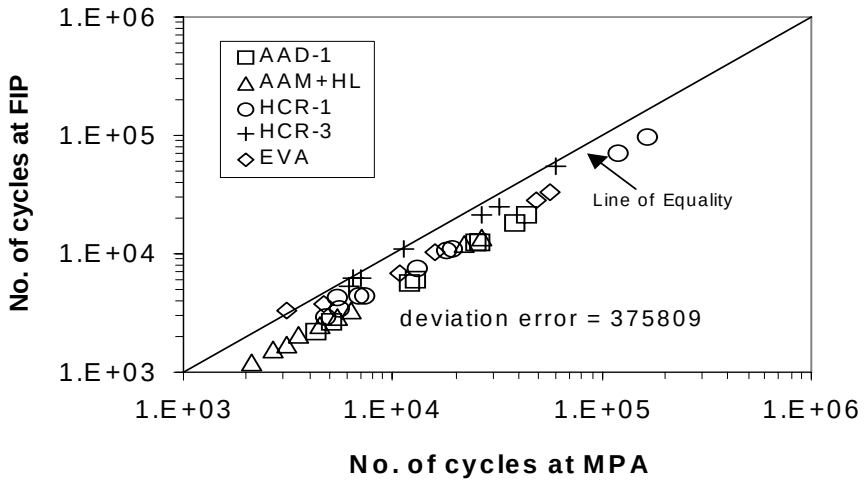

Figure 34. Cross-Plot between the Number of Loading Cycles at the First Inflection Points and the Number of Loading Cycles at the Maximum Phase Angle (Sand Asphalt Mixtures: AAD, AAM+HL, HCR-1, HCR-3, and EVA).

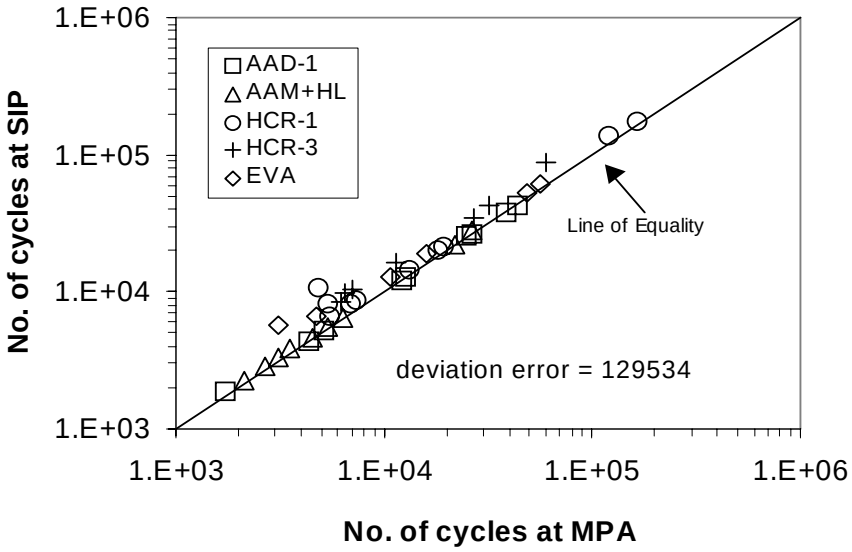

Figure 35. Cross-Plot between the Number of Loading Cycles at the Second Inflection Points and the Number of Loading Cycles at the Maximum Phase Angle (Sand Asphalt Mixtures: AAD, AAM+HL, HCR-1, HCR-3, and EVA).

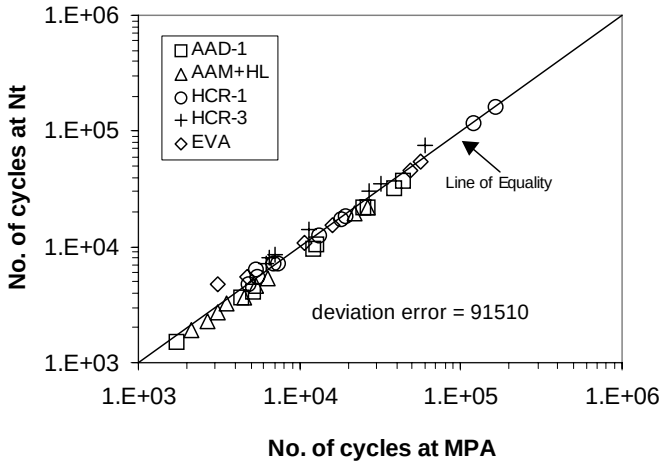

Figure 36. Cross-Plot between the Number of Loading Cycles at the Transition Points and the Number of Loading Cycles at the Maximum Phase Angle (Sand Asphalt Mixtures: AAD, AAM+HL, HCR-1, HCR-3, and EVA).

Table 5. Average Value and Standard Deviation of the Normalized Nonlinear Dynamic Modulus at FIP, SIP, N_t, and MPA.

		AAD	AAM	AAD+LS	AAD+HL	AAM+HL	HCR-1	HCR-2	HCR-3
Nor. NLDM[1] at FIP	Average	0.533	0.477	0.482	0.435	0.435	0.403	0.238	0.196
	S. D.[2]	0.0331	0.0264	0.0229	0.0124	0.0102	0.0280	0.0191	0.0242
Nor. NLDM at SIP	Average	0.232	0.223	0.198	0.177	0.183	0.188	0.127	0.116
	S. D.	0.0319	0.0270	0.0228	0.0145	0.0151	0.0201	0.0151	0.0201
Nor. NLDM at Nt	Average	0.436	0.383	0.396	0.355	0.359	0.340	0.196	0.162
	S. D.	0.0309	0.0224	0.0338	0.0200	0.0168	0.0220	0.0143	0.0211
Nor. NLDM at MPA	Average	0.258	0.292	0.227	0.232	0.255	0.336	0.208	0.183
	S. D.	0.0504	0.0373	0.0196	0.0260	0.0508	0.0206	0.0184	0.0242

		BASE	AirBlown	SBS-LG	EVA	ELVALOY
Nor. NLDM at FIP	Average	0.440	0.458	0.424	0.368	0.404
	S. D.	0.0267	0.0244	0.0290	0.0289	0.0125
Nor. NLDM at SIP	Average	0.184	0.198	0.208	0.190	0.185
	S. D.	0.0236	0.0170	0.0078	0.0124	0.0066
Nor. NLDM at Nt	Average	0.351	0.370	0.338	0.306	0.341
	S. D.	0.0258	0.0222	0.0241	0.0311	0.0142
Nor. NLDM at MPA	Average	0.217	0.289	0.409	0.312	0.340
	S. D.	0.0537	0.0510	0.0795	0.0224	0.0162

Note
[1]: Normalized Nonlinear Dynamic Modulus
[2]: Standard Deviation

Average values and standard deviations of the normalized nonlinear dynamic modulus at FIP, SIP, N_t, and MPA are calculated and presented in Table 5. The normalized nonlinear dynamic moduli at N_t, which is adopted as a point of fatigue failure in this study, are shown for each sand mixture in Figure 37. Approximately 60 percent of stiffness reduction was observed at fatigue failure for the SHRP binders, filled binders, and polymer-modified binders. On the other hand, unaged high cure rubber binder HCR-1 and aged binders HCR-2 and HCR-3 show approximately 70 percent and 80 to 85 percent stiffness reduction, respectively. It was observed that the residual stiffness at fatigue failure is dependent on binder type (modified and unmodified) as well as the level of aging. This representation of fatigue is considerably more accurate and logical than simply determining failure as an arbitrary condition, e.g., when 50 percent of the initial stiffness is reached.

Based on this finding, a complete fatigue test for each mixture was performed by testing replicate specimens to failure (N_t) at different strain levels. The number of loading cycles to failure at each strain level was plotted on a log-log scale in Figure 38. Fatigue test results can be described by a phenomenological regression model, Equation (31), and model coefficients are presented in Table 6.

$$N_f = A(\gamma_o)^{-B} \quad (31)$$

Where N_f = fatigue life,

γ_o = applied strain amplitude, and

A, B = regression constants.

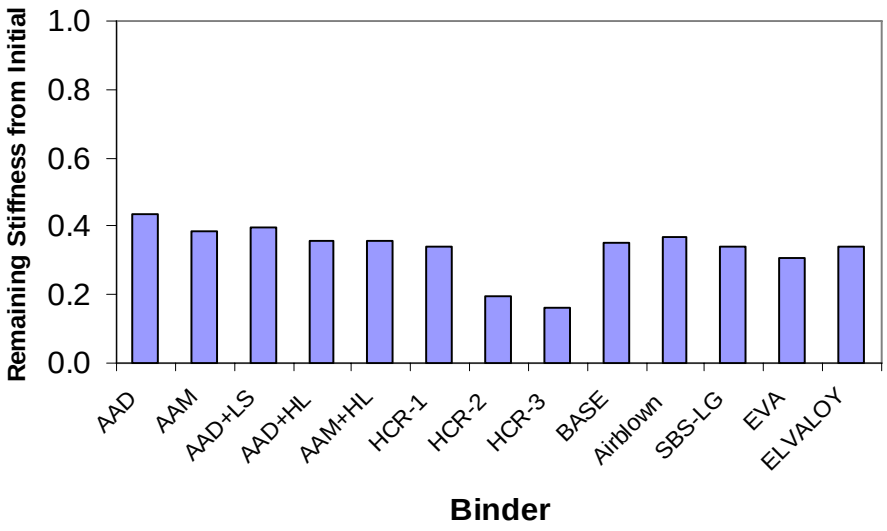

Figure 37. Average Values of Normalized Nonlinear Dynamic Modulus at Fatigue Failure of Each Sand Asphalt Mixture.

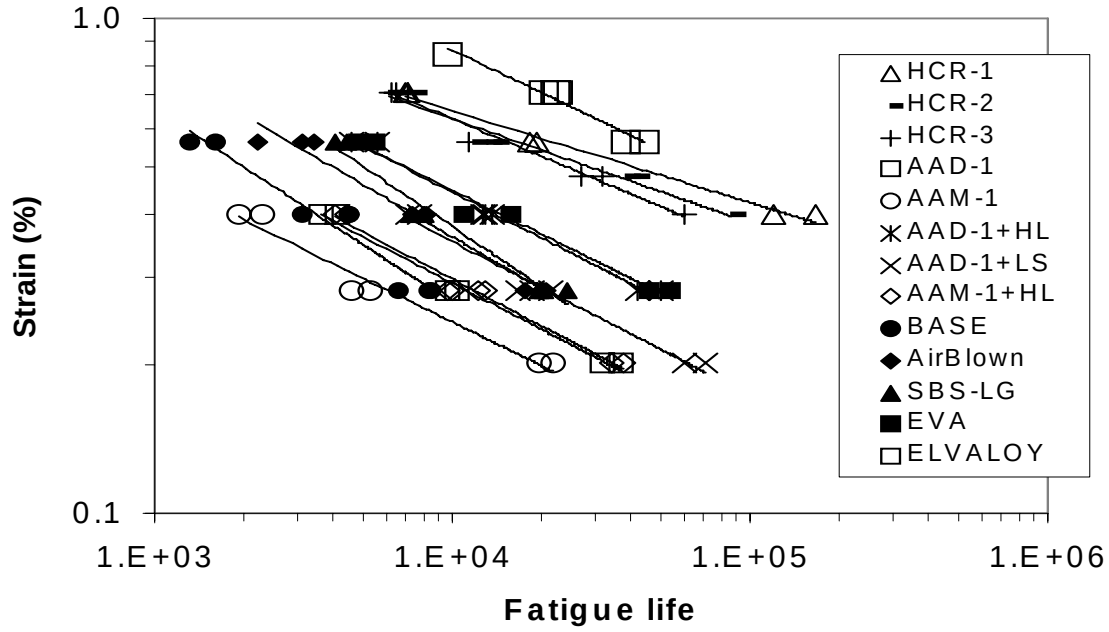

Figure 38. Applied Strain versus the Number of Loading Cycles to Failure.

Table 6. Phenomenological Fatigue Model Parameters.

	Phenomenological Fatigue Model	
Mixture	A	B
AAD-1	205.47	3.1566
AAM-1	94.771	3.2869
HCR-1	912.43	5.4616
AAD-1+LS	438.64	3.0591
AAD-1+HL	757.25	3.1987
AAM-1+HL	234.06	3.0992
BASE	399.83	2.3886
AirBlown	593.06	2.7695
SBS-LG	979.18	2.3976
EVA	716.64	2.3036
ELVALOY	6407.4	2.3037

Fatigue Life Prediction Model for Torsional Loading Mode

Fatigue life can be expressed in the form of work potential theory and continuum damage mechanics. Lee et al. originally developed such a model for asphalt concrete samples under uniaxial cyclic loading (2000). The original model was modified in two different ways so that it could be applied to data from the torsional shear cyclic loading mode without rest periods.

The first approach is to use dissipated pseudo strain energy and pseudo stiffness, which is a secant modulus of a hysteresis loop between stress and pseudo strain, as indicators of damage evolution. This approach requires measurements of sufficient numbers of fatigue testing data at each loading cycle to develop hysteresis behavior. As mentioned, the use of stress-pseudo strain domain is technically sound, since the hysteretic behavior between stress and pseudo strain does not include linear viscoelastic time-dependency, and additional time-dependency can be considered nonlinear damage due to fatigue.

Dissipated strain energy (damage indicator employed for second approach) can be alternatively used to derive a mechanistic fatigue life prediction model. As illustrated in Figure 24, reduction in normalized values of dissipated strain energy showed similar behavior, as it is compared to pseudo stiffness reduction that is a damage indicator in stress-pseudo strain domain. However, it should be noted that the dissipated strain

energy represents energy dissipation due to fatigue damage as well as linear viscoelastic stress relaxation.

Use of Dissipated Pseudo Strain Energy Concept

The general form of the constitutive equation under the torsional loading mode for a viscoelastic body during damage is presented as:

$$\tau_m = I_P C(S)\gamma_m^R \tag{32}$$

Where I_P = initial pseudo stiffness, which is introduced for elimination of sample-to-sample variability,
C = pseudo stiffness that is a function of the damage parameter, S,
γ_m^R = peak shear pseudo strain in each cycle, and
τ_m = physical shear stress corresponding to γ_m^R.

The corresponding stress-strain relationship in terms of pseudo strain can be expressed as:

$$\tau_m = \frac{\partial W_m^R}{\partial \gamma_m^R} \tag{33}$$

Where W_m^R = pseudo strain energy density function when $\gamma^R = \gamma_m^R$.

The time-dependent damage evolution law for viscoelastic materials is typically rate-dependent (Park et al., 1996) and is expressed as:

$$\frac{dS}{dt} = \left(-\frac{\partial W_m^R}{\partial S} \right)^{\alpha} \tag{34}$$

Where dS/dt = damage evolution rate, and
α = a material constant.

Combining Equations 32 and 33 yields:

$$W_m^R = \frac{I_P}{2} C(S)(\gamma_m^R)^2 \tag{35}$$

A graphical expression explaining Equation 35 in stress – pseudo strain domain is presented in Figure 39. Substituting Equation 35 into equation 34 yields:

$$\frac{dS}{dt} = \left[-\frac{I_P}{2} \frac{dC}{dS} (\gamma_m^R)^2 \right]^{\alpha} \tag{36}$$

The function $C(S)$ can be characterized by the chain rule:

$$\frac{dC}{dS} = \frac{dC}{dt} \frac{dt}{dS} \tag{37}$$

Substituting Equation 37 into equation 36 and integrating yields:

$$S \cong \sum_{i=1}^{N} \left[\frac{I_P}{2} (\gamma_{m,i}^R)^2 (C_{i-1} - C_i) \right]^{\frac{\alpha}{1+\alpha}} (t_i - t_{i-1})^{\frac{1}{1+\alpha}} \tag{38}$$

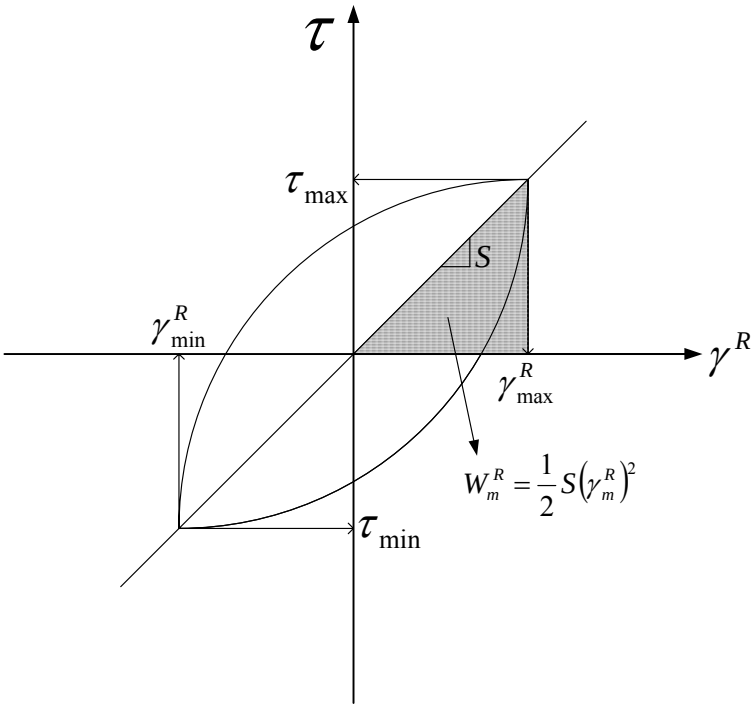

Figure 39. Graphical Expression of Dissipated Pseudo Strain Energy.

The damage parameter S can be calculated at each discrete cycle by obtaining the peak pseudo strain ($\gamma_{m,i}^{R}$) and pseudo stiffness (C_i) corresponding to time (t_i). The material constant α is initially assumed and then varied until cross-plotting the measured C against S at several different strain-levels results in closure. The load-level dependency is eliminated if α is a true material property. According to Schapery, α is related to the material's creep or relaxation properties (1975). Figure 40 shows cross-plotting of the pseudo stiffness versus the calculated damage parameter for the same value of loading cycles, before and after the strain level dependency was eliminated by varying the value of α. An appropriate value of α successfully eliminates load-level dependency, as demonstrated in Figure 40. The strain-level independence of the relationship between pseudo stiffness and the calculated damage parameter indicates that the pseudo strain based stiffness parameter and the internal state variable are effective representatives to reflect damage growth and damage state, respectively. Figure 41 shows cross-plots of the pseudo stiffness versus the calculated damage parameter of each system tested, after the strain level dependency was eliminated.

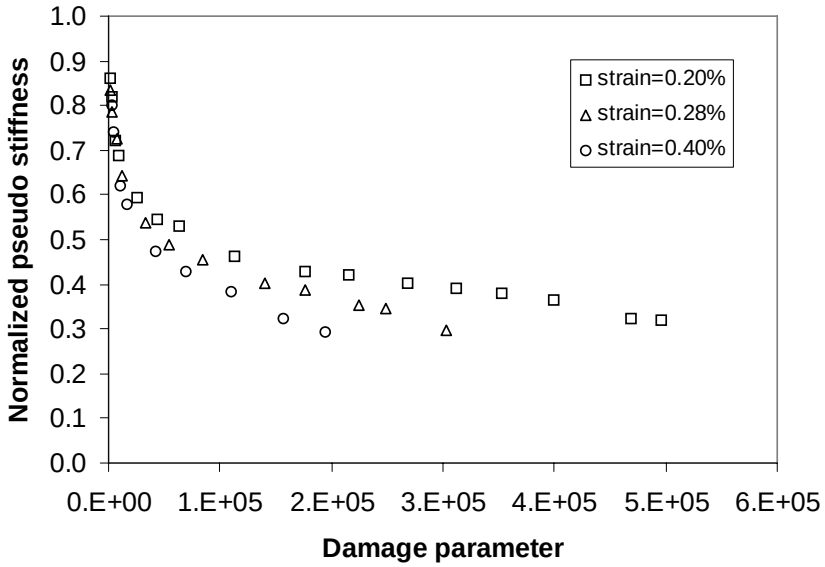

(a)

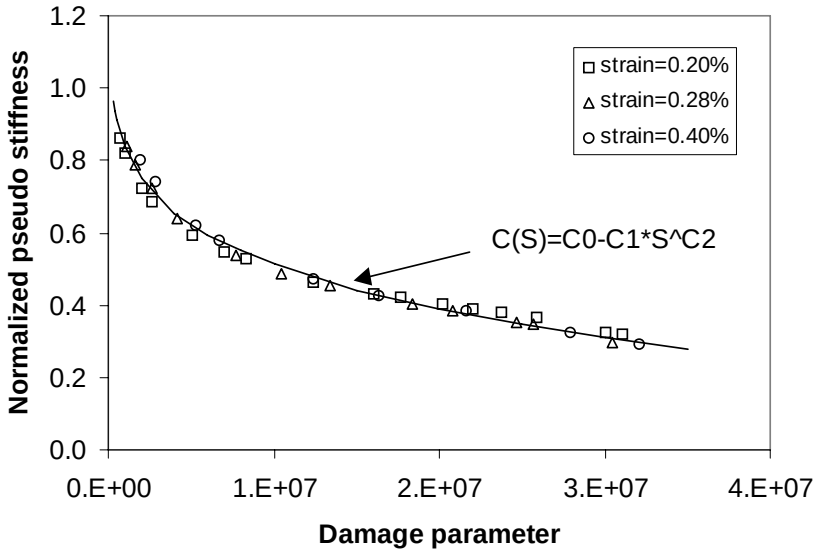

(b)

Figure 40. Normalized Pseudo Stiffness versus Calculated Damage Parameter (a) before and (b) after the Strain Level Dependency was Eliminated.

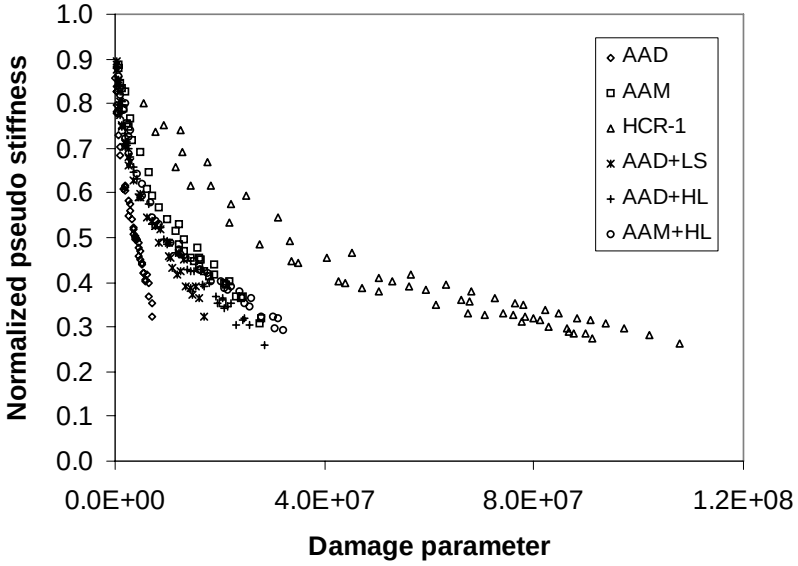

Figure 41. Normalized Pseudo Stiffness versus Calculated Damage Parameter of Each Sand Mixture after the Strain Level Dependency was Eliminated.

As Lee proposed, the curve of C versus S typically follows a power relation (1996):

$$C(S) = C_0 - C_1(S)^{C_2} \tag{39}$$

Where C_0, C_1, and C_2 are regression constants.

Substituting Equation 39 into Equation 35 and taking the derivative with respect to the damage parameter S gives:

$$\frac{dW_m^R}{dS} = -\frac{I_P}{2} C_1 C_2 (S)^{C_2 - 1} (\gamma_m^R)^2 \tag{40}$$

Combining Equations 28, 34, and 40 and integrating yields the following fatigue life prediction model for the torsional loading mode:

$$N_f = \frac{f(S_f)^k}{k(0.5 I_P C_1 C_2)^\alpha} \left|G^*(\omega)\right|^{-2\alpha} (\gamma_o)^{-2\alpha} \tag{41}$$

Where $k = 1 + (1 - C_2)\alpha$,

f = loading frequency, and
S_f = damage parameter when the samples approach fatigue failure.

The determination of S_f is clearly related to the fatigue failure criteria. The proposed model is a function of the damage evolution characteristics of the material: C_1 and C_2 and linear viscoelastic material properties: $|G^*(\omega)|$ and α. Strain amplitude and loading frequency are given as testing input, and the linear viscoelastic dynamic shear modulus $|G^*(\omega)|$ and material parameter α are determined from linear viscoelastic constitutive testing, such as static creep, static relaxation, or dynamic frequency sweep tests. Parameters $I_P, k, S_f, C_1,$ and C_2 represent damage evolution characteristics and are obtained from fatigue tests.

The mechanistic fatigue model in Equation 41 can be rewritten in the generalized form of Equation 31 as:

$$N_f = A_1(\gamma_o)^{-B_1} \tag{42}$$

$$\text{Where } A_1 = \frac{f(S_f)^k}{k(0.5 I_P C_1 C_2)^\alpha |G^*(\omega)|^{2\alpha}} \tag{43}$$

$$B_1 = 2\alpha \tag{44}$$

Use of Dissipated Strain Energy Concept

The constitutive equation in the oscillatory torsional loading mode can be alternatively expressed as follows:

$$\tau_m = I_D |G^*(D)| \gamma_m \tag{45}$$

Where I_D = initial nonlinear dynamic modulus, which is introduced for elimination of sample-to-sample variability,
$|G^*(D)|$ = damage-affected dynamic modulus at each cycle, and
D = damage parameter.

By introducing the damage-affected phase angle, $\phi(D)$, the dissipated strain energy (hysteresis loop area between shear stress and shear strain) can be expressed as:

$$W(D) = \pi I_D \gamma_m \tau_m \sin\phi(D) \tag{46}$$

Where $W(D)$ = dissipated strain energy at each cycle, and
$\phi(D)$ = phase angle between stress and strain at each cycle.

Substituting loss modulus in Equation 46, the equation can be rewritten as:

$$W(D) = \pi I_D (\gamma_m)^2 G^{"}(D) \tag{47}$$

Where $G^{"}(D)$ = damage-induced loss modulus at each cycle.

Equation 47 is graphically illustrated in Figure 42. The hysteresis loop area between measured stress and measured strain represents energy dissipation, and the dissipated energy can be calculated by monitoring loss modulus at each cycle.

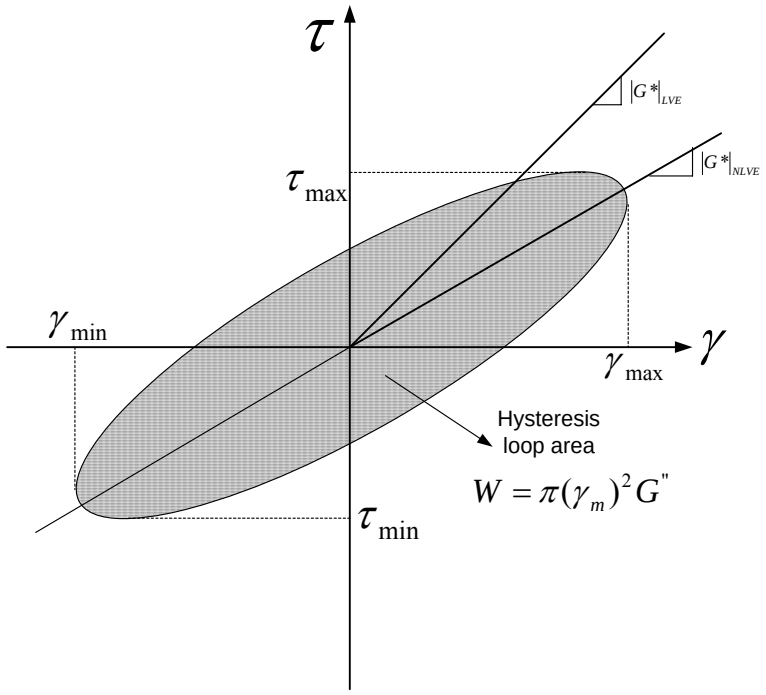

Figure 42. Graphical Expression of Dissipated Strain Energy.

The damage evolution law for this approach can be expressed as a similar form shown in Equation 34.

$$\frac{dD}{dt} = \left(-\frac{\partial W}{\partial D} \right)^{\alpha} \tag{48}$$

Substituting Equation 47 into Equation 48 yields:

$$\frac{dD}{dt} = \left[-\pi I_D (\gamma_m)^2 \frac{\partial G^{"}}{\partial D} \right]^{\alpha} \tag{49}$$

The function $G^{"}(D)$ can be characterized by the chain rule:

$$\frac{\partial G^{"}}{\partial D} = \frac{\partial G^{"}}{\partial t} \frac{\partial t}{\partial D} \tag{50}$$

Substituting Equation 50 into Equation 49 and integrating yields a similar form as expressed in Equation 38.

$$D \cong \sum_{i=1}^{N} \left[\pi I_D (\gamma_m)^2 (G^{"}_{i-1} - G^{"}_{i}) \right]^{\frac{\alpha}{1+\alpha}} (t_i - t_{i-1})^{\frac{1}{1+\alpha}} \tag{51}$$

The curve of $G^{"}$ versus D follows a power relation:

$$G^{"}(D) = C_3 - C_4 (D)^{C_5} \tag{52}$$

Where C_3, C_4, and C_5 are regression constants.

Substituting Equation 52 into Equation 47 and taking the derivative with respect to the damage parameter, D yields:

$$\frac{dW}{dD} = \pi I_D (\gamma_m)^2 \left[-C_4 C_5 D^{C_5 - 1} \right] \tag{53}$$

Combining Equations 50 and 53, and integrating yields the following final form of fatigue life prediction model:

$$N_f = \frac{f (D_f)^k}{k (\pi I_D C_4 C_5)^{\alpha}} (\gamma_m)^{-2\alpha} \tag{54}$$

Where $k = 1 + (1 - C_5)\alpha$,

f = loading frequency, and

D_f = damage parameter when the sample approaches fatigue failure.

By introducing linear viscoelastic dynamic shear modulus, $\left|G^*(\omega)\right|$, Equation 54 can be expressed as:

$$N_f = \frac{f(D_f)^k}{k\left(\pi \frac{I_D}{\left|G^*(\omega)\right|} C_4 C_5\right)^{\alpha}} \left|G^*(\omega)\right|^{-\alpha} (\gamma_m)^{-2\alpha} \tag{55}$$

The derived fatigue model, Equation 55, based on the dissipated strain energy concept, can be rewritten in the generalized form of Equation 31 as:

$$N_f = A_2 (\gamma_m)^{-B_2} \tag{56}$$

$$\text{Where } A_2 = \frac{f(D_f)^k}{k\left(\pi \frac{I_D}{\left|G^*(\omega)\right|} C_4 C_5\right)^{\alpha} \left|G^*(\omega)\right|^{\alpha}} \tag{57}$$

$$B_2 = 2\alpha \tag{58}$$

Model Validation and Discussion

The predicted fatigue lives using Equations 41 and 54 are cross-plotted to the measured fatigue lives in Figures 43 and 44, respectively. The deviation from the line of equality is very small. It can be inferred that the model parameters provide a reasonable representation of the fatigue response.

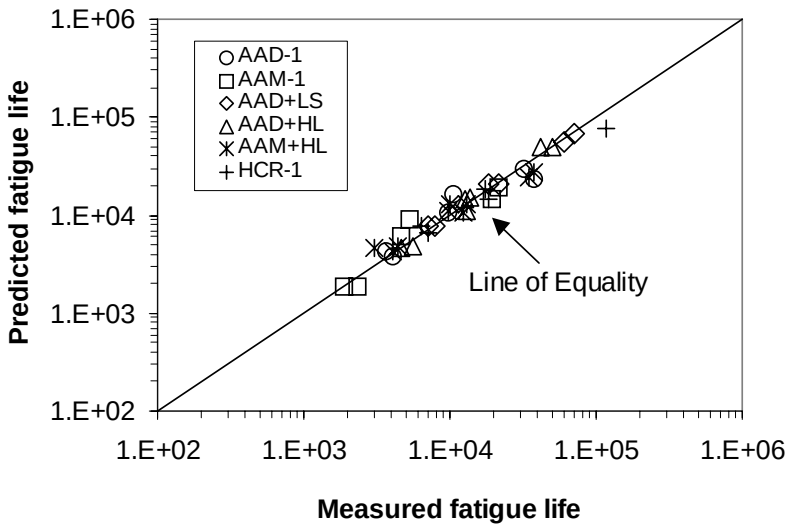

Figure 43. Cross-Plot of Measured Fatigue Life versus Predicted Fatigue Life from the Mechanistic Fatigue Prediction Model (Dissipated Pseudo Strain Energy).

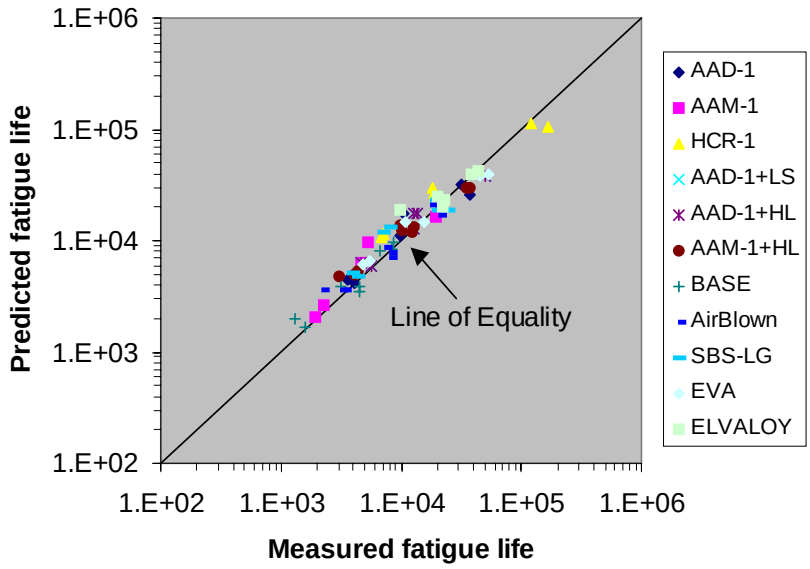

Figure 44. Cross-Plot of Measured Fatigue Life versus Predicted Fatigue Life from the Mechanistic Fatigue Prediction Model (Dissipated Strain Energy).

The empirically derived model coefficient and exponent: A and B, respectively, are replaced by mechanistic model parameters A_1, A_2, B_1, and B_2. Figures 45 and 46 indicate that each mechanistic model is quite compatible with a simple phenomenological model. A good agreement exists between the model parameters. The clear advantages of using the parameters A_1, B_1 or A_2, B_2 are that they are derived based on measurable material parameters and are not derived simply from curve fitting. The ability to derive mechanistic model parameters from measurable engineering properties provides the potential to engineer better material properties based on fundamental properties and to investigate how these fundamental properties affect fatigue life. Table 7 summarizes the model parameters included in Equations 41 and 54 determined from test data .

Assessing the effect of each model parameter on fatigue resistance is difficult, since the parameters are interactive. For example, the material parameter α is associated with the damage parameter, dynamic shear modulus, shear strain input, and other factors. The parameter k is an exponent in the numerator and appears in the denominator as well. A physical meaning for each parameter can be described as follows:

- I_P, I_D, initial pseudo stiffness and initial nonlinear dynamic modulus, respectively: higher initial value infers a lower level of early damage.
- k, combined effect of C_2 (or C_5) and α: a higher k value means an extended fatigue life since it is an exponent of the term S_f or D_f, which has a relatively large value.

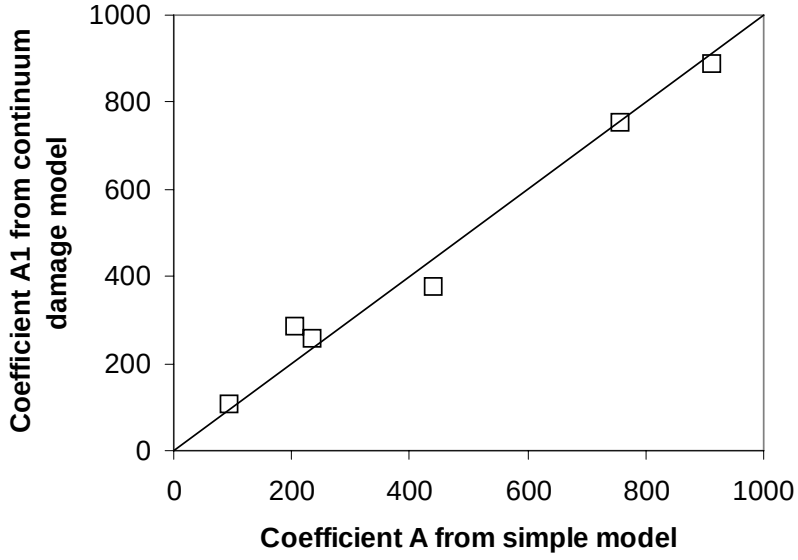

(a)

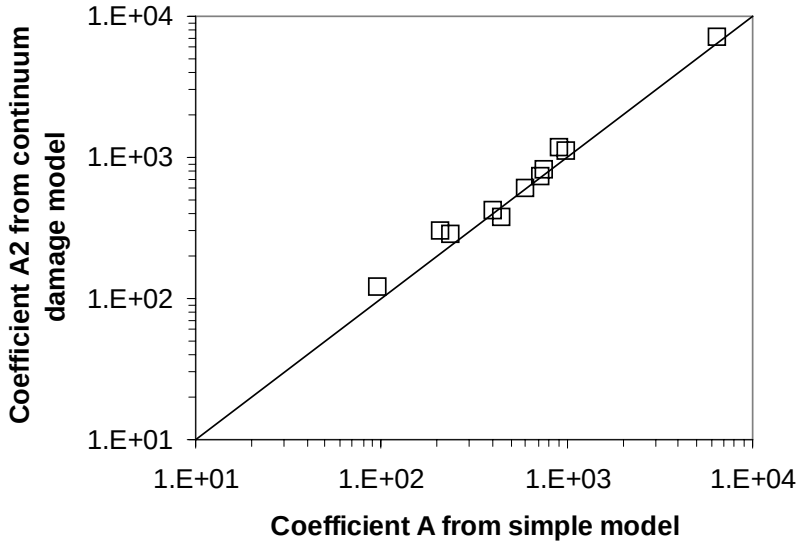

(b)

Figure 45. Comparison Plots of Model Coefficient between Phenomenological Model and Continuum Damage Model Using (a) Dissipated Pseudo Strain Energy, and (b) Dissipated Strain Energy.

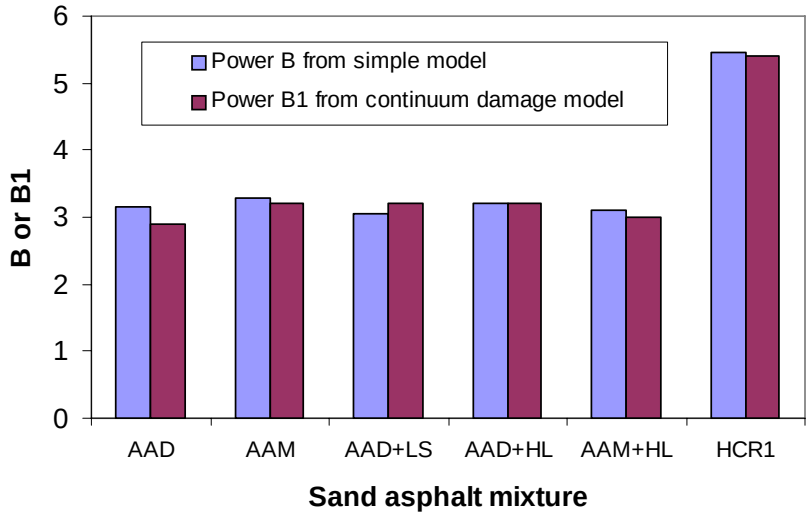

(a)

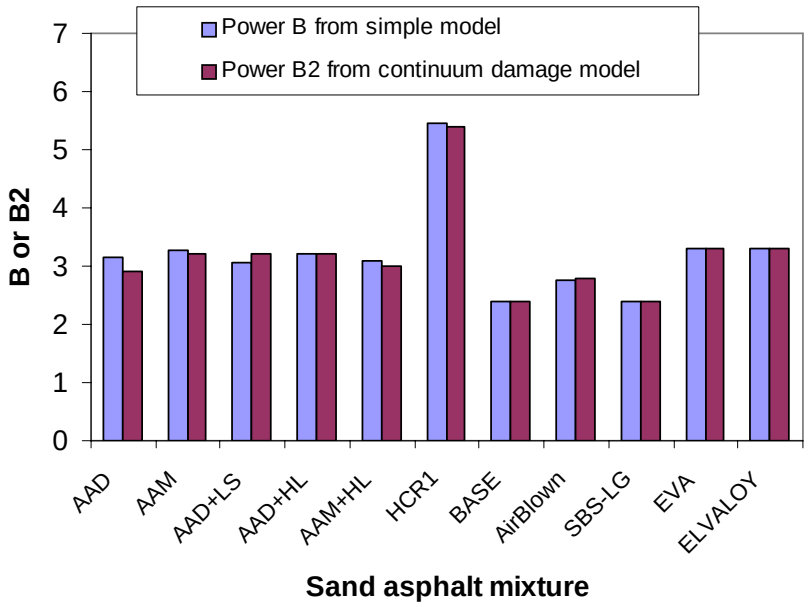

(b)

Figure 46. Comparison Plots of Model Exponent between Phenomenological Model and Continuum Damage Model Using (a) Dissipated Pseudo Strain Energy, and (b) Dissipated Strain Energy.

Table 7. Mechanistic Fatigue Model Parameters.

	Mechanistic Fatigue Model (Dissipated Pseudo Strain Energy)						
Mixture	Average I_P	C_2	C_1C_2	$\lvert G^* \rvert$, MPa	α	k	Average S_f
AAD-1	0.6379	0.4028	0.000439	50.2	1.45	1.866	6,181,814
AAM-1	0.6528	0.2952	0.001594	135.2	1.60	2.128	24,482,752
HCR-1	0.4602	0.0685	0.061540	45.1	2.70	3.515	94,588,211
AAD-1+LS	0.6643	0.275	0.002224	68.0	1.60	2.16	16,067,051
AAD-1+HL	0.6807	0.28	0.001987	73.0	1.60	2.152	24,512,617
AAM-1+HL	0.5675	0.1565	0.013461	184.0	1.50	2.265	29,929,693

	Mechanistic Fatigue Model (Dissipated Strain Energy)					
Mixture	Average I_D, Pa	C_5	C_4C_5	α	k	Average D_f
AAD-1	29200000	0.5122	0.01114	1.45	1.7073	515.928
AAM-1	70700000	0.4364	0.01542	1.60	1.9018	708.764
HCR-1	17400000	0.2622	0.04117	2.70	2.9921	924.753
AAD-1+LS	40600000	0.4282	0.01553	1.60	1.9149	778.977
AAD-1+HL	45400000	0.3379	0.02369	1.60	2.0594	1113.50
AAM-1+HL	98500000	0.2949	0.02957	1.50	2.0577	1053.21
BASE	66200000	0.4087	0.01882	1.20	1.7096	810.162
AirBlown	61500000	0.3828	0.01813	1.40	1.8641	1041.51
SBS-LG	45500000	0.2046	0.05138	1.20	1.9545	916.314
EVA	42100000	0.2496	0.04346	1.65	2.2382	1057.83
ELVALOY	29000000	0.0970	0.09184	1.65	2.4900	1753.11

- $\left|G^*(\omega)\right|$, linear viscoelastic dynamic shear modulus: representing the fundamental stiffness of the material.
- S_f (or D_f), damage parameter at fatigue failure: inferring cumulative amount of damage to failure, a higher value of this parameter indicates that the sample can absorb more damage before failure and correspondingly shows a higher fatigue resistance.
- C_1C_2 (or C_4C_5), multiplication of regression constants: typically a higher value shows a faster decrease in stiffness (faster damage) when compared against the damage parameter.

By observing the fatigue prediction model in Equations 41 and 54, one can conclude that more fatigue resistant materials show lower values of stiffness, C_1 (or C_4), and C_2 (or C_5), and higher values for S_f (or D_f) and k, if the α value does not vary significantly among the materials evaluated. As a result, a material that is soft (low stiffness) but capable of cumulating more damage before failure (high S_f or D_f) due to a slow rate of stiffness reduction (low C_2 or C_5 and high k) will demonstrate a longer fatigue life.

Effect of Mineral Fillers on Fatigue Fracture

The effects of fillers can be identified from DMA fatigue testing results. As demonstrated in Figure 38, the contribution of fillers to the extended fatigue life of the mastic is clear. Average fatigue life and percent increase of fatigue life due to filler addition were calculated, as shown in Table 8. However, this effect is complex and is probably synergistically derived from mechanical, chemical, physical, and even rheological mechanisms. Table 7 indicates that fillers stiffen the binder, which is easily verified by higher stiffness. Furthermore, fillers increase the damage parameter at fatigue failure S_f (or D_f), increase the value of the parameter k, and reduce the value of regression coefficient C_2 (or C_5). It can also be observed that the dynamic shear modulus (or initial loss modulus) and the fatigue failure damage parameter are the most dominant parameters in defining fatigue life because they are relatively large numbers. Even though fillers stiffen the binder, they contribute to better resistance in microcracking due to a lower rate of damage evolution and a higher tolerance for total damage accumulation.

Comparison of model parameters between limestone filled and hydrated lime filled systems show that hydrated lime is a more effective filler than limestone. Hydrated lime provides a much longer fatigue life because it allows the accumulation of more microdamage from initial loading to failure. It is apparent that since the same filler

volume (10 percent) was used for each filler (hydrated lime and limestone), other mechanisms than the volume filling effect must come into play. These other effects may include crack pinning efficiency and physico-chemical interactions between the binder and the filler.

The difference between filled binders and unfilled binders can also be identified by monitoring dissipated pseudo strain energy in fatigue tests. The dissipated pseudo strain energy is typically defined as dissipated energy due to additional time-dependency after linear viscoelastic time-dependency was eliminated. The additional time-dependency can be expressed as a quantity due to non-linearity and/or damage. The theoretical background for the dissipated pseudo strain energy is well described in the previous chapter.

Table 8. Average Fatigue Life and Percent Increase Due to Filler Addition.

Strain (%)	AAD-1			AAM-1	
	Neat[1]	LS[2]	HL[3]	Neat	HL
0.20	34,555	65,610 (89.9)[4]	Not tested	20,660	36,210 (75.3)
0.28	10,060	18,843 (87.3)	45,960 (356.9)	4,510	11,235 (149.1)
0.40	3,860	7,577 (96.3)	13,110 (239.6)	2,110	4,210 (99.5)
0.56	Not tested	Not tested	5,110 (N/A)	Not tested	Not tested

Note
[1]: Unfilled system
[2]: Mastic mixed with limestone filler
[3]: Mastic mixed with hydrated lime
[4]: Average fatigue life in number of loading cycles (percent increase of fatigue life compared to fatigue life of unfilled system)

As illustrated in Figures 22 and 23, the inside area of the stress-pseudo strain hyteresis loop at each discrete loading cycle and summation of the hysteresis loop area until complete fatigue failure for each unfilled and filled mixture at different strain levels were calculated. Figure 47 shows the cumulative dissipated pseudo strain energy values corresponding to fatigue failure for each mixture at different strain levels (0.20, 0.28, 0.40, and 0.56 percent). Average values of the cumulative pseudo strain energy for each mixture at a 0.28 percent strain level were calculated for better clarity. The percent increase in the average cumulative pseudo strain energy at a 0.28 percent strain level for AAD-1 mixed with limestone, AAD-1 mixed with hydrated lime, and AAM-1 mixed with hydrated lime were 133, 588, and 442 percent, respectively.

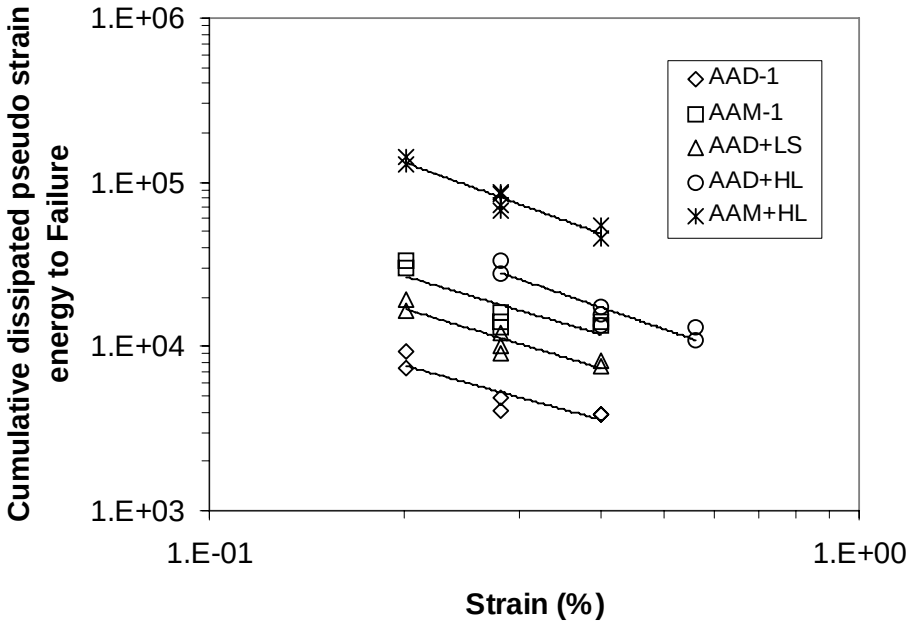

Figure 47. Cumulative Dissipated Pseudo Strain Energy at Fatigue Failure of Each Mixture at Different Strain Levels.

The effect of filler addition on fatigue life can be easily verified by studying Figure 47. Filled systems show greater damage accumulation capability than do unfilled systems. It is also evident that hydrated lime is a better material than limestone filler in terms of fatigue resistance under the strain-controlled mode of loading. The percent increase in average cumulative dissipated pseudo strain energy at a 0.28 percent strain level further infers that the degree of interaction and effectiveness of hydrated lime may be dependent on the type of bitumen with which it is used. The hydrated lime is more effective with bitumen AAD-1 than bitumen AAM-1. This is consistent with results from Lesueur and Little (1999).

CHAPTER 6. EVALUATION OF THE EFFECT OF MOISTURE

Moisture damage is a primary mode of distress in asphalt concrete mixtures and accelerates structural degradation of the mixtures in conjunction with cracking and plastic deformation. Moisture typically reduces stiffness of the binder and/or mastic through diffusion and degrades the adhesive bond between the mastic and aggregate particles. Moisture damage mechanisms are complex, and attempts have been made to simplify them by categorizing them. Still, an identification of the fracture mechanisms of asphalt-aggregate systems in the presence of water is difficult, and a synergistic interaction of mechanisms often remains the best explanation of the moisture damage process. A promising approach to assess moisture damage potential is to identify fundamental material properties that affect and control moisture damage and then compare the mechanical behavior of asphalt mixtures dry and in the presence of water to see if the fundamental properties can indeed predict moisture-related damage.

As an example, Cheng et al. investigated moisture effects on asphalt mixtures using two different moisture damage models: an adhesion failure model and a moisture diffusion model based on surface energy characteristics, which are fundamental material properties (2003). Cheng et al. were able to measure the surface energies of the asphalt binder or mastic and the aggregate and then calculate the cohesive bond energy of the mastic as well as the adhesive bond between the binder or mastic and the aggregate. They used the Wilhelmy Plate to measure binder surface energies (both non-polar and polar components) and the Universal Sorption Device to measure aggregate surface energy (both non-polar and polar components). Cheng et al. also used the Universal Sorption Device to measure the diffusion of moisture vapor into various asphalt cement binders. They found that the migration of moisture into the binder is binder dependent. For example, considerably more moisture vapor diffuses into the asphalt identified in the Strategic Highway Research Program as AAD-1 than into SHRP asphalt AAM-1. They further found that the quantities of vapor absorbed by the asphalt were surprisingly high, in the range of parts per thousand. They speculated that this diffusion alone could alter the rheological properties of the binder and affect the ability of the binder or mastic to resist moisture damage.

Asphalt concrete mixtures are typically composed of two dominant phases – relatively coarse aggregate particles and matrix phase that is a combination of binder, air voids, and fine aggregates. The quality of the matrix phase influences damage and fracture of the entire mixture. The matrix phase is considerably weaker and less stiff than the coarse aggregate phase and more susceptible to the effects of damage through moisture diffusion. Therefore, a relatively accurate and repeatable methodology to assess damage susceptibility of the matrix phase is necessary, and a more accurate evaluation of the response of the matrix phase will lead to better understanding of the overall mixture performance in the presence of water.

Data from DMA were used to successfully differentiate among the damage potential of several different systems comprised of different neat binders' (five binders) different levels of modification and different types of mineral fillers (smaller than 74-μm particles). Two types of filled systems were evaluated: limestone and hydrated lime of approximately the same particle size distribution. These different fillers were evaluated with two very different asphalt cements: AAD-1 and AAM-1. The simplicity, repeatability, and accuracy of the DMA make it a very attractive tool by which to evaluate fatigue damage and fracture of asphalt mixtures, including the effect of moisture.

Based on this history of success with the DMA analytical approach, the main objectives discussed in Chapter 6 are:

- to develop a simple and reasonable test method to evaluate moisture damage of asphalt mixtures with emphasis on the mastic or mastic and fine aggregate fraction,

- to evaluate the effects of moisture damage on fundamental material characteristics and fatigue damage resistance of asphalt mixtures, and

- to consider how this tool can be used to validate the prediction of moisture damage sensitivity of a mastic and/or a fine aggregate mixture based on surface energy properties of the mixture components and/or moisture diffusions characteristics of the binder and mastic.

DEVELOPMENT OF METHODOLOGY

Researchers evaluated the impact of moisture on the rate and level of fatigue damage potential of asphalt binders and mastics by measuring fundamental viscoelastic material properties and by performing fatigue tests using DMA.

To evaluate the DMA testing methodology, cylindrical DMA specimens were fabricated from SHRP-classified binder AAD-1, which was mixed with Ottawa sand. Ottawa sand is a relatively clean and uniformly graded aggregate. Approximately 70 percent of the sand particles are within the #30 sieve (0.6-mm mesh size) and #50 sieve (0.3-mm mesh size). The selected Ottawa sand satisfied the particle gradation required for standard sand (ASTM C-778).

Eight-percent binder by weight of dry sand was mixed and compacted at a pre-determined mixing temperature (164^{o}C) and compaction temperature (145^{o}C). The 11.5 grams of loose sand asphalt mixture was compacted in a specially fabricated mold to produce sample geometry of 50-mm long with a 12-mm diameter. Chapter II provides a

detailed description of the specially designed DMA specimen mold. To prevent undue distortion, each sample was removed from the mold after an approximately 30-minute cooling period. Each end of the compacted sample was trimmed neatly to produce final target sample weight of 11 grams. The allowable weight tolerance was with ± 0.05 gram. Any sample exceeding the tolerance was excluded.

Of course, it is necessary to precondition the DMA samples with moisture prior to testing in order to evaluate the influence of moisture. The initial step in achieving this objective is to allow moisture to penetrate the specimens until an equilibrium condition is reached. Figure 48 illustrates the variation in weight of the sand asphalt samples versus soaking time in distilled water at room temperature (approximately 25^{o}C). To accelerate moisture saturation, a vacuum was applied so that air voids of the sample were removed efficiently. Approximately 17 percent of air voids was monitored based on the measurements of bulk specific gravity of each compacted sand asphalt sample. Asphalt absorption was not considered to determine the percentage of air voids for simplicity. As illustrated in Figure 48, approximately 1.2 gram of water, which corresponds to 11 percent of dry sample weight, penetrated into the sample, and the sample reached a weight equilibrium after about 30 minutes of soaking. This represents an average saturation of approximately 125 percent, which means that some of moisture could have diffused into the mastic. It can also be inferred that the vacuum saturation conditioning might alter void structure somewhat and account for some of the extra saturation of moisture recorded. Based on results presented in Figure 49, each wet sample for DMA tests was soaked for 1 hour in the distilled-water vacuum bath.

To retain the moisture absorbed in the sample during DMA testing, a thin polyethylene film was wrapped around the wet sample. Other methods of retaining the water were considered, including a thin polymer spray around the sample. However, the polyethylene film was selected as it was not only able to retain the water, but it also fit loosely enough around the sample so as not to stiffen the sample in the torsional loading. In fact, use of the polyethylene film limited moisture fluctuation to less than 0.01 gram, which is 1 percent of the total absorbed water, during the course of the experiment. To compare samples tested dry and wet on an equal basis, dry samples were also wrapped with the polyethylene film.

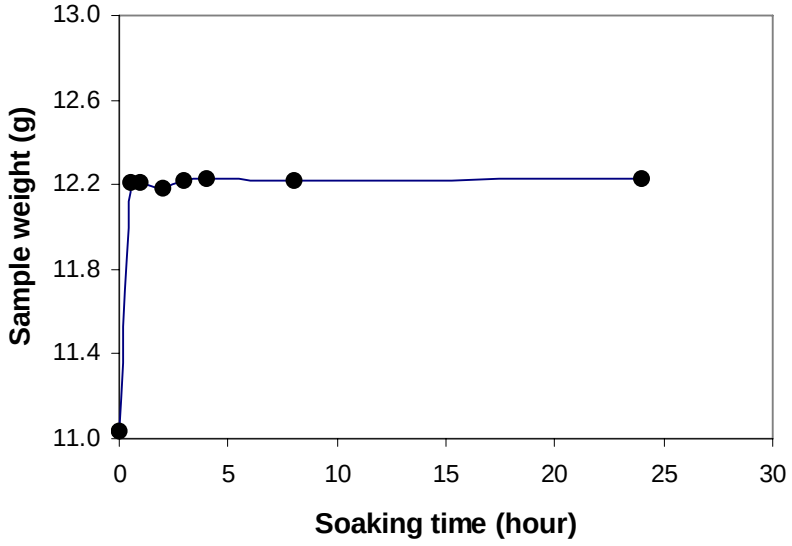

Figure 48. Sand-Asphalt Sample Weight versus Soaking Time.

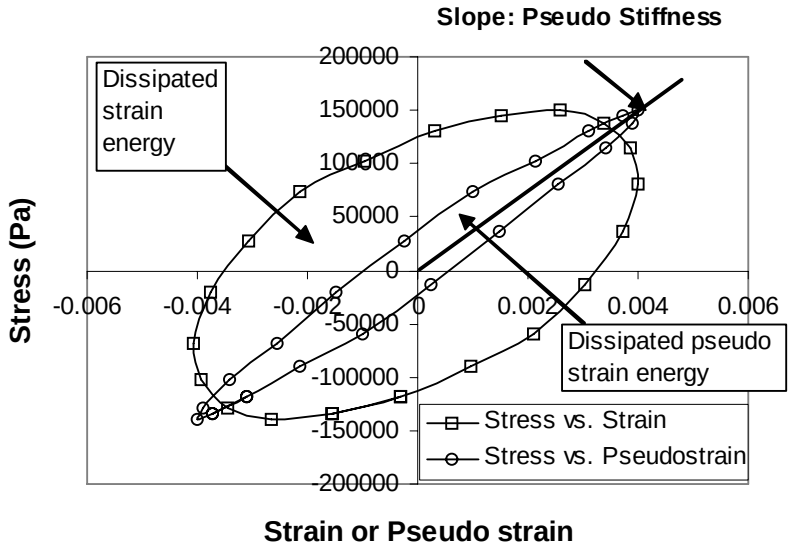

Figure 49. Typical Nonlinear Viscoelastic Hysteretic Behavior Resulting from DMA Fatigue Tests.

After sample fabrication and preconditioning, each sample was mounted in the DMA, and the chamber was closed and allowed to equilibrate to the desired testing temperature (25°C). Every test was begun after a 20-minute period of equilibration at the test temperature.

As Kim et al. proposed, pseudo stiffness (S^R), which is a ratio of corresponding stress to maximum pseudo strain, can also be used to quantify damage (1998). A graphical expression of the pseudo stiffness is illustrated in Figure 49.

$$S^R = \frac{\tau_m}{\gamma_m^R} = \frac{\tau_m}{\gamma_0} \tag{59}$$

Where τ_m = physical stress corresponding to γ_m^R.

Viscoelastic mechanical behavior due to fatigue damage can be scientifically analyzed by the use of a continuum mechanics-based fatigue life prediction model. The continuum mechanics-based fatigue model was originally developed by Lee et al. based on the pseudo strain concept and work potential theories (2002). A more detailed description of the model can be found in elsewhere (2000, 2002). Recently, Kim et al. modified the model to be used for DMA torsional fatigue testing data to investigate filler effects on fatigue resistance of asphalt mastics (2003). The use of this model is also appropriate to study the effects of moisture on asphalt mastic sensitivity to fatigue damage. A usable form of this model is presented as:

$$N_f = \frac{f(S_f)^k}{k(0.5 I_P C_1 C_2)^\alpha}(\gamma_0)^{-2\alpha} \tag{60}$$

Where I_P = initial pseudo stiffness,

$k = 1 + (1 - C_2)\alpha$,

f = as defined previously,

S_f = damage parameter to fatigue failure,

α = material parameter relating to the material's viscoelastic properties, and

C_1, C_2 = regression constants determined by plotting of pseudo stiffness versus damage parameter.

It should be noted that Equation 60 is described differently from the fatigue life prediction model presented in the previous study by Kim et al., since the reference shear modulus in Equation 60 is the linear viscoelastic dynamic modulus to convert pseudo strain expression into applied physical strain (2003).

LABORATORY TESTS AND RESULTS

Researchers performed two different sets of DMA tests. Dynamic shear frequency sweep tests were conducted on both wet and dry sand asphalt samples to define linear viscoelastic material properties. A shear strain, 0.009 percent, which is low enough not to cause any nonlinear damage, was selected and applied as loading frequencies increased from 0.01Hz to 10Hz at 25^{o}C. Linear viscoelastic material property measurements are summarized in Table 9. As can be seen, dynamic shear moduli were somewhat lower due to the presence of moisture, while phase angle and m-value (slope of the log modulus versus the log of loading frequency graph) did not show any significant difference due to moisture in this present study. However, the effect of moisture on linear viscoelastic material properties should be studied in a more general way with a sufficient amount of testing data. Based on testing results, one might infer that moisture penetrated into the mastic (binder and mineral filler – black phase) and/or into the binder-sand particle interfaces so that the infiltrated moisture reduces stiffness of the sample. The linear viscoelastic dynamic modulus and the phase angle presented in Table 9 are used for nonlinear viscoelastic pseudo variable analyses.

Table 9. Linear Viscoelastic Material Properties and Damage Characteristics Resulted from DMA Tests

	Dry	Wet
	Material Properties	
Dynamic modulus (in MPa at 10 Hz)	76.7	65.9
Phase angle (in degree at 10 Hz)	46.2	45.4
m-value	0.482	0.480

	CDPSE[1] to Sample Failure			
	0.28% strain	0.40% strain	0.28% strain	0.40% strain
Sample #1	2115397	2143803	1346249	1554611
Sample #2	2980019	2583839	1301590	1235635

	Fatigue Life[2]			
	0.28% strain	0.40% strain	0.28% strain	0.40% strain
Sample #1	21610(24690)	9810(10318)	11310(9997)	6310(5634)
Sample #2	27910(24322)	11110(10720)	10010(11182)	5110(5905)

	Continuum Fatigue Model Parameters	
Average I_P	50732133	48610941
C_0	1.230	1.075
C_2	0.2130	0.2888
C_1C_2	0.05267	0.03699
α	1.2	0.9
k	1.9445	1.6400
Average S_f	334.88	280.02

Note
[1:] CDPSE: cumulative dissipated pseudo strain energy
[2]: measured fatigue life (calculated fatigue life from continuum fatigue model)

To simulate fatigue damage, researchers repeated the strain-controlled dynamic time sweep tests for several samples at two different shear strain levels: 0.28 and 0.40 percent; at 25°C and 10Hz. The applied shear strains are high enough to produce fatigue damage. Hysteretic behavior, which is illustrated in Figure 50, clearly demonstrates that each sample experiences fatigue damage. The existence of an area within the hysteretic loop (dissipated pseudo strain energy) reflects that microdamage has occurred during fatigue loading cycles. It is also obvious that wet samples undergo a higher level of damage compared to dry samples. This can be monitored by the lower values of pseudo stiffness and lower levels of dissipated pseudo strain energy.

A representative data set at different strain levels is compared in Figure 51 using the reduction in normalized pseudo stiffness versus the number of loading cycles to complete fatigue failure as the indicator of damage. Clearly, the rate of pseudo stiffness reduction increases when higher levels of strain are applied and when samples contain moisture. Moisture accelerates fatigue damage and correspondingly reduces fatigue life. In this study, the fatigue life was defined as described in previous studies (2003). Kim concluded that a transition point in the plot of shear modulus versus loading cycles in the DMA test is the most reasonable estimate of fatigue failure. This transition point occurs between two inflection points. Furthermore, as explained by Kim (2003), the transition point corresponds to the point at which the phase angle reaches a maximum value, as defined by Reese (1997). Using this fatigue failure criterion, fatigue life at each strain level with and without moisture is presented in Table 9. Dry samples demonstrate a longer fatigue life and less strain level dependency than wet samples. Moisture clearly reduces fatigue resistance, and the impact of moisture becomes more dominant, especially when higher level of strain was applied.

Figure 52 is a plot of dissipated pseudo strain energy on a linear-log scale at different strain levels: results from both dry and moisture-conditioned samples. As mentioned, the dissipated pseudo strain energy is considered a simple and theoretically sound damage indicator to estimate viscoelastic material behavior under nonlinear damage. As can be seen in Figure 50, samples in a controlled-strain experiment generally experiences a higher rate of damage in the early stage of fatigue, and the rate of damage then decreases and eventually drops to a very low level. Stiffness reduction during the early stages of the experiment is rapid. This damage might be due to structural fatigue damage such as microcracking. In fact, a detailed experiment was undertaken and discussed by Kim et al. to ensure that the cause of degradation in the modulus was primarily microcrack damage and not heating (2001).

The area below the curve between the dissipated pseudo strain energy and the number of loading cycles represents cumulative dissipated pseudo strain energy. CDPSE physically defines the sample's ability to accumulate damage to failure. Correspondingly, CDPSE at fatigue failure (transition point of fatigue curve) can be employed as a quantitative indicator to define fatigue resistance and/or the ability of a

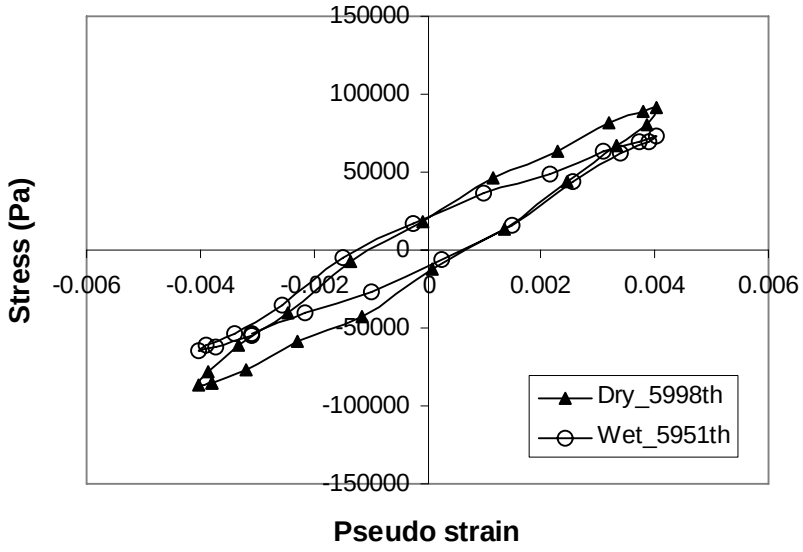

Figure 50. Stress versus Pseudo Strain Hysteretic Fatigue Behavior with and without Moisture.

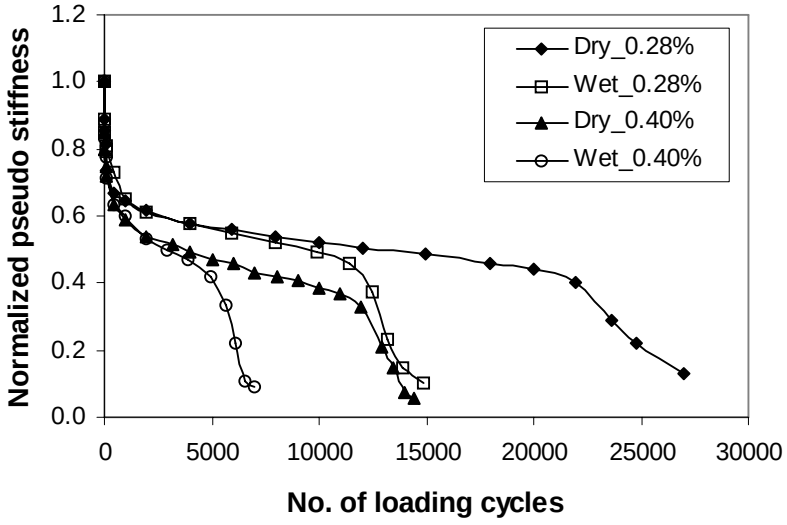

Figure 51. Pseudo Stiffness versus Number of Loading Cycles.

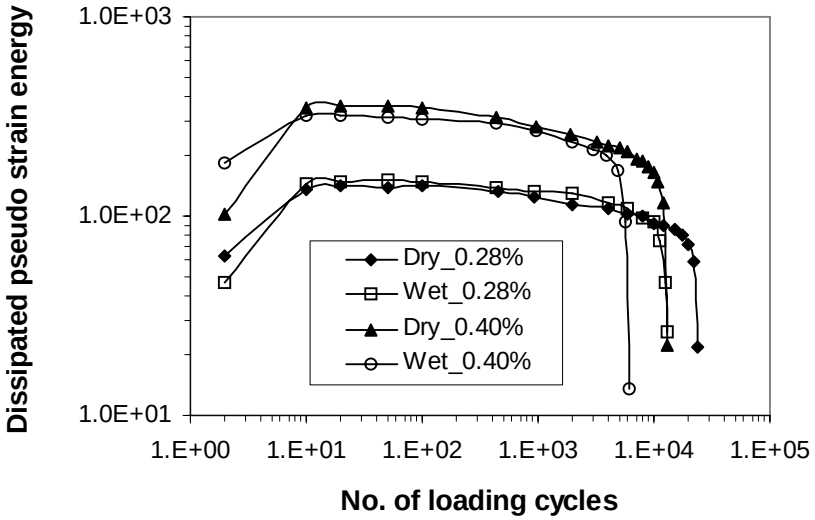

Figure 52. Dissipated Pseudo Strain energy versus Number of Loading Cycles.

specimen to withstand damage before failing. The CDPSE values corresponding to fatigue failure for each sample at different strain levels with and without moisture were calculated and presented in Table 9. As expected, wet samples show less damage accumulation capability than do dry samples. The difference in CDPSE between wet and dry samples can be considered to be a loss of the ability to resist fatigue-damage due to the presence of moisture.

The effect of moisture on fatigue damage can also be estimated by monitoring continuum damage fatigue model parameters. As presented in previous studies, the model parameters are strongly associated with fundamental material properties as well as damage characteristics (2000, 2003). Parameter I_P represents initial level of fatigue damage. Higher values of I_P infer that the sample experiences less initial damage. Regression constants C_1 and C_2 are related to the rate of damage accumulation, and the S_f term defines how much damage the sample can withstand before failure. Assessing the effect of the material parameter α on fatigue resistance is somewhat complex, since α is interactive with several terms. A higher α value tends to increase fatigue life because it increases the value of k (an exponent in the numerator) and affects strain as a negative exponent. On the other hand, α is an exponent in the denominator, and a higher α in the denominator would work against efficient fatigue behavior. If one realizes that

the α represents a curve slope between applied strain levels and fatigue life in Equation 60, it can be concluded that the overall effect of an increase in α is to increase fatigue life. A higher value of α infers a lower rate of curve slope and a correspondingly longer fatigue life.

Table 9 summarizes the model parameters included in Equation 60 are summarized in Table 9. Wet samples typically show lower values of I_P, α, k, and S_f, and a higher value of C_2 than dry samples. Based on the observations of the model parameters, it can be concluded that moisture reduces fatigue resistance and fatigue life of materials due to a higher level of initial damage and strain level dependency, a faster rate of damage evolution, and a lower tolerance for total damage accumulation. These findings are quite consistent with the analyses based on the use of dissipated pseudo strain energy and cumulative dissipated pseudo strain energy.

APPLICATON OF DMA TESTING TO ASSESS MOISTURE DAMAGE POTENTIAL

Recent work at Texas A&M University as described by Cheng et al. (2002, 2003) show that moisture damage potential in asphalt mixtures can be assessed by measuring surface energies of the components: asphalt binder or mastic and the aggregate. If the non polar (Lifshitz Van der Waals) and polar (acid-base) parts of each component are measured, then cohesive bond energies and adhesive bond energies can be and have been calculated. Furthermore, Cheng et al. used the Universal Sorption Device (USD) to determine how much water can be absorbed into various asphalt binders. They were able to develop a methodology to separate the moisture vapor absorbed into the asphalt binder from that adsorbed onto the asphalt surface using Ficks second law. They found that the rate of diffusion and the amount of water that is actually absorbed into the binder varies considerably from asphalt binder to asphalt binder. They also found that the amount of moisture vapor absorbed ranged from approximately 2500 parts per million in asphalt AAD-1, to approximately 1000 parts per million, in asphalt AAM-1. This degree of absorption can significantly alter the rheological response of the asphalt binder and/or mastic. Furthermore, work by Kim et al. (2003) have shown that the ability of an asphalt mastic to resist damage is strongly influenced by the mineral filler present in the asphalt cement. The DMA testing methodology presented in this paper offers a tool by which to directly assess the impact of moisture damage on a blend of asphalt mastic and fine aggregate, in this case Ottawa sand. The DMA test results can be used to validate predictions of cohesive and adhesive bond strength in fine aggregate mixtures based on the application of surface energy principles, as previously discussed. Since the adhesive bond between binder or mastic and aggregate in the presence of moisture can also be calculated based on surface energy principles, use of DMA testing to assess moisture damage based on surface energy calculations has great potential. DMA testing can also

be used to assess the impact of mineral filler and comparison of damage analyses of various fine aggregate mixtures, dry and in the presence of moisture.

According to Cheng et al. (2002), adhesive surface energies can be calculated by measuring surface energies of each mixture constituent: asphalt binder, aggregate, and water.

$$\Delta G_d = 2\left(\sqrt{\Gamma_b^{LW}\Gamma_a^{LW}} + \sqrt{\Gamma_b^{+}\Gamma_a^{-}} + \sqrt{\Gamma_b^{-}\Gamma_a^{+}}\right) \tag{61}$$

$$\begin{aligned}\Delta G_w = {} & 2\Gamma_w^{LW} + 2\sqrt{\Gamma_b^{LW}\Gamma_a^{LW}} - 2\sqrt{\Gamma_b^{LW}\Gamma_w^{LW}} - 2\sqrt{\Gamma_a^{LW}\Gamma_w^{LW}} + \\ & 4\sqrt{\Gamma_w^{+}\Gamma_w^{-}} - 2\sqrt{\Gamma_w^{+}}\left(\sqrt{\Gamma_b^{-}} + \sqrt{\Gamma_a^{-}}\right) - 2\sqrt{\Gamma_w^{-}}\left(\sqrt{\Gamma_b^{+}} + \sqrt{\Gamma_a^{+}}\right) + \\ & 2\sqrt{\Gamma_b^{+}\Gamma_a^{-}} + 2\sqrt{\Gamma_b^{-}\Gamma_a^{+}}\end{aligned} \tag{62}$$

Where Γ^{LW} = Lifshitz-van der Waals component of the surface energy,

Γ^{+} = Lewis acid component of the surface energy,

Γ^{-} = Lewis base component of the surface energy, and

b, a, w = each subscript represents asphalt binder, aggregate, and water, respectively.

The power of this relationship can be illustrated by the following simple equation:

$$R_i = \frac{\Delta G_d (1 - P_i) + \Delta G_w P_i}{\Delta G_d} \tag{63}$$

Where R_i = ratio of a damage indicator between wet and dry conditions,

P_i = percentage of surface area of the aggregate that is replaced by moisture,

ΔG_d = adhesive surface energy between asphalt and aggregate without moisture,

ΔG_w = adhesive surface energy between asphalt and aggregate with moisture, and

i = i th number of loading cycle.

In DMA testing, the ratio of damage indicator is defined as:

$$R_i = \frac{PS_{i,w}^{N}}{PS_{i,d}^{N}} \tag{64}$$

Where $PS_{i,w}^{N}$ = normalized pseudo stiffness of a wet sample at i th loading cycle, and

$PS_{i,d}^{N}$ = normalized pseudo stiffness of a dry sample at i th loading cycle.

Equations 63 and 64 relate the ratio of wet modulus of a mixture to the dry modulus of the mixture. Note that the modulus ratio is related to the ratio of the total bond strength of the wet system to the total bond strength of the dry system. Furthermore, the total bond strength of the wet system is the summation of the product of the dry bond strength between the aggregate and the asphalt cement or mastic, ΔG_d, and the area of the bond $(1 - P_i)$, and the bond strength between the aggregate and asphalt cement in the presence of moisture, ΔG_w, and the area influenced by moisture, P_i. Table 10 compares surface energies for three binder-aggregate systems. In case 1, the binder is asphalt AAD-1 and the aggregate is quartz sand. In case 2, the same quartz sand aggregate is blended with asphalt AAM-1 instead of AAD-1. In case 3, the AAD-1 binder is blended with a limestone in lieu of a quartz sand. The Γ-values in Table 10 are surface energies for the binder (subscript b) and aggregates (subscript a), respectively. The ΔG-values are adhesive bond energies for the dry (subscript d) and wet (subscript w) conditions, respectively. Note that the value of ΔG_w is always a negative value, indicating that bond energy between the asphalt cement and aggregate is released in the presence of moisture or that moisture will replace asphalt cement at the interface. The potential of water to replace the asphalt cement bond is directly proportional to the magnitude of this negative value. The more negative the value of ΔG_w is, the greater is the potential for asphalt-aggregate bond loss. Therefore, as Cheng et al. conclude, the most moisture-resistant asphalt mixtures are those that have the highest (most positive) value of ΔG_d and the least negative value of ΔG_w (2002). The DMA test can be used in conjunction with or to validate this approach. In addition, the DMA test can be used to validate the logical hypothesis that the binder or mastic that absorbs the most water is more susceptible to moisture damage. Actually, Cheng et al. (2002, 2003) have already validated these hypotheses via full scale mixture testing; however, the DMA experiment is much more efficient and easier to analyze than full scale mixture testing. It therefore, provides an excellent test by which to assess the moisture resistance of the black phase or sand asphalt of the asphalt mixture, which is often the most moisture damage prone phase.

As a test of this hypothesis, case 1 (AAD-1 and quartz sand) and case 2 (AAM-1 and quartz sand) were evaluated using the DMA moisture damage test. Using the ratio of number of load cycles to failure as a criterion, the effect of moisture on the case 1 mixture was more severe than the effect of moisture on the case 2 mixture $(N_{f\,wet}/N_{f\,dry})_{case\ 1} = 0.45$ while $(N_{f\,wet}/N_{f\,dry})_{case\ 2} = 0.60$.

Table 10. Arbitrarily Determined Adhesive Surface Energies (Unit: ergs/cm^2)

	Surface Energies		
	Case 1	Case 2	Case 3
Γ_b^{LW}	8.59	9.33	8.59
Γ_b^+	5.96	17.79	5.96
Γ_b^-	14.48	21.40	14.48
Γ_a^{LW}	64.8	64.8	86.5
Γ_a^+	11.0	11.0	0.4
Γ_a^-	250.8	250.8	285.5
ΔG_d	149.8	213.5	141.8
ΔG_w	-63.7	-27.4	-66.9

Note: For every case, surface energy of water: $\Gamma_w^{LW} = 21.8,\ \Gamma_w^+ = 25.5,\ \Gamma_w^- = 25.5$

Figure 53 presents the calculated values of R_i at a strain level of 0.28 percent (large enough to cause damage) and the P_i value based on Equation 70. This plot represents asphalt AAD-1 and sand, Case 1 in Table 10. Similar plots for Cases 2 and 3 can be developed and compared. The value of P_i indicates moisture damage evolution represented by adhesive fracture at the interfaces between binder and aggregate due to the presence of moisture. By observing the value of P_i as the number of loading cycles increases, potential moisture damage susceptibility of each different asphalt-aggregate system can be estimated, since each different system possesses different combinations of surface energy characteristics and damage evolution behavior between wet and dry conditions.

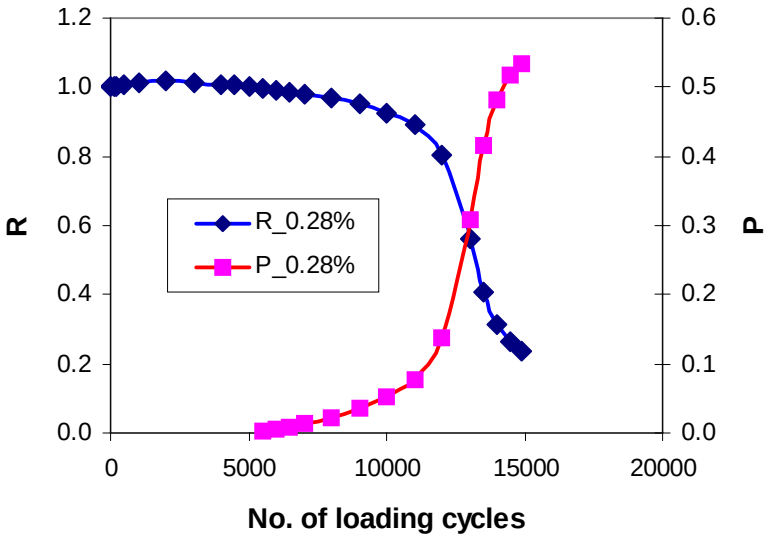

Figure 53. Variation of Wet-to-Dry Pseudo Stiffness Ratios and Percentage of Aggregate Surface Exposed to Moisture as the Number of Loading Cycles Increases.

CONCLUDING REMARKS

The effects of moisture on fatigue damage and fracture of asphalt binders and/or mastics were evaluated successfully using the DMA for one SHRP-classified binder, AAD-1 in this study. The experimental procedure described in this project using the DMA offers a macroscopic evaluation of moisture damage that can be related to fundamental material properties such as viscoelastic properties and surface energy characteristics and damage evolution characteristics. The testing method is relatively fast and efficient and offers a valuable tool to directly assess moisture damage potential in a fine aggregate mixture where moisture damage is often of considerable concern.

The use of two reliable nonlinear viscoelastic damage indicators, pseudo stiffness and dissipated pseudo strain energy; clearly demonstrated that moisture significantly reduces fatigue resistance and ultimately fatigue life of asphalt mixtures. Based on scientific observations using a continuum damage fatigue model, we conclude that mixtures in the presence of moisture usually experience a higher level of initial damage as well as a faster rate of damage evolution.

Mechanical fatigue testing results from DMA should be performed in conjunction with cohesive bond and adhesive bond (dry and in the presence of water) calculations as

a validation of the calculations and to monitor the impact of the bond strength calculation from these basic material properties on measured performance. Analysis results indicate that moisture damage susceptibility depends strongly on surface energy characteristics of individual mixture constituents.

Future research will extend this approach to other DMA mixtures composed of different binders and fine aggregates. Effects of material aging and/or binder additives on moisture damage can also be evaluated. Since each system has different material characteristics such as viscoelastic material properties and surface energies, the DMA test together with surface energy principles can be used as a landmark to maximize moisture damage resistance.

CHAPTER 7. FURTHER DEVELOPMENT OF DMA ANALYSIS

METHODOLOGY

Zollinger (2005) developed a new fabrication method for DMA specimens based on the previous work of Kim (2003). In this approach, the filler is mixed with the pure binder at the pre-determined mixing temperature. The binder-filler mixture is then mixed with aggregate using a mechanical mixer, as is used to produce gyratory specimens at the mixing temperature. The loose mixture is then placed in the oven and aged at the proper aging temperature for 2 hours for short-term oven aging. The temperature is then changed to the compaction temperature for 1 hour.

The theoretical maximum specific gravity is determined for the mixtures used to prepare the DMA specimens. The loose mixture is placed in a 150 mm diameter gyratory mold and compacted using a Superpave gyratory compactor to a target air void content of 11 percent and a height of 85 mm. The sample is allowed to cool for 1 day. Each side of the specimen is trimmed about 17.5 mm to a sample height of 50 mm. Approximately 32 DMA specimens are cored from the 150 mm diameter and 50 mm tall gyratory compacted sample, as illustrated in Figure 54.

To use the DMA testing methodology to evaluate moisture damage, some DMA samples are tested in the dry condition, while others are preconditioned with moisture. Preconditioning is achieved following the method described in Chapter 6. The first step is to allow moisture to penetrate the specimen by placing the specimen in distilled water and applying vacuum pressure to accelerate moisture permeation. The specimen remains under vacuum for 1 hour. As described in Chapter 6, the average saturation level (volume of absorbed water to the volume of air voids) is approximately 125 percent, meaning some moisture may have diffused into the mastic.

DMA testing was performed (by Zollinger 2005) using a Bohlin Instruments CVOR 200 rheometer. The sample holders that came with the device required tightening of two screws on each end, which caused some misalignment. Therefore, sample holders and solid fixtures for the cylindrical samples were fabricated at the TTI machine shop. The new solid fixtures require tightening one set screw, which eliminated misalignment problems.

DMA testing begins with placing a DMA sample in the sample holder using glue as shown in Figure 55a. The glue requires 20 minutes to stiffen. The specimen is then mounted into the DMA chamber (Figure 55b) solid fixtures and time given to equilibrate to the desired testing temperature of 25^{o}C, as shown in Figure 55c.

Figure 54. A Cored Superpave Gyratory Specimen.

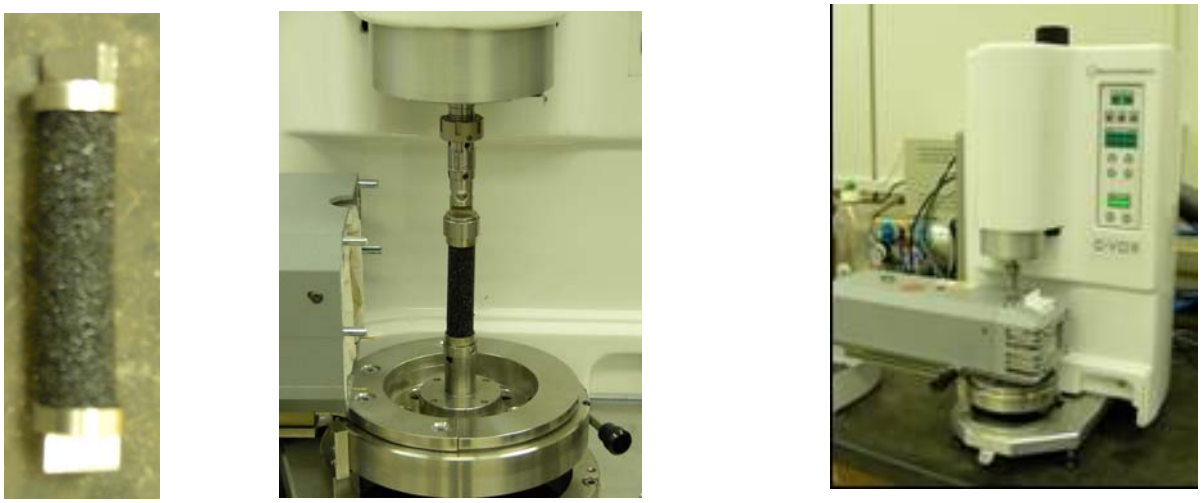

(a) **(b)** **(c)**

Figure 55. (a) Specimen Placed in Sample Holders for DMA Testing, (b) A Sample Mounted in DMA, (c) Temperature Equilibrium.

A DMA specimen is subjected to sinusoidal torsional strain loading. The resulting stress is also sinusoidal but out of phase with strain with a magnitude equal to the phase angle, as seen in Figure 56. To determine the linear viscoelastic material properties, dynamic modulus, and phase angle, a strain-controlled torsional cyclic test is

conducted at a strain of 0.0065 percent, which is within the linear viscoelastic range, and at a frequency of 10 Hz. These properties are subsequently used to compute pseudostrain during the fatigue damage portion. To simulate fatigue damage, the same sample is then subjected to strain-controlled cyclic torsion at 0.3 percent strain at 10 Hz until failure. It is assumed that the total dissipated energy is the same irrespective of the loading strain level.

Researchers also used the DMA to conduct a relaxation test within the LVE range on DMA specimens. In this test, a constant shear strain γ_o was applied, and the stress response $\tau(t)$ was recorded.

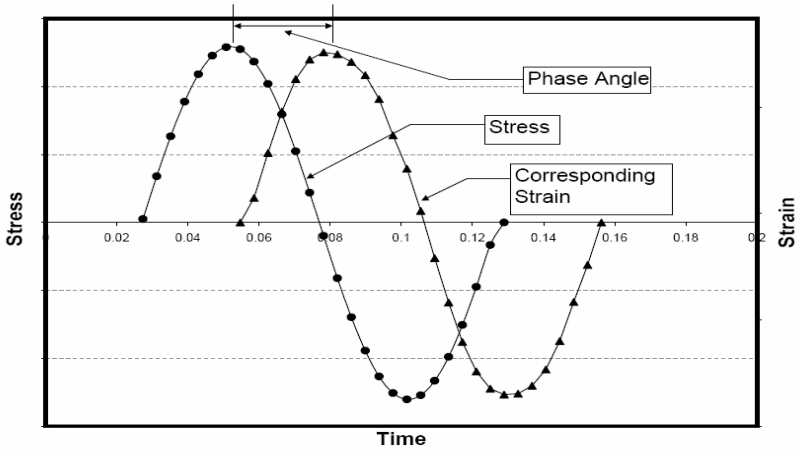

Figure 56. Typical DMA Sample Time Profile of Stress and Strain.

The eight mixtures selected represent varying mixture designs, geological origins of aggregates, and binder grades. Table 11 includes a summary of these mixtures. The details on mix design and aggregate gradations are given by Zollinger (2005).

Table 11. Mixture Descriptions.

Mix #	Location	Reported Field Moisture Performance	Binder Grade
1	Wichita Falls, TX	Hamburg Data Only	PG 76-22
2	Wichita Falls, TX	Hamburg Data Only	PG 76-22
3	Atlanta, TX	Good	PG 76-22
4	Atlanta, TX	Good	PG 76-22
5	Atlanta, TX	Good	PG 76-22
6	Atlanta, TX	Good	PG 76-22
7	Ashland County, OH	Poor	PG 64-22
8	Wayne County, OH	Poor	PG 64-28

Zollinger (2005) prepared DMA cylindrical specimens by mixing the binder with the finer portion (minus 1.18 mm to pan) of the aggregate gradation. The DMA specimen aggregate gradation was proportioned according to the job mix formula (JMF), as shown in Table 12.

Table 12. DMA Aggregate Gradations.

Sieve Size (mm)	**Mix 3**			**Mix 4**		
	Quartzite Screenings	**Granite Donnafill**	**Hyd Lime**	**Sandstone Screenings**	**Granite Donnafill**	**Hyd Lime**
1.18	100.0	100.0	100.0	100.0	100.0	100.0
0.6	61.4	94.8	100.0	61.1	94.8	100.0
0.3	22.8	57.3	100.0	49.7	57.3	100.0
0.15	12.3	22.4	100.0	26.9	22.4	100.0
0.075	1.8	1.8	100.0	1.7	1.7	100.0
Sieve Size (mm)	**Mix 5**			**Mix 6**		
	Limestone Screenings	**Hyd Lime**		**Sandstone Screenings**	**Field Sand**	**Hyd Lime**
1.18	100.0	100.0		100.0	100.0	100.0
0.6	61.2	100.0		-	-	-
0.425	-	-		40.2	98.5	100.0
0.3	49.7	100.0		-	-	-
0.15	26.9	100.0		18.0	28.8	100.0
0.075	1.8	100.0		-	-	-
Sieve Size (mm)	**Mix 7**			**Mix 8**		
	Limestone Sand	**Natural Sand**		**Limestone Sand**	**Natural Sand**	
1.18	100.0	100.0		100.0	100.0	
0.6	60.1	64.0		60.1	64.0	
0.425	-	-		-	-	
0.3	25.4	23.3		25.4	23.3	
0.18	-	-		-	-	
0.15	6.3	2.9		6.3	2.9	
0.075	1.8	1.8		1.8	1.8	

The aggregate passing the 0.075 mm sieve is considered to be filler and is mixed with the pure binder at the pre-determined mixing temperature for the mixture. If the volume of filler is 10 percent of the binder volume, then 8 percent binder-filler mixture by mass of aggregate is mixed with the aggregate at the mixing temperature.

The DMA was used to evaluate each mixture's ability to accumulate damage. The DMA applies a cyclic, torsional strain-controlled loading to cylindrical asphalt mastics until failure. For each mixture, a minimum of 10 samples were tested in both the wet and dry conditions.

Linear viscoelastic properties were determined with a cyclic loading strain amplitude equal to 0.0065 percent during the low-strain portion of the testing protocol and are presented in Table 13. Mixture 5 has the highest dry LVE dynamic modulus of 242×10^6 Pa, with the lowest dry LVE phase angle of 19.2°. Mixture 8 has the lowest dry LVE dynamic modulus of 108.4×10^6 Pa, with the highest dry LVE phase angle of 33.5°.

The relaxation test results were used to calculate the relaxation modulus as in Equation (1):

$$G(t) = \frac{\tau(t)}{\gamma_o} = G_\infty + G_1 t^{-m} \tag{65}$$

The parameters of Equation 65 are shown in Table 14. G_∞ was almost equal to zero for the specimens tested in this study.

Table 13. DMA Linear Viscoelastic Dynamic Modulus and Phase Angle at 10 Hz in Both Dry and Wet Conditions.

Mix	LVE Modulus (G*) (Pa)		LVE Phase Angle (δ) (°)	
	Dry ($\times 10^6$)	Wet ($\times 10^6$)	Dry	Wet
3	177.9	174.6	24.0	24.1
4	188.9	143.5	22.9	29.0
5	242.0	206.0	19.2	26.3
6	163.3	146.7	30.5	33.7
7	158.1	190.8	26.6	22.8
8	108.4	134.2	33.5	29.9

Table 14. Average G_1 and m Values.

Mix	G_1 (Pa)		m	
	Dry ($\times 10^6$)	Wet ($\times 10^6$)	Dry	Wet
3	65.8	36.7	0.38	0.26
4	40.9	27.6	0.34	0.30
5	79.4	57.6	0.31	0.23
6	23.9	20.4	0.42	0.38
7	30.1	34.1	0.54	0.37
8	12.1	18.0	0.45	0.45

Empirical Parameters for Evaluation of Moisture Damage

As described by Kim (2003), the peak of the product of NxG′/G proved to be the best indicator of fatigue failure (Figure 57).

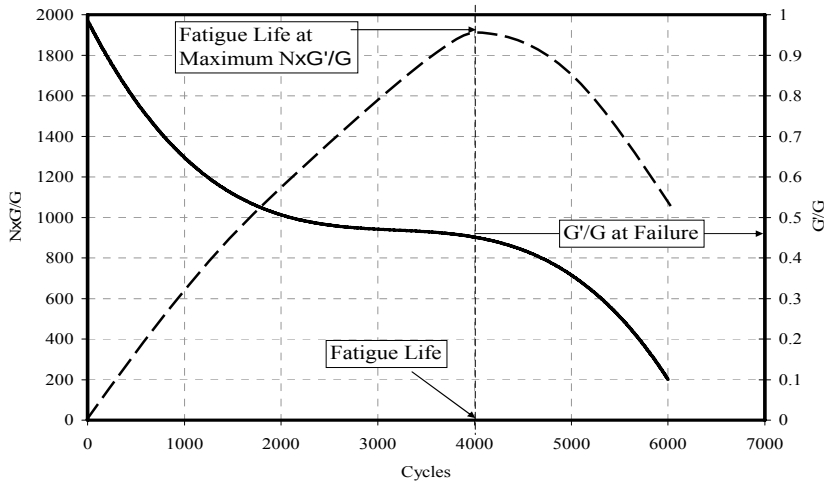

Figure 57. Typical Plot of N×G*'/G* and G*'/G* versus Number of Load Cycles.

Table 15 provides the average fatigue life in both the wet and dry conditions, along with the moisture damage parameter wet N_f/Dry N_f. The higher the wet/dry ratio, the better the mixture performs, as the wet fatigue life is closer to the dry fatigue life. Mixture 4 has the highest ratio of 0.9, while Mixture 3 has the lowest at 0.08. This parameter correlates very well with the reported field performance and surface energy parameters, except for Mixture 3. Mixture 3 had the highest dry fatigue life; however, it had the lowest wet fatigue life. A possible reason for this poor resistance to moisture damage is the high angularity of the Mixture 3 quartzite particles as compared to those used in the other mixtures. Particles retained on the 0.3 mm sieve were analyzed for

angularity using AIMS and are reported in Figure 58. This discussion regarding the effect of angularity is developed further by Zollinger (2005).

The Mixture 3 quartzite particles are 20 percent more angular than the next highest angular aggregate. As discussed earlier in this paper, high angularity of aggregates could cause puncturing of asphalt film, which accelerates water intrusion to the asphalt-aggregate interface and moisture damage.

Table 15. Mixture Rankings According to Average Fatigue Life in Both Dry and Wet Conditions.

Mix	Reported Performance	Average Fatigue Life (N_f)		$\frac{\text{Wet } N_f}{\text{Dry } N_f}$
		Dry	Wet	
3	Good	25,205	2,083	0.08
4	Good	16,349	14,671	0.90
5	Good	13,628	5,330	0.39
6	Poor	13,541	5,603	0.41
7	Poor	3,159	803	0.25
8	Poor	8,767	2,231	0.25

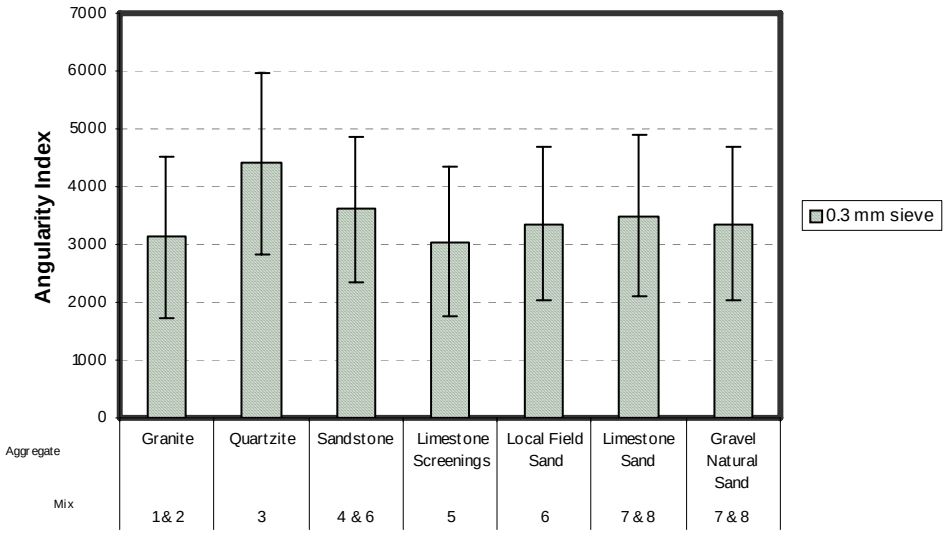

Figure 58. Fine Aggregate Angularity Index.

Table 16 shows the ratio of the dynamic modulus at failure to the initial dynamic modulus. This parameter describes the amount the mastic dynamic modulus can decrease while still accumulating damage. Mixture 5 has the highest dry G^{*}'/G^{*} at 0.549. Mixture 7 has the lowest dry reduced dynamic modulus at 0.387, yet the highest wet value of 0.672. Since the Mixture 3 dry value is 0.448 and wet value is 0.608, the wet samples clearly failed prematurely, supporting the effect of high angularity as the cause. The lower the moisture damage parameter of Wet/Dry, the better the mixture resistance to moisture damage. Based on this parameter, Mixture 4 had the lowest value of 0.91, and Mixture 7 had the highest value of 1.74. The results in Table 16 indicate that the 50 percent reduction in stiffness, which is commonly taken as the threshold of damage, does not represent all materials.

Table 16. Mixture Rankings According to Reduction in Dynamic Modulus (G^{*}'/G^{*}) at Fatigue Life in Both Dry and Wet Conditions.

Mix	Reported Performance	G^{*}'/G^{*} at Fatigue Life		Wet / Dry
		Dry	Wet	
3	Good	0.44	0.60	1.36
4	Good	0.46	0.42	0.91
5	Good	0.54	0.62	1.14
6	Poor	0.37	0.40	1.08
7	Poor	0.38	0.67	1.74
8	Poor	0.43	0.49	1.16

This work by Zollinger (2005) lends considerable credibility to the work described in Chapters 1-6 describing the development of the DMA methodology used to assess the impact of mineral filler and fine aggregate on HMA fracture fatigue, for both dry and wet mixtures.

CHAPTER 8. CONCLUSIONS AND RECOMMENDATIONS

CONCLUSIONS

Based on the study, the following conclusions can be drawn.

- Dynamic mechanical analysis can be effectively used to characterize basic material properties, the fatigue behavior of asphalt binders, and the fine aggregate mastics in a torsional mode.

- The DMA is a tool that is capable of defining the impact on fatigue life of asphalt cement mastics and fine aggregate. The protocol described in this project using sand asphalt mixtures in the form of a cylindrical sample provides acceptable data.

- Among the first inflection point, the second inflection point, and the transition point (N_t) based on the product of stiffness and the number of load cycles, the N_t is a reasonable point by which to identify failure and correlates well with the point of maximum phase angle.

- Three different damage parameters, a decay in pseudo stiffness, a loss of nonlinear dynamic modulus, and a change in dissipated strain energy, showed similar behavior when normalized. The three different damage parameters proved to be effective as monitors of fatigue damage during torsional loading.

- Careful analysis of the shape of the relationship between normalized NDM and number of load cycles can be effectively used to understand the mechanisms of fatigue failure, which were shown in this study to vary among asphalt systems. For example, the high cure rubber modified binders fatigue in a very different manner and due to a different mechanism than the traditional, unmodified binders. This is evident based on the slopes of the damage curves, which indicate rate of damage and the impact of the binder-modifier structure that impacts the response mechanism.

- Modified binders generally show much longer fatigue life than other neat binders, even though the modified binders were aged. The aged HCR binders generally approached failure faster than the unaged binder especially at a lower strain level, and the degree of aging clearly influences fatigue life.

- The continuum damage mechanical fatigue prediction model developed by Lee et al. (2000) was successfully extended from uniaxial fatigue, as developed by Lee

et al., to the torsion mode. In addition, the definition of fatigue failure was based on the transition definition of fatigue damage rather than 50 percent of PS reduction as proposed by Lee et al. (2000).

- By observing continuum damage mechanical model parameters, it can be concluded that the polymer and/or rubber modified binder demonstrates longer fatigue life because it is soft but capable of accumulating more damage before failure due to a slow rate of stiffness reduction.

- Fillers that contribute to fatigue life increase in strain-controlled fatigue testing, even though they stiffen the binders. By employing the continuum damage mechanical fatigue prediction models, one can conclude that fillers provide better resistance to microcracking due to a lower rate of damage evolution and higher capability for total damage accumulation. Hydrated lime was more effective than limestone filler, which infers that mechanisms other than a volume filling effect occur.

- The improvement in fatigue life due to hydrated lime is much greater for the AAD-1 mix than for the AAM-1 mix. This indicates that the physico-chemical interaction between binder and filler is dependent on the types of material. This is quite consistent with previous research findings.

- Work by Zollinger (2005) has developed a DMA test methodology based on the empirical and theoretical development by Kim (2003), which successfully applied the DMA analysis to asphalt mixtures prepared with aggregate passing the No. 16 sieve. This technique defines the impact of fine aggregate and mineral filler on the fatigue damage of asphalt mixtures in both a dry and wet environment.

REFERENCES

Allen, D. H., Jones, R. H., and Boyd, J. G., (1994), "Micromechanical Analysis of a Continuous Fiber Metal Matrix Composite Including the Effects of Matrix Viscoplasticity and Evolving Damage," *Journal of Mechanical Physic Solids,* Vol. 42, No. 3, pp.505-529.

Allen, D. H. and Searcy, C. R., (2000), "Numerical Aspects of a Micromechanical Model of a Cohesive Zone," *Journal of Reinforced Plastics and Composites*, Vol. 19, No. 3, pp. 240-248.

Allen, D. H. and Searcy, C. R., (2001a), "A Micromechanical Model for a Viscoelastic Cohesive Zone," *International Journal of Fracture*, Vol. 107, pp. 159-176.

Allen, D. H. and Searcy, C. R., (2001b), "A Micromechanically Based Model for Predicting Dynamic Damage Evolution in Ductile Polymers," *Mechanics of Materials*, Vol. 33, pp. 177-184.

Anderson, D. A., (1987), "Guidelines for Use of Dust in Hot Mix Asphalt Concrete Mixtures," *Proceedings Association of Asphalt Paving Technologists*, Vol. 56, pp. 492-516.

Anderson, D. A. and Goetz, W. H., (1973), "Mechanical Behavior and Reinforcement of Mineral Filler-Asphalt Mixtures," *Proceedings Association of Asphalt Paving Technologists,* Vol. 42, pp. 37-66.

Anderson, D. A., Le Hir, Y. M., Marasteanu, M. O., Planche, J., and Martin, D., (2001), "Evaluation of Fatigue Criteria for Asphalt Binders." *Transportation Research Record 1766*, Transportation Research Board, Washington, D. C., pp. 48-56.

Bahia, H., Zhai, H., Bonnetti, K., and Kose, S., (1999), "Non-linear Viscoelastic and Fatigue Properties of Asphalt Binders," *Journal Association of Asphalt Paving Technologists*, Vol. 68, pp. 1-34.

Barenblatt, G. I., (1962), "The Mathematical Theory of Equilibrium Cracks in Brittle Fracture," *Advances in Applied Mechanics*, Vol. 7, pp. 55-129.

Bhurke, A. S., Shin, E. E., and Drzal, L. T., (1997), "Fracture Morphology and Fracture Toughness Measurement of Polymer-modified Asphalt Concrete," *Transportation Research Record*, *1590*, Transportation Research Board, Washington, D. C., pp. 23-33.

Bonnetti, K. S., Nam, K., and Bahia, H., (2002), "Measuring and Defining Fatigue Behavior of Asphalt Binders," *Paper Presented at 81th Annual Meeting*, Transportation Research Board, Washington, D. C.

Buttlar, W. G., Bozkurt, D., Al-Khateeb, G. G., and Waldhoff, A. S., (1999), "Understanding Asphalt Mastic Behavior through Micromechanics," *Transportation Research Record 1681*, Transportation Research Board, Washington, D. C., pp. 157-169.

Cheng, D., (2002), "Surface Free Energy of Asphalt-Aggregate System and Performance Analysis of Asphalt Concrete Based on Surface Free Energy," Ph.D. dissertation, Texas A&M University, College Station, Texas.

Cheng, D., Little, D. N., Lytton, R. L., and Holste, J., (2002), "Use of Surface Free Energy of Asphalt-Aggregate System to Predict Moisture Damage Potential," *Journal of the Association of Asphalt Paving Technologists*, Vol. 71, pp. 59-88.

Cheng, D., Little, D. N.., Lytton, R. L., and Holste, J., (2003), "Moisture Damage Evaluation of Asphalt Mixture by Considering Both Moisture Diffusion and Repeated Load Conditions," paper presented at the meeting of the *Transportation Research Board*, Washington D. C.

Christensen, D. W. and Anderson, D. A., (1992), "Interpretation of Dynamic Mechanical Test Data for Paving Grade Asphalt Cements," *Journal Association of Asphalt Paving Technologists*, Vol. 61, pp. 67-116.

Christensen, R. M., (1982), *Theory of Viscoelasticity: An Introduction,* Academic Press, N. Y.

Cooley, L. A., Stroup-Gardiner, M., Brown, E. R., Hanson, D. I., and Fletcher, M. O., (1998), "Characterization of Asphalt-Filler Mortars with Superpave Binder Tests," *Journal of Association of Asphalt Paving Technologists*, Vol. 67, pp. 42-65.

Costanzo, F. and Allen, D. H., (1993), "A Continuum Mechanics Approach to Some Problems in Subcritical Crack Propagation," *International Journal of Fracture*, Vol. 63, pp. 27-57.

Costanzo, F. and Walton, J. R., (1997), "A Study of Dynamic Crack Growth in Elastic Materials Using a Cohesive Zone Model," *International Journal of Engineering Science*, Vol. 35, pp. 1085-1114.

Craus, J., Ishai, I., and Sides, A., (1978),"Some Physico-Chemical Aspects of the Effect and the Role of the Filler in Bituminous Paving Mixtures," *Journal of Association of Asphalt Paving Technologists,* Vol. 47, pp. 558-588.

Dugdale, D. S., (1960), "Yielding of Steel Sheets Containing Slits," *Journal of the Mechanics and Physics of Solids*, Vol. 8, pp. 100-104.

Glover, C. J., Estakhri, C. K., and Williamson, S. A., (2000), "A Comprehensive Laboratory and Field Study of High-Cure Crumb-Rubber Modified Asphalt Materials," Research Report 1460-1, Texas A&M University, College Station, Texas.

Golden, H. J., Strganac, T. W., and Schapery, R. A., (1999), "An Approach to Characterize Nonlinear Viscoelastic Material Behavior Using Dynamic Mechanical Tests and Analyses," *Journal of Applied Mechanics*, Transactions of the ASME, Vol. 66, pp. 872-878.

Goodrich, J. L., (1988), "Asphalt and Polymer Modified Asphalt Properties Related to the Performance of Asphalt Concrete Mixes," *Journal Association of Asphalt Paving Technologists*, Vol. 57, pp. 116-175.

Goodrich, J. L., (1991), "Asphaltic Binder Rheology, Asphalt Concrete Rheology, and Asphalt Concrete Mix Properties," *Journal Association of Asphalt Paving Technologists*, Vol. 60, pp. 80-120.

Griffith, A. A., (1920), "The Phenomena of Rupture and Flow in Solids," *Philosophical Transactions of the Royal Society of London*, Vol. A221, pp. 163-197.

Gurtin, M. E., (1979), "Thermodynamics and the Griffith Criterion for Brittle Fracture," *International Journal of Solids and Structures*, Vol. 15, pp. 553-560.

Harris, B. M. and Stuart, K. D., (1995), "Analysis of Mineral Fillers and Mastics Used in Stone Matrix Asphalt," *Journal Association. of Asphalt Paving Technologists*, Vol. 64, pp. 54-95.

Helms, K. L. E., Allen, D. H., and Hurtado, L. D., (1999), "A Model for Predicting Grain Boundary Cracking in Polycrystalline Viscoplastic Materials Including Scale Effects," *International Journal of Fracture*, Vol. 95, pp. 175-194.

Helms, K. L. E., (2000), "Modeling the Mechanical Response and Damage Evolution in Inelastic Polycrystalline Solids," Ph.D. Dissertation, Texas A&M University, College Station, Texas.

Hopman, P. C., Kunst, P. J., and Pronk, A. C., (1989), "A Renewed Interpretation Method for Fatigue Measurement, Verification of Miner's Rule," *Proceedings, Fourth Eurobitume Symposium*, Vol. 1, pp. 557-561.

Hopman, P., Vanelstraete, A., Verhasselt, A., and Walter, D., (1999), "Effects of Hydrated Lime on the Behaviour of Mastics and on Their Construction Aging,"

Proceedings of the Durable and Safe Road Pavements, International Conference, Kielce, Poland, Vol. I, pp. 59-67.

Huang, Y. H., (1993), *Pavement Analysis and Design,* Prentice-Hall, Englewood Cliffs, N. J.

Hui, J., Morrison, G. R., and Hesp, S., (1994), "Improved Low-temperature Fracture Performance for Rubber-modified Asphalt Binders," *Transportation Research Record*, *1436*, Transportation Research Board, Washington, D. C., pp. 83-87.

Kavussi, A. and Hicks, R. G., (1997), "Properties of Bituminous Mixtures Containing Different Fillers," *Journal Association of Asphalt Paving Technologists*, Vol. 66, pp. 153-186.

Kim, Y. R., (1988), "Evaluation of Healing and Constitutive Modeling of Asphalt Concrete by Means of the Theory of Nonlinear Viscoelasticity and Damage Mechanics," Ph.D. Dissertation, Texas A&M University, College Station, Texas.

Kim, Y. R., and Little, D. N., (1990), "One-Dimensional Constitutive Modeling of Asphalt Concrete," *Journal of Engineering Mechanics*, ASCE, Vol. 116, No. 4, pp. 751-772.

Kim, Y. R., Whitmoyer, S. L., and Little, D. N., (1994), "Healing in Asphalt Concrete Pavements: Is It Real?" *Transportation Research Record 1454*, Transportation Research Board, Washington, D. C., pp. 89-96.

Kim, Y. R., Lee, Y. C., and Lee, H. J., (1995), "Correspondence Principle for Characterization of Asphalt Concrete," *Journal of Materials in Civil Engineering*, ASCE, Vol. 7, No. 1, pp. 59-68.

Kim, Y. R., Lee, H. J., and Little, D. N., (1997), "Fatigue Characterization of Asphalt Concrete Using Viscoelasticity and Continuum Damage Theory," *Journal Association of Asphalt Paving Technologists*, Vol. 66, pp. 520-569.

Kim, Y. R., Lee, H. J., and Little, D. N. (1998), *Fundamental Properties of Asphalts and Modified Asphalts - Task K: Microdamage Healing in Asphalt and Asphalt Concrete*, Volume 4. Report DTFH61-92-C-00170. FHWA, U.S. Department of Transportation,.

Kim, Y., Little, D. N., and Lytton, R. L., (2001)"Evaluation of Microdamage, Healing, and Heat Dissipation of Asphalt Mixtures Using a Dynamic Mechanical Analyzer," In *Transportation Research Record 1767*, Transportation Research Board, Washington, D. C., pp. 60-66.

Kim, Y., Little, D. N., and Lytton, R. L., (2002) "Use of Dynamic Mechanical Analysis (DMA) to Evaluate the Fatigue and Healing Potential of Asphalt Binders in Sand Asphalt Mixtures", *Journal of the Association of Asphalt Paving Technologists*, Vol. 71, pp. 176-206.

Kim, Y., Little, D. N., and Lytton, R. L. (2003), "Fatigue and Healing Characterization of Asphalt Mixtures," *Journal of Materials in Civil Engineering*, ASCE, Vol. 15, No. 1, pp. 75-83.

Kim, Y.R., (2003) "Mechanistic Fatigue Characterization and Damage Modeling of Asphalt Mixtures," Ph.D., Dissertation, Texas A&M University, College Station, Texas.

Kim, Y., Little, D. N., and Song, I., (2003)"Mechanistic Evaluation of Mineral Fillers on Fatigue Resistance and Fundamental Material Characteristics," Paper Presented at the meeting of the *Transportation Research Board*, Washington D. C.

Kim, Y., Song, I., and Little, D. N., (2003) "Use of Dynamic Mechanical Analysis to Predict Damage in Asphalt Mastic," *Proceeding of 11th Annual International Center for Aggregate Research Symposium*, Austin, Texas.

Kim, Y.R., Little, D.N., and Lytton, R.L.,(2004) "Effect of Moisture Damage on Material Properties and Fatigue Resistance of Asphalt Mixtures," Transportation Research Record 1891, Transportation Research Board, National Research Council, Washington, D.C., pp. 48-54.

Knauss, W. G., (1993), "Time Dependent Fracture and Cohesive Zones," *Journal of Engineering Materials and Technology*, Vol. 115, pp. 263-267.

Lagoudas, D. C., Ma, X., and Xu, S., (1998), "Surface Damage Modeling of Oxidized Metal Matrix Composite Laminates under Axial and Transverse Tension," *International Journal of Damage Mechanics*, Vol. 7, pp. 209-237.

Lee, H. J., (1996), "Uniaxial Constitutive Modeling of Asphalt Concrete Using Viscoelasicity and Continuum Damage Theory," Ph.D. Dissertation, North Carolina State University, Raleigh, N. C.

Lee, H. J., Daniel, J. S., and Kim, Y. R., (2000), "Continuum Damage Mechanics-Based Fatigue Model of Asphalt Concrete," *Journal of Materials in Civil Engineering*, ASCE, Vol. 12, No. 2, pp. 105-112.

Lee, N. K., and Hesp, S., (1994), "Low-temperature Fracture Toughness of Polyethylene-modified Asphalt Binders," *Transportation Research Record*, *1436*, Transportation Research Board, Washington, D. C., pp. 54-59.

Lesueur, D. and Little, D. N., (1999), "Effect of Hydrated Lime on Rheology, Fracture, and Aging of Bitumen," *Transportation Research Record*, 1661, pp. 93-105.

Little, D. N., Lytton, R. L., Williams, D., Chen, C. W., Kim, Y. R., and Lee, H. J., (1998), "Fundamental Properties of Asphalts and Modified Asphalts, Task K - Microdamage Healing in Asphalt and Asphalt Concrete, Volume 1: Microdamage and Microdamage Healing," FHWA Report.

Little, D. N., Lytton, L. R., Williams, D. A., and Kim, Y. R., (1999), "An Analysis of the Mechanism of Microdamage Healing Based on the Application of Micromechanics First Principles of Fracture and Healing," *Journal of Association of Asphalt Paving Technologists*, Vol. 68, pp. 501-542.

Moulthrop, J. S., (1990), "Memorandum to SHRP Asphalt Research Program Coordinators."

Needleman, A., (1987), "A Continuum Model for Void Nucleation by Inclusion Debonding," *Journal of Applied Mechanics*, Vol. 54, pp. 525-531.

Park, S. W., (1994), "Development of a Nonlinear Thermo-viscoelastic Constitutive Equation for Particulate Composites with Growing Damage," Ph.D. Dissertation, University of Texas, Austin, Texas.

Park, S. W., Kim, Y. R., and Schapery, R. A., (1996), "A Viscoelastic Continuum Damage Model and Its Application to Uniaxial Behavior of Asphalt Concrete," *Mechanics of Materials*, Vol. 24, pp. 241-255.

Reese, R., (1997), "Properties of Aged Asphalt Binder Related to Asphalt Concrete Fatigue Life," *Journal of Association of Asphalt Paving Technologists*, Vol. 66, pp. 604-632.

Rowe, G. M., (1993), "Performance of Asphalt Mixtures in the Trapezoidal Fatigue Test," *Journal Association of Asphalt Paving Technologists*, Vol. 62, pp. 344-384.

Rowe, G. M. and Bouldin, M. G., (2000), "Improved Techniques to Evaluate the Fatigue Resistance of Asphaltic Mixes," *Proceedings of 2nd Enraphalt and Eurobitume Congress*, Barcelona, Spain.

Schapery, R. A., (1974), "Viscoelastic Behavior and Analysis of Composite Materials," *Mechanics of Composite Materials*, Vol. 2, pp. 85-168.

Schapery, R. A., (1975a), "A Theory of Crack Initiation and Growth in Viscoelastic Media: Part I," *International Journal of Fracture*, Vol. 11, No. 1, pp. 141-159.

Schapery, R. A., (1975b), "A Theory of Crack Initiation and Growth in Viscoelastic Media: Part II," *International Journal of Fracture*, Vol. 11, No. 3, pp. 369-387.

Schapery, R. A., (1975c), "A Theory of Crack Initiation and Growth in Viscoelastic Media: Part III," *International Journal of Fracture*, Vol. 11, No. 4, pp. 549-562.

Schapery, R. A., (1984), "Correspondence Principles and a Generalized J-Integral for Large Deformation and Fracture Analysis of Viscoelastic Media," *International Journal of Fracture*, Vol. 25, pp. 195-223.

Schapery, R. A., (1990), "A Theory of Mechanical Behavior of Elastic Media with Growing Damage and Other Changes in Structure," *Journal of Mechanical Physics Solids*, Vol. 38, pp. 215-253.

Schapery, R. A., (1991), "Analysis of Damage Growth in Particulate Composites Using a Work Potential," *Composites Engineering*, Vol. 1, No. 3, pp. 167-182.

Seidel, G. D., (2002), "A Model for Predicting the Evolution of Damage in the Plastic Bonded Explosive LX17," Master's thesis, Texas A&M University, College Station, Texas.

Shin, E. E., Bhurke, A. S., Scott, E., Rozeveld, S., and Drzal, L. T., (1996), "Microstructure, Morphology, and Failure Modes of Polymer-modified Asphalt," *Transportation Research Record*, *1535*, TRB, Washington, D. C., pp. 61-73.

Smith, B. J. and Hesp, S., (2000), "Crack Pinning in Asphalt Mastic and Concrete: Regular Fatigue Studies," *Transportation Research Record 1728*, Transportation Research Board, Washington, D. C., pp. 75-81.

Soenen, H. and Eckmann, B., (2000), "Fatigue Testing of Bituminous Binders with a Dynamic Shear Rheometer," *Proceedings of 2nd Enraphalt and Eurobitume Congress,* Barcelona, Spain.

Tvergaard, V., (1990), "Effect of Fiber Debonding in a Whisker-Reinforced Metal," *Materials Science & Engineering A: Structural Materials: Properties, Microstructure, and Processing*, Vol. A125, No. 2, pp. 203-213.

Ungsuwarungsri, T. and Knauss, W. G., (1988), "A Nonlinear Analysis of an Equilibrium Craze: Part I – Problem Formulation and Solution," *Journal of Applied Mechanics*, Vol. 55, pp. 44-51.

Williams, J. J., (2001), "Two Experiments for Measuring Specific Viscoelastic Cohesive Zone Parameters," Master's thesis, Texas A&M University, College Station, Texas.

Yoon, C. and Allen, D. H., (1999), "Damage Dependent Constitutive Behavior and Energy Release Rate for a Cohesive Zone in a Thermoviscoelastic Solid," *International Journal of Fracture*, Vol. 96, pp. 55-74.

Zhou, F. P., Lydon, F. D., and Barr, B. I. G., (1995), "Effect of Coarse Aggregate on Elastic Modulus and Compressive Strength of High Performance Concrete," *Cement and Concrete Research*, Vol. 20, pp. 177-186.

Zocher, M. A., Allen, D. H., and Groves, S. E., (1997), "A Three Dimensional Finite Element Formulation for Thermoviscoelastic Orthotropic Media," *International Journal for Numerical Methods in Engineering*, Vol. 40, pp. 2267-2288.

Zollinger, C., (2005) "Measurement of Surface Energy and its Relationship to Moisture Damage," Master Thesis, Department of Civil Engineering, Texas A&M University, College Station, Texas.